uc3m | Universidad Carlos III de Madrid

TESIS DOCTORAL

Design of high temperature cobalt-based alloys processed by powder metallurgy route

Autor:

Rafael Casas Ferreras

Directores:

Mónica Campos Gómez

Francisco Gálvez Díaz-Rubio

Tutora:

Mónica Campos Gómez

Programa de Doctorado de Ciencia e Ingeniería de los Materiales

Leganés, octubre 2018

TESIS DOCTORAL

Design of high temperature cobalt-based alloys processed by powder metallurgy routes

Autor:	Rafael Casas Ferreras
Directores:	Dra. Mónica Campos Gómez
	Dr. Francisco Gálvez Díaz-Rubio

FIRMA TRIBUNAL CALIFICADOR:

Presidente:

Vocal:

Secretario:

Calificación:

Leganés (Madrid), octubre de 2018

The secret, dear Alice,

is to surround yourself with people who make your heart smile.

It's then, only then, that you'll find Wonderland

"Alice in Wonderland"

Datum Universitate Carolo III Matritensis, ante diem IX kalendas november, in sollemnitate Archangeli Raphaeli, cordubensis civitatis Custodis. ann. Domini MMXVIII.

Agradecimientos

"Cuando te de vértigo y algo de miedo, pero te haga inmensamente feliz. Entonces, simplemente, arriésgate" Rivera.

La llegada al final de esta tesis doctoral me sirve para hacer una breve reflexión de las infinitas vivencias que han pasado en mi vida durante estos últimos años. Todo aquel que ya anduvo este camino sabe bien que no es un recorrido fácil, donde muchas de las cosas que queremos van quedando atrás, no siendo siempre ese nuestro deseo.

Una vez acabada la escritura, es momento de dar las gracias a todo aquel que ha querido acompañarme durante todo este pasaje, siendo los primeros mis directores, Mónica Campos y Francisco Gálvez. Os agradezco la plena confianza y el temperamento que me habéis ofrecido durante estos años, así como vuestros buenos consejos, valores y sugerencias, ayudándome a crecer como investigador en un mundo muy complicado, hasta conseguir llevar a buen puerto esta tesis.

Estoy muy feliz de haber formado parte del GTP. Por ello me gustaría agradecer de corazón a las profesoras Elena Gordo y Antonia Morales su aprecio y consejos, ya que fueron grandes responsables de decidirme a hacer la tesis. A José M. Torralba por elegirme doctorando. A Elisa, Maru, Juan, Sandra, Sofía, Paula y Eva, con quien he compartido miles de momentos, desayunos y comidas, y alguna que otra porra deportiva. A mis compañeros de múltiples despachos donde he estado durante algún tiempo; Estela, Pedro, Andrea Galán, Guille, George, Andrea Alcántara, Alberto, Edu y obviamente a Eric, un gallego que vale la pena conocer y tener como compañero, gracias. Nunca podría olvidarme de mis dos compañeros, Miguel, por tantas buenas conversaciones y momentos juntos; y Julia, por ayudarme siempre en todos mis agobios y ser la responsable de los mejores recuerdos de esta etapa. He echado tanto de menos vuestra ausencia en este final, pero me voy sabiendo que he tenido la suerte de haber compartido los mejores momentos de mi doctorado durante todos estos años con vosotros. No importa la cantidad de tiempo, sino la calidad del tiempo que hemos disfrutado juntos. Aún así, he intentado siempre no fallar a las personas que de verdad quiero y que han querido seguir a mi lado sin importar que pasase.

Pese haber llegado a la UPM en mi etapa final, no ha sido menos el cariño y la amistad recibida, ya que, gracias a Rafa, Victor, Sandra, Dani, Andrés, Blanca, Fede, Marta y el resto de los compañeros del departamento, Rosa, Ana, Alberto, Josemi, David, Bea, Gustavo, Álvaro, Elena y José Ignacio, me he sentido en casa. No me olvido del instituto IMDEA-materiales, otro de los centros que he pisado, donde he tenido la suerte de tener siempre los consejos de la Dra. Teresa Perez-Prado, la ayuda de Andrea, Marcos y Miguel, grandes responsables de que los resultados finales fueran positivos, y del resto de los chicos y chicas que trabajan allí.

También quiero agradecer a los profesores David N Seidman y David S Dunand, su bienvenida y apoyo durante mi estancia en Northwestern University. Fue una bonita y enriquecedora experiencia que jamás olvidaré, donde tuve la oportunidad de conocer a dos grandes personas como son Filipe y Edwin.

El mayor de los agradecimientos va dirigido a mi familia. Mamá, Papá Jose y mi sobri… menos mal que estáis ahí siempre… ¡mi orgullo hacía todos vosotros hace no quepa en mí! Quiero agradecer todo el apoyo y cariño de mis seres queridos más cercanos, María del Mar, Mercedes y Francisco porque sois simplemente mi familia. Vuestro amor y cariño hacía mi no tiene fronteras y es el mejor tesoro que guardo, así que esto también os corresponde. Titos, primos, somos tantos… pero no os olvido a ninguno porque siempre me hacéis sentir especial cuando estamos juntos. Pepe Castroviejo, D. Jesús, Lilu, Julia, Juan B, Nacho, Gonzalo, Juanma, Pove, Lorenzo, Valen, grandes amigos y personas. Gracias, de corazón.

"Solo quien te quiere de verdad comprenderá el dolor detrás de tu sonrisa, el amor detrás de tu rabia y las razones detrás de tus silencios" Sirva esta frase para agradecer con todo mi corazón a todos aquellos que de quisieron compartir conmigo algún momento de su vida durante esta etapa.

Table of contents

Abstract

The superalloys are a family of alloys with great interest for their application in severe conditions due to their high specific resistance at high temperatures up to 800 °C. Traditionally, different industries have focused their efforts on implementing nickel-based superalloys due to their excellent performance in extreme environments as for example in hot gas turbine parts of aerospace industry.

The discovery of Sato *et al.* [1] marked a milestone, when a Co-Al-W ternary system with a γ/γ' dual phase microstructure was developed. The resulted precipitate phase has a stable stoichiometry $L1_2$ at high temperatures. This new family of cobalt-based alloys allowed to develop an alternative to conventional nickel-based. During the last decade, many investigations have confirmed its excellent versatility, suitable corrosion resistance and good mechanical properties and in severe conditions at high temperature.

On the other hand, the processing by powder metallurgy route of this family of superalloys, has been advanced, in general terms, to improve the mechanical properties of compositions already developed. This type of technology has made the powder metallurgy route, a very attractive alternative for the design and development of new superalloys with a high degree of distribution elements and good mechanical properties.

The main objective of this research work has been to design a new cobalt-based superalloy by powder metallurgy route with a dual γ/γ' microstructure, with a nominal composition of Co-12Al-10W (at.%) and Co-12Al-10W-2Ti-2Ta (at.%), as well as, the study of its mechanical properties at high strain rate conditions.

To be suitable, the defined compositions were processed by Mechanical Alloying (MA) and consolidated by Field Assisted Sintering Techniques (FAST). To be able to perform a more precise comparison, both compositions were also processed by conventional casting route in a controlled atmosphere.

Once the alloys were consolidated, different heat treatments were suggested to choose the most suitable γ/γ' microstructure. All samples were characterized by Scanning Electron Microscope and Transmission Electron Microscope, as well as study composition by Energy

Dispersive Spectrometer and the present phases by X-ray diffraction. The mechanical properties in terms of hardness were also studied by means of micro and nano indentation. Finally, the mechanical behavior under dynamic conditions (at high strain rate of 10^3 s^{-1}), and simultaneously modifying the temperature in a range from room temperature to 850 °C was studied. A thermos-visco-plastic Johnson-Cook model was constituted to simulate the behavior the cobalt-based processed alloys in dynamic regimes.

Resumen

Las denominadas *superaleaciones* son una familia de aleaciones de gran interés para aplicaciones en condiciones severas, al proporcionar una elevada resistencia específica a unas temperaturas cercanas a 800 °C. Tradicionalmente, industrias como la aeroespacial, han focalizado sus esfuerzos en implementar las superaleaciones base níquel, debido a su excelente comportamiento en ambientes extremos como, por ejemplo, en zonas calientes de turbinas de gas.

El descubrimiento por Sato *et al.* [1] marcó un hito, al constatar que en el sistema ternario Co-Al-W se podía conseguir una microestructura de tipo dual γ/γ', donde la fase precipitada tenía una estequiometria $L1_2$ estable a altas temperaturas. Esta nueva familia de superaleación base cobalto permitió desarrollar una alternativa a las convencionales base níquel. Durante esta última década, diversas investigaciones han confirmado su excelente versatilidad, buenas propiedades mecánicas y resistencia a corrosión en condiciones extremas a alta temperatura.

Por otro lado, el procesamiento por la ruta pulvimetalúrgica de esta familia de las superaleaciones, ha ido consiguiendo, en términos generales, mejorar las propiedades mecánicas de las composiciones ya desarrolladas anteriormente. Este tipo de tecnología ha hecho de la vía pulvimetalúrgica, una opción muy atractiva para el diseño y creación de nuevas superaleaciones con un alto grado de distribución de elementos y buenas propiedades mecánicas.

El principal objetivo de esta tesis ha sido plantear a partir de la ruta pulvimetalúrgica una nueva superaleación base cobalto con una composición nominal Co-12Al-10W (at.%) y Co-12Al-10W-2Ti-2Ta (at.%), así como el estudio de sus propiedades mecánicas en condiciones de alta velocidad de deformación.

Para cumplir con él, las composiciones definidas se fabricaron en polvo mediante molienda mecánica de alta energía (MA del inglés *Mechanical Alloying*) y se consolidaron mediante técnicas asistidas por campo (FAST, del inglés *Field Assisted Techniques*). Para poder realizar de forma más precisa una comparativa con respecto a las mismas aleaciones obtenidas por moldeo, también fueron procesadas las dos composiciones por colada convencional en atmosfera controlada.

Una vez consolidadas las aleaciones, se estudiaron diferentes tipos de tratamientos térmicos para poder elegir la microestructura más adecuada. Todas las muestras se caracterizaron mediante

microscopia electrónica de barrido y transmisión, así como estudio de composición por EDS y de las fases presentes por difracción de Rayos X. También se estudiaron sus propiedades mecánicas mediante micro y nano identación. Finalmente se estudió el comportamiento mecánico en condiciones dinámicas (a alta velocidad de deformación, $\dot{\varepsilon}=10^3\,s^{-1}$), y modificando simultáneamente las temperaturas en un rango desde temperatura ambiente hasta 850 °C. Se constituyó así, un modelo termo-visco plástico de Johnson-Cook que simula el comportamiento del material en regímenes dinámicos

Published and submitted content

Authors	**R. Casas**, F. Gálvez, M. Campos
Title	Microstructural development of powder metallurgy cobalt-based superalloys processed by field assisted sintering techniques (FAST)
Review	Materials Science & Engineering A Volume 724, (2018), pp 461-468 DOI 10.1016/j.msea.2018.04.004

This work is included mainly on Chapter 3 and Chapter 4.

Congress	XIV Congreso Nacional de Materiales Gijón (España), June 2016
Authors	**R. Casas**, M. Campos, F. Gálvez
Title	Aleaciones base Co sinterizadas para su aplicación en condiciones severas: Diseño de microestructuras γ/γ'
Participation	Oral

This work is included mainly on Chapter 3 and Chapter 4.

Congress	World PM 2016 Hamburg (Germany), October 2016 ISBN: 978-1-899072-48-4
Authors	**R. Casas**, M. Campos, F. Gálvez
Title	High Temperature Co alloys processed by PM route: Designing γ/γ' microstructures.
Participation	Oral

This work is included mainly on Chapter 3 and Chapter 4.

Congress	AMPT 2016 Kuala Lumpur (Malaysia), November 2016
Authors	M. Cartón, **R. Casas**, M. Campos, José M. Torralba
Title	Microstructural possibilities of Co-Al-W alloys processed by SPS: Effects of Al and W contents.
Participation	Oral

This work is included mainly on Chapter 3 and Chapter 4.

Congress	VI Congreso Nacional de Pulvimetalurgia Ciudad Real (España), June 2017 ISBN: 978-84-697-3650-0
Authors	**R. Casas**, M. Campos, F. Gálvez
Title	Diseño de microestructuras γ-γ' mediante tratamientos térmicos para la obtención de aleaciones de cobalto por vía pulvimetalúrgica
Participation	Oral

This work is included mainly on Chapter 3, Chapter 4 and Chapter 5

Congress	EuroPM 2017 Milan (Italy), October 2017 ISBN: 978-1-899072-49-1
Authors	**R. Casas**, M. Campos, F. Gálvez, David C. Dunand, David N. Seidman
Title	Design of γ-γ ' microstructures through heat treatments for strengthening Co base PM alloys

This work is included mainly on Chapter 3 and Chapter 5

Congress	Eurosuperalloys 2018 Oxford (United Kingdom), September 2018
Authors	**R. Casas**, M. Campos, F. Gálvez
Title	Poster Research on design of γ/γ' microstructures in cobalt-based superalloys processed by powder metallurgy route

This work is included mainly on Chapter 3 and Chapter 6.

Preface

The Ph.D. thesis here presented has been carried out at the department of Materials Science and Engineering of the University Carlos III de Madrid and Universidad Politécnica de Madrid – Escuela de Caminos, Canales y Puentes.

This work has been developed in the frame of a DIMMAT project funded by Madrid region under program S2013/MIT-2775.

This doctoral thesis has been recognized with the mention of International Ph.D. part of the effect of heat treatments test research work has been carried out at the Northwestern University (Evanston, Illinois, USA) during more than 3 months to obtain a better result and to get in touch with two of the most important word's experts in the cobalt superalloy area. Moreover, two international experts in high temperature alloys and dynamic behavior at high strain rates, Dra. Raquel de Oro Calderón, from TU Wien, (Vienna, Austria) and Dr. Sidney Chocron, from South West Research Institute in San Antonio (Texas, USA), have reviewed the present manuscript.

The results obtained during this thesis have been published in top journals in the field of metallurgy, such as, Materials Science and Engineering A. In addition, this work has been shared and well received at international conferences and workshops on the field of powder metallurgy and superalloys.

1. Motivation and Objectives

The range of application for superalloys has increased to many areas since their development for use in the aviation industry [2, 3]. An increasing market demand requires new finding associates with such alloys. The cobalt-based superalloys have been studied in the literature since the discovery of the stable ternary $Co_3(Al,W)$ compound with an ordered $L1_2$ precipitates structures by Sato *et al.* in 2006 [1]. It is well known that the Co-Al-W system has provided a good alternative for these demanding applications due to an ability to retain most of their strength even after long exposition times and temperatures [4]. Xue *et al.* [5] reported that the novel ternary system has been designed to form rafted γ'-cuboidal precipitates embedded in a continuous γ-matrix, with many similarities with the γ/γ' dual phase of nickel based superalloys.

However, to compete better with nickel based alloys it is necessary to increase the temperature range of stability of γ'-$Co_3(Al,W)$. Yan *et al.* [6] reported that ternary Co-Al-W alloys were previously discarded due to their lower high temperature strength, limited by the γ' solvus temperature, about 100 °C ~ 300 °C lower than the present nickel based alloys. Bauer *et al.* [7], shows how addition of 2 at. % -Ta as well as -Ti on the ternary alloy produced a substantial increase in the γ' volume fraction. However, Suzuki *et al.* [8] determined how cobalt-based with -Ta element addition has a strength comparable to a conventional nickel-based alloys at 900 °C. Suzuki and Pollock [9] also studied that -Ta element is effective for stabilization of the γ' phase, while an addition of Cr decreases the γ' solvus temperature. Pollock *et al.* [10] reported that cobalt-based alloys have significantly higher solidus and liquidus temperatures compared to the nickel-based alloys, typically 100 to 150 °C higher. Bauer *et al.* [7] studied how different alloying elements, as Ta, Nb, W, Ti, and V, increase the γ' volume fraction and γ' solvus temperature. The tensile creep behavior was studied by Xue *et al.* [11] indicating that the creep properties of experimental alloy exceeded commercial 1st generation nickel-based single crystal superalloy.

Two alloying elements, such as -Ti and –Ta, are of special attention as they are known to increase the range of stability of γ' and the volume fraction of the phase. Ishida [12] reported that the addition of alloying elements was found to be very similar to that of nickel-based alloys, where Ti, -Ta, -Nb and V are the γ' stabilizing elements. Xue *et al.* [5] remarked that γ'-phase stabilize

better by adding -Ti and -Ta elements. It is also shown that -Ta addition in the cobalt system can improve the high temperature strength.

The mechanical response of cobalt-based alloys has been usually measured at low strain rates, such as, compression and tensile tests. No evidences of high strain rates studies have been found in the cobalt superalloys literature. The majority of the material data properties were obtained under quasi-static loading conditions but in a wide range of situations, materials are subjected to impact or explosion conditions. A better knowledge of the fundamentals of dynamic behavior in these materials could be critical for enhancing alloy development.

The major objective of this thesis is *to develop a novel cobalt-based superalloy with a dual γ/γ' microstructure processed by powder metallurgy (PM) route and to study the dynamic behavior of this alloy at high strain rates.*

With this aim, a powder route based on the mix of elemental powders processed by Mechanical Alloying (MA) and consolidated by Field Assisted Sintering Techniques (FAST) was proposed. Previously, the ternary system was designed by thermodynamic simulation (CALPHAD), to predict the nominal composition Co-12Al-10W. Based on prior research works, another composition with -Ti and -Ta (2 at. %) was also developed.

Subsequently, different alternatives of heat treatments have been suggested to investigate their effect in the γ/γ' two phase microstructures and to optimize the morphological properties of the desired alloys. In addition, a conventional casting route was also determined to compare the morphological properties, as well as mechanical properties.

Finally, a dynamic study with Hopkinson bar test was performed with the aim of characterizing the impact behavior of cobalt-based specimens under high strain rates (10^3 s^{-1}) and different temperatures, allowing to identify an anomalous positive flow stress in the range of temperatures of (700 – 800 °C). A modified Johnson-Cook model was considered with the aim of adjusting the mathematical model with the experimental tests.

The work described above has been structured in the following chapters:

- Chapter 2: Literature review highlighting the state of the art, microstructure and common phases, manufacturing routes and mechanical properties of cobalt-based alloys.

- Chapter 3: Description of the materials used in this work, their preparation and characterization methods to study their microstructure and mechanical properties.

- Chapter 4: Development of the γ/γ' microstructure with the design of the optimal composition by thermodynamical simulation (CALPHAD). Processing of the powders of ternary system by Mechanical Alloying (MA) and subsequently consolidated by Field Assisted Sintering Techniques (FAST). The cobalt-based samples were studied by morphological and mechanical characterization.

- Chapter 5: Study of the effect of possible heat treatments to achieve an optimal γ/γ' microstructure. Additional cast route samples were used to compare to them by microstructural characterization and mechanical properties.

- Chapter 6: Analysis of the dynamic behavior of PM cobalt-based alloys at high strain rates. Determination of a modified model of Johnson-Cook to adjust the experimental results obtained at high temperature range.

2. Literature Review

2.1. Brief introduction of the superalloys

In the modern industrial world, there is a strong need to go further and develop a wide range of materials with the ability to maintain their mechanical properties at elevated temperatures. This kind of materials are called as high-temperature materials. Their application in the industry is determined by the operating conditions which can be tolerated. For this reason, Reed [2] reported that the desirable characteristics of this materials, is *the ability to withstand loading at an operating temperature close to its melting point, the substantial resistance to mechanical degradation over extended periods of time and the tolerance of severe operating environments.* These severe conditions demand materials called as a high-temperature materials or superalloys.

Superalloys are a wide family of alloys that exhibit high strength and oxidation resistance for high temperature applications [13]. Many intermetallic compounds and ceramic materials have been investigated in the last two decades due to ever-increasing demands of structural materials with high operating temperatures and significant resistance to loading under fatigue and creep conditions. Nevertheless, to date only nickel-based superalloys have the extreme requirements in the hottest area of the turbine due to their balanced properties in terms of creep and thermomechanical fatigue, strength, ductility and oxidation resistance with good density and acceptable costs. A schematic perspective of the different process developments occurred since first superalloys began to appear in 40s decade is shown in Fig. 2.1.

Superalloys are traditionally separated into three main groups, depending on their main element compound. The first superalloy to be developed was iron or iron-nickel, (Incoloy 800 series) [2], and containing high wt.% Fe which act as a joint base material with nickel [13]. Most of these alloys show a solid-solution strengthening mechanism similar to nickel-based alloys but exhibit spherical precipitation rather than cuboidal precipitation of the strengthening γ'-phase [13]. This type of alloys are used as wrought rather than cast material [2,13].

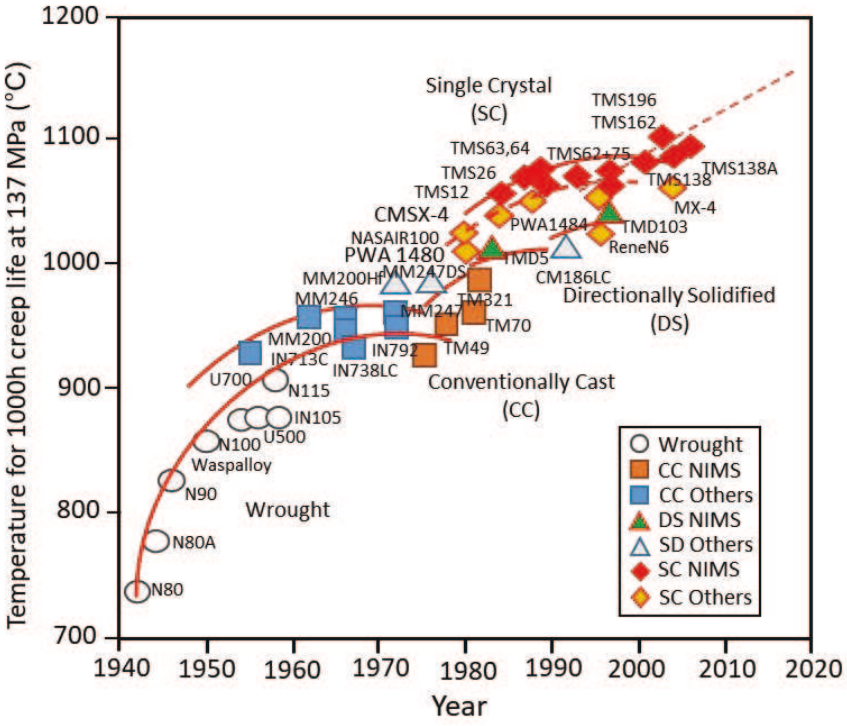

Fig. 2.1 Development of the high-temperature capability of the superalloys over a 70 year period and new perspective for 2020 [2].

Nickel-based is the second category of superalloys which contains the most widely used high temperature structural materials in aircraft engines and power generation systems, constituting over 50 % of the engine weight. They are represented by the use of nickel as the sole base element [13], and can be used in cast, wrought and powder metallurgy route, depending on the application. The nickel-based alloys contain at least 50 % nickel and are characterized by the high phase stability of the face centered-cubic (fcc) austenitic (γ) matrix. The most commonly used alloying elements in nickel-based alloys are chromium, aluminum, cobalt and small amounts of boron, zirconium, niobium, tantalum, tungsten and rhenium. Chromium and aluminum provide oxidation resistance by forming the oxides Cr_2O_3 and Al_2O_3, respectively. In addition, the appearance of the γ' precipitate is very important in the austenitic matrix, due to strengthening increases with increasing amounts of γ' precipitate, which is a function of the combined aluminum and titanium content. Depending on the volume fraction of γ'-phase, the precipitate particle can change from spherical (γ' less than about 25 %) to cuboidal shape (γ' greater than 35 %). It is generally recognized that the high temperature resistance rises with increasing γ'-phase.

The last category of superalloy is the cobalt-based alloys, typically rely on strengthening by elements within solid-solution and the formation of carbides for their high temperature properties. Polycrystalline cobalt usually has a combination of hexagonal close-packed (hcp) structure and

face-centered cubic (fcc) phases at room temperature, which transforms martensitically into the cubic close-packed below 420 °C. The HCP-FCC transitions depends of the thermal history, shape, purity and grain size [14, 15]. No strengthening precipitates were found in cobalt-based alloys, which limited their use in many applications until the discovery of a novel stable ternary $Co_3(Al,W)$ system by *Sato et al.* [1]. This novel ternary compound provides a possible potential cobalt-based dual phase γ/γ' microstructures for superalloys performance at high temperatures.

2.2. Industrial applications

The superalloys have emerged as the most powerful candidates for industrial applications with specific requirements of high-strength creep deformation and oxidation resistance at high temperatures.

One of the most important demand in the aerospace industry has been the development of better superalloys for gas turbine engines. Jet engines are complex systems made using various type of materials. Fig. 2.2 shows the design of a typical turbofan engine which about 50 % is made up of superalloys, including four main parts: compressor, fan combustor and turbine. Must be considered that each alloy is chosen depending on the function of the component, cost and mechanical, thermal and environmental properties. Superalloys can be divided in two groups for gas turbines:

- Rotating parts: Shafts, Discs and blades.
- Stationary parts: Combustor can, nozzles, guide vanes, seals and casing.

The efficiency of gas turbine engines generally increases with the operating temperature of the engine. The new class of cobalt-based superalloys with dual γ/γ' microstructure may help improve the design of this turbines, increasing the operating temperature, due to the melting temperature, oxidation and wear resistance of cobalt is higher than nickel. It would improve turbine efficiency and lead to substantial fuel cost savings [13, 16].

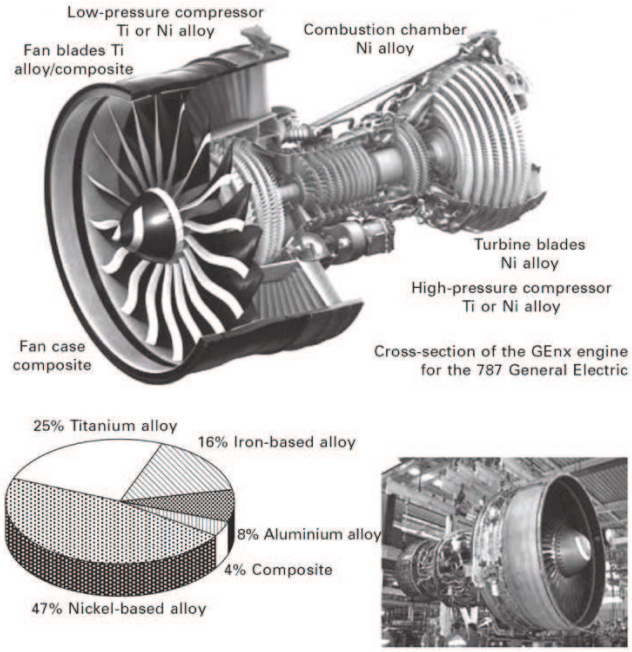

Fig. 2.2 Material distribution in an General Electric (CF6) turbofan engine used in the Boeing 737 [16, 17].

Other applications can include chemical and petrochemical plants (valves, reaction vessels, piping, pumps), marine equipment (blades, bolts), metal processing (hot work tools and dies, casting dies), automotive components (turbochargers, exhaust valves) and nuclear reactors (control-rod drive mechanism, valve stems, springs, ducting). It is worth to mention that cast superalloys present some challenges due to specific conditions during machining, such as, low thermal conductivity, hot hardness, chemical affinity towards tool materials, and presence of abrasive carbide particles in their microstructure [17–20]. For this reason, compared to conventionally produced superalloys, powder metallurgy technology may help to develop new possibilities in the industry providing improved strength, creep resistance, creep fatigue and better low cycle fatigue properties, as well as saving extra costs.

2.3. Nickel and Cobalt based alloys

Materials for high-temperature service must withstand considerable loads at high temperature for extended periods of time. This is the primary concept of any superalloy, to demonstrate high strength, as high creep, yield, rupture or fatigue strength at high temperature. Table. 2.1 summarizes some typical physical properties of both superalloys.

Nickel-based superalloy is the primary family of metallic materials for high temperature applications. As it was explained, the good behavior of nickel-based under high temperature conditions is due to a γ/γ' microstructure. These superalloys are the most used materials in turbine

engines due to their good combination of high strength, long fatigue life and good resistance to oxidation and corrosion at high temperature.

Table. 2.1 Normal physical properties of Ni and Co superalloys [21].

Property	**Typical ranges of Ni-based**	**Typical ranges of Co-based**
Density	7.6 – 9.1 g/cm^3	8.3 - 9.4 g/cm^3
Melting temperature (*liquidus*)	1310 – 1450 °C	1315 - 1495 °C
Elastic Modulus	Room T: 210 GPa	Room T: 211 GPa
	800 °C: 160 GPa	800 °C: 168 GPa
Thermal expansion	8-18 x 10^{-6} /°C	12.1-16 x 10^{-6} /°C
Thermal conductivity [22]	Room T: 9 - 11 W/m · K	Room T: 10 - 13 W/m · K
	800 °C: 22 - 23 W/m · K	800 °C: 25 W/m · K

Cobalt-based superalloys exhibits the same fcc structure at high temperatures of nickel-based alloys. Despite being high melting point (1494 °C vs 1454 °C), the potential of nickel alloys is much greater due to the specific microstructure observed, which is based on the precipitation of an ordered phase, γ' onto the fcc matrix. The γ' phase exhibits stoichiometry of the type A_3B, as in $Ni_3(Al,Ti)$ which has an $L1_2$ structure.

In order to have another possibility of choice in superalloys, γ/γ' dual phase in cobalt-based must exhibit at least, same mechanical properties at higher operating temperatures. Typical applications for cobalt-based in gas turbine engines are vanes and other stationary components, due to their superior stress-rupture properties and hot corrosion resistance. It can also be used for blades but in this case, it is better to use nickel-based alloys than cobalt-based due to their limitation to lower stresses.

The outstanding resistance again creep and stress rupture at high temperature are the most remarkable properties of superalloys. Creep is an important property in superalloy to avoid seizure and failure of engine parts that involves the gradual plastic deformation occurs at stress levels below the yield strength of the material [16]. Compared with other aerospace materials, the stress strength of superalloys at high temperature is outstanding, as shown in Fig. 2.3.

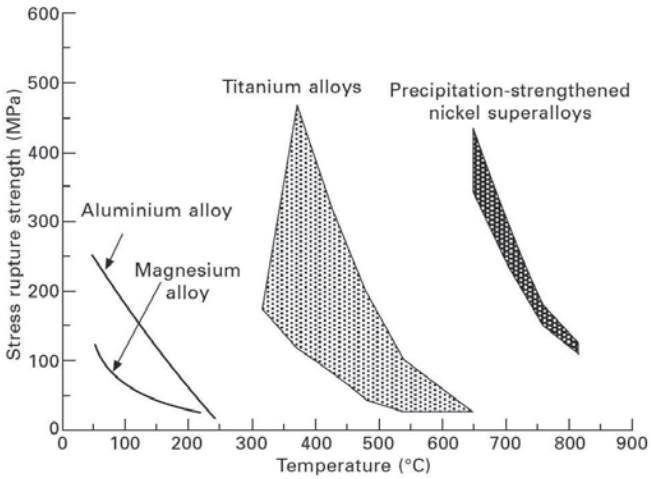

Fig. 2.3 Stress rupture curves for typical materials used in aircraft structures [16].

In 1971, Charles S. Lee [23] was the first who reported that two-phase alloys within the ternary system, consist of an fcc (γ) matrix strengthened by coherent $L1_2$-ordered precipitates (γ'), analogous to nickel-based alloys. In 2006, *Sato et al.* [1] reported an intermetallic γ'-($L1_2$) ordered fcc phase in the Co-Al-W system. This route has resulted in a new class of high temperature alloys, which may increase the maximum operating temperatures of gas turbine engines. In the another hand, other intermetallic results were reported for the Cobalt system, such as Co_3Ti [24, 25] or Co_3Ta [26, 27], but none of these alloys were capable of undergoing heat treatments at high temperatures. In addition, there are some matters needing to be addressed, such as, lower γ' solvus temperature compared to Ni-based [1, 10], increased mass density due to the large amounts of W needed to stabilize the γ'-phase, and reduced strength and yield stress anomaly compared to $Ni_3(Al,Ti)$ [28, 29].

The existence of this new class of precipitation-strengthened Cobalt-based opens the door to the possibility of obtaining a dual phase γ/γ' with satisfactory properties at high temperatures, similar to nickel alloys.

In summary, the advantages of cobalt-based alloys are summarized below:

- Higher melting temperatures and flatter stress-rupture curves. This provide a useful stress capability to a higher absolute temperature than polycrystalline nickel or iron-based superalloys.
- Superior hot corrosion resistance. High concentration of cobalt, nickel, chromium and tungsten provide good resistance against lead oxides, sulfur oxides and other corrosive compounds in the combustion gas turbine.

- Superior thermal fatigue resistance and weldability compared to nickel-based alloys.

2.4. Phases and microstructure of superalloys

The microstructure of the standard superalloys is complex, with a large amount of intermetallics and secondary phases that can modify the alloy behavior through their location, composition and morphology. This microstructure can be represented as a face-centered cubic (fcc) γ-phase matrix that contains secondary phases as fcc carbides, ordered fcc γ'-phase, body-centered tetragonal (bct) γ''-phase, ordered hexagonal η-phase, ordered orthorhombic intermetallic compounds and others that can be beneficial or harmful depending the alloy properties [13].

One of the most important essential factors that determinates the properties of these alloys is the morphology of the precipitates. Nickel and cobalt-based have a bimodal γ' morphology, achieved by precisely heat treatments that can modify the precipitation morphology. The evolution of superalloy microstructure, showing the morphology of both useful and harmful phases is shown in Fig. 2.4.

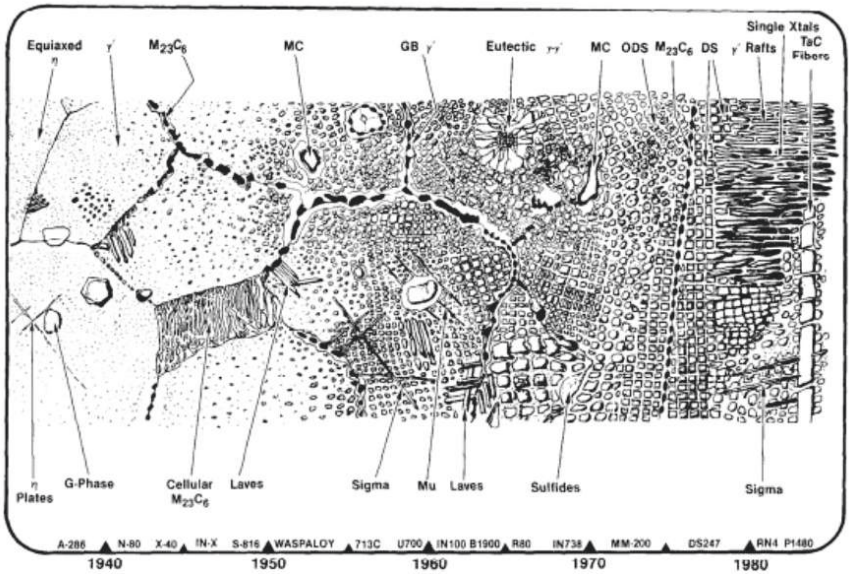

Fig. 2.4 Evolution of Ni superalloy microstructure, showing both beneficial and detrimental phases [30].

It can be seen the influence of the particular elements and their amount, distribution and shape of the of the γ' phase during the development of these superalloys. It should also be considered that depending on the developed microstructure, the field of application has been changing, thus allowing an evolution over the years to acquire microstructures with more effective

hardening mechanisms. The volume fraction of γ' precipitates has increased up to 80 % and their high temperature properties was also optimized.

The major phases present of typical nickel or cobalt superalloys have been shown from the following list.

- *The gamma phase (γ).* This exhibits a solid solution of face-centered-cubic (fcc) structure, and it forms a continuous matrix phase which the other phases reside. This phase can contain elevated amounts of alloying elements such a Cr and Mo.
- *The gamma prime phase (γ').* This is a coherent precipitate phase, with an ordered $L1_2$ cubic crystal structure. It is hardened by the precipitation of the coherent γ'-phase (Ni_3Al) in nickel-based alloys, and $Co_3(Al,W)$ for cobalt-based alloys, respectively. Both superalloys are typically heat treated to form the cuboidal structure.
- *The gamma double prime (γ'').* This is a strong coherent metastable precipitate of composition Ni_3Nb with a body center tetragonal (bct) structure. It is precipitates in nickel and nickel-iron based superalloys. At certain high temperatures and time conditions, δ precipitate of the same Ni_3Nb composition forms instead. Careful heat treatment is required to ensure precipitation of γ'' instead of δ.
- *Carbides and borides.* Carbon, often present at concentration up to 0.2 wt.%, combines with other reactive alloying elements such as titanium, tantalum and hafnium to form MC carbides. During processing, can decompose to other secondary species, such as $M_{23}C_6$ and M_6C, residing on the γ grain boundaries. Borides can be formed from Cr or Mo placed at grain boundaries.

Other phases can be found in superalloys after aged conditions, i.e. close-packed (tcp) phases, as μ, η, χ, σ, etc. However, the composition of the superalloys are chosen to avoid the formation of these secondary phases [2]. A schematic of different phases on the cobalt-based superalloy have been studied by Mottura *et al.* [31] with a representation of the typical unit cell for the γ/γ' dual phase (see: Fig. 2.5).

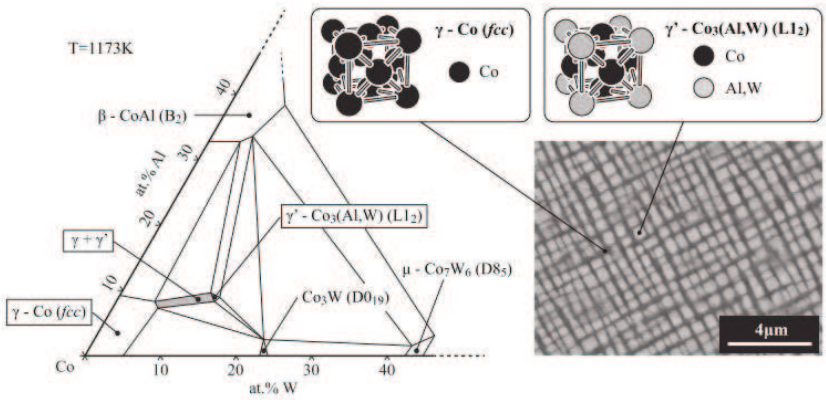

Fig. 2.5 A schematic diagram of the ternary Cobalt-based system at 900 °C with a representation of the unit cells for γ and γ' phase [31].

2.4.1. Strengthening mechanisms

The superalloys can be strengthened by a mix of three mechanisms, solid solution hardening, precipitation hardening and the presence of different carbides at the grain boundaries.

2.4.1.1. Solid Solution Hardening

Because of its electronic structure, the fcc lattice of the matrix has a large solubility for many other elements [32]. Solid solution strengthening is caused partly by lattice distortion. This technique works by adding atoms of one element into the crystalline lattice of a different soluble element. The alloying elements diffuses into the matrix, forming a solid solution and the distortion of the atomic lattice caused by the misfit of atomic radius inhibits dislocation movement. This method depends on the concentration, shear modulus, size and valency of solute atoms. High melting point elements provide strong lattice cohesion and reduces diffusion particularly at high temperatures. Molybdenum and tungsten are thus particularly effective for both these reasons. By adding tungsten and molybdenum together with chromium and aluminum, can also strengthened the matrix due to the electronic effect of an atomic clustering or short-range order. However, strengthening due to short range order generally diminishes rapidly above about 0.6 Tm, due to increased diffusion [33].

2.4.1.2. Precipitation Hardening

Precipitation hardening can impart a considerable increase in creep strength for most high temperature applications in superalloys. Nickel-based superalloys are commonly strengthened by γ' precipitates of the type Ni_3Al, in the disordered fcc matrix γ-phase. The main principle to

precipitate the γ' phase is to apply solution heat treatments and then aged to produce the desired properties. The primary carbides located at grain growth can be dissolved by applying long exposure times at solution temperatures. Aging heat treatments are used to strengthen precipitation alloys by precipitation one or more phases (γ' or γ'').

The origin of precipitation hardening is complex. The size and spacing of the particles and therefore their volume fraction and lattice parameter is an important factor [34]. Pure γ' is quite unusual in that its intrinsic strength is low at low temperatures and increases with temperature up to a maximum at about 700-750 °C. In the case of nickel-based alloys, precipitation hardening can be achieved by elemental addition such as aluminum, titanium or niobium.

The four key factors to control the effectiveness of precipitation hardening are, [3, 13]:

- Coherency strains between the matrix (γ) and the precipitate (γ', γ'') due to the difference in their lattice parameters
- Antiphase-boundary energy (APB) in the presence of an ordered precipitate (γ', γ'') The (APB) represents the energy needed for the dislocation to cut through the ordered precipitate
- Volume fraction of the precipitate (γ', γ'')
- Particle size

2.4.1.3. Role of carbides

The carbides are also an important constituent of superalloys. They can increase or decrease the alloy properties, depending on location, composition and shape. Carbides tend to locate at grain boundaries in nickel-based superalloys, but it is possible to find intragranular carbides in cobalt and iron-based alloys. In general, this phases provide a beneficial effect on rupture strength at high temperature if present in the right composition and morphology [3].

Primary carbides, MC ("M" is tantalum, titanium or tungsten), are formed typically at high temperature as coarse, random, globular or discrete blocky microstructure. They usually have an fcc crystal structure. The preferred order of carbide in this class of superalloys is as follows: TaC, NbC, TiC.

Secondary carbides, $M_{23}C_6$ and M_7C_3, form mainly on the grain boundaries and usually occur as irregular, and discontinuous blocky particles. The M_6C carbides also precipitate in blocky form on grain boundaries and can form Widmanstätten structures (see: Fig. 2.6).

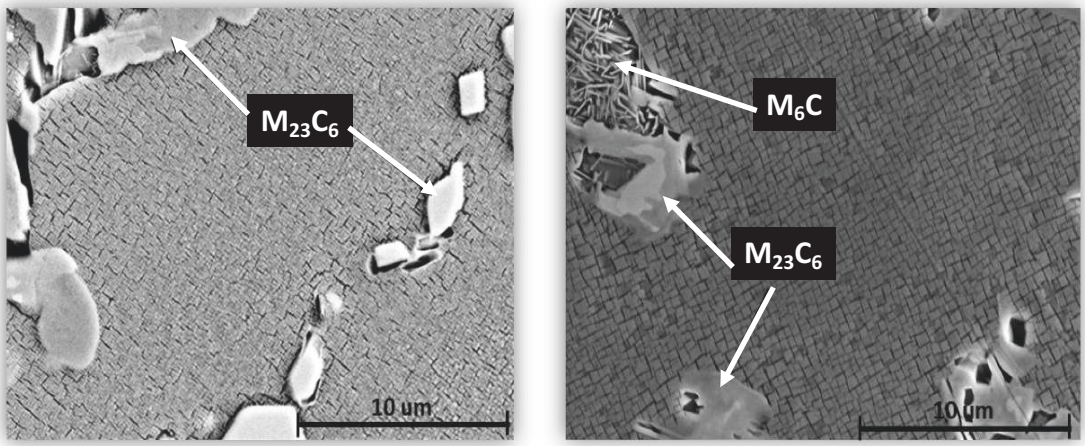

Fig. 2.6. SEM micrographs of powder metallurgy cobalt-based superalloy processed in this project with typical carbides $M_{23}C_6$ and M_6C (Widmanstätten pattern)

Stress-rupture strength and tensile strength are mechanical properties affected by carbides. The benefit of MC carbides is to provide a stable source of carbon for precipitation of secondary carbides. However, they also serve as crack initiation sites and crack propagation paths. *Jiang et al.* [35] reported that secondary carbides formed during heat treatments provide beneficial effect as fine secondary carbide dispersions pinning dislocations and hardening the alloy. The amount of carbides present in the microstructure must be controlled due to at the grain boundaries provide paths of crack propagation. Moreover, MC carbide is a metastable phase and can be decomposed easily into secondary carbide at temperature higher than 1140 °C and dissolves into the matrix partially at or above 1180 °C. *Sim et al.* [34] presented the fundamental understanding of the structure carbides (see: Fig. 2.7). It is also noted that MC carbides break down into $M_{23}C_6$ carbides at the grain boundaries by the following reaction: $\gamma + MC \rightarrow M_{23}C_6 + \gamma'$.

In addition, the role of the carbide has been studied as crack initiation by *Engler-Pinto et al.* [36] on creep and thermo-mechanical fatigue, but is in the study completed by *Doherty et al.* [37], where is indicated that it is the "thin-film" carbides formation which are most negative in terms of crack initiation and propagation.

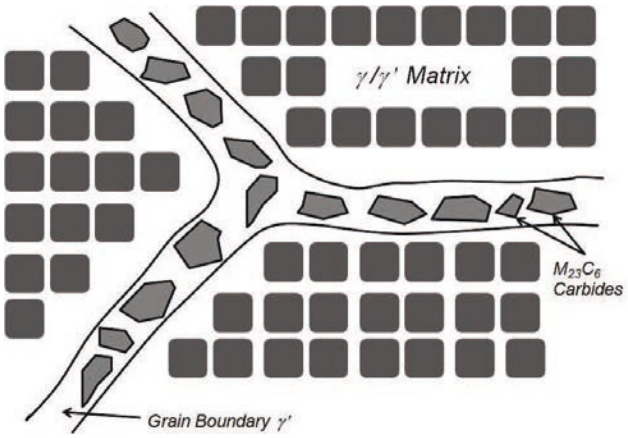

Fig. 2.7 Scheme of typical grain boundary carbide structure [34].

2.4.2. The γ/γ' dual phase structure

The γ/γ' dual phase structure is the main responsible for mechanical properties of superalloys. This microstructure leads to high-temperature creep resistance because of the large interfacial area between the γ and γ' phases, which blocks the motion of dislocations [21]. It is important to understand the atomic structure of both phases separately; the γ-nickel (or cobalt) and γ'-Ni_3Al, (or $Co_3(Al,W)$) phases exhibit a fcc and $L1_2$ structure, respectively (see: Fig. 2.8, above) [13]. This γ-phase matrix is ideal for high temperature because it has optimal mechanical properties, i.e. tensile, rupture, creep and thermomechanical fatigue. The densely packed fcc matrix is also ideal for use at high relative temperatures (T/T_m), due to the low diffusivity of alloying elements. In addition, the fcc matrix has a broad solubility of secondary elements that allows the precipitation of intermetallic compounds, such as γ' and γ'' for strengthening.

The γ'-phase shows an ordered structure ($L1_2$); in the case of nickel-based superalloys, it could be said that the upper and lower planes consist of a nickel atom surrounded by aluminum atoms at each corner of the square. Aluminum atoms are at the cube corners and nickel atoms are placed at the center of the cube faces. The middle plane, placed between the upper and the lower face of the unit cell, shows simply four nickel atoms lying in the face-centered positions. These atoms form an entire plane of nickel which separates each plane of ordered nickel and aluminum. In Fig. 2.9a, it is shown the diagram of the ordered plane and how this combines with nickel planes, Fig. 2.9b. [13]. Same case applies for cobalt-based alloys (see: Fig. 2.8, below). Cobalt atoms occupy the (½, ½, 0) face-center positions whereas Al, W atoms prefer to occupy the (0, 0, 0) cube corner position in the $L1_2$ phase [1, 38].

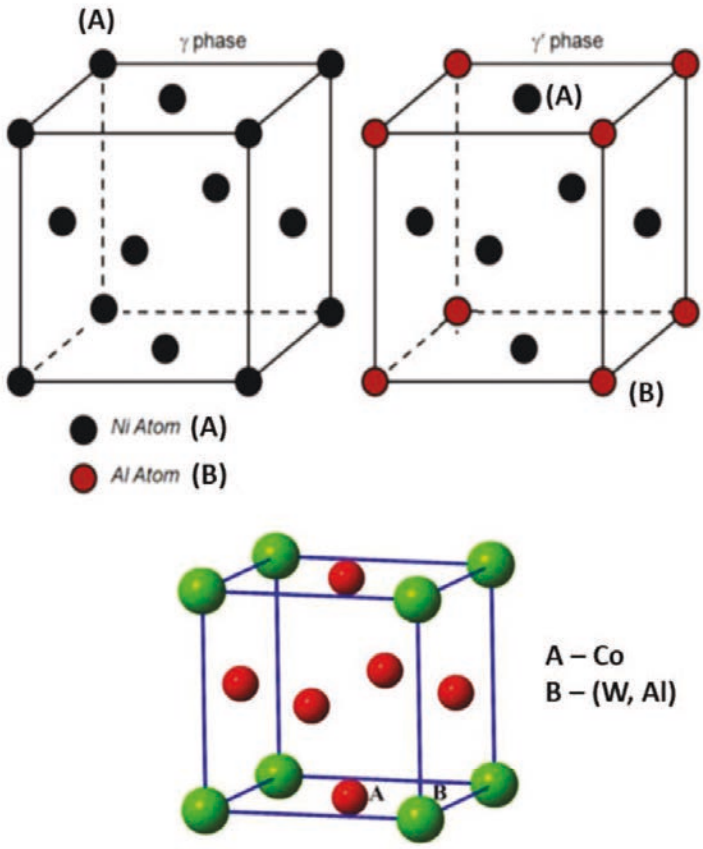

Fig. 2.8 (Above) Diagram of the atomic structure of both γ (Ni) and γ' (Ni_3Al). Black spheres denotes the nickel atoms, and red circles denote the aluminum atoms in Ni-based superalloys [13] (Below) Atomic structure of an $L1_2$ unit cell in cobalt-based superalloys.

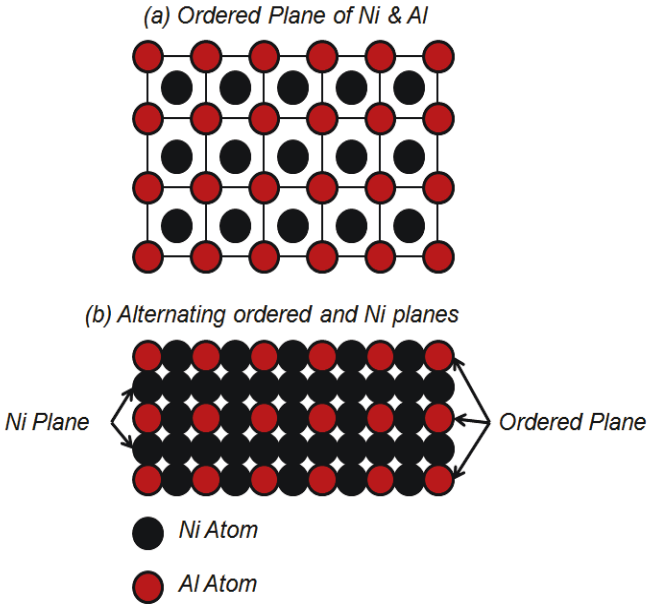

Fig. 2.9 Illustration of the ordered plane structure within the γ' phase (a) and how these planes combine with nickel planes (b) [13].

An aging heat treatment may be used to precipitate the γ'-phase in the form of discrete particles. This particles structure is desirable as it confers good creep properties. With short aging heat treatments, the γ'-phase will form small spherical particles, however further ageing will produce characteristic cuboidal shapes precipitates typical in more recent superalloys. *Ricks et al.* [39] discussed the transition from spherical to cuboidal particle during aging treatments. This change is dependent directly on the lattice misfit parameter (δ), between the γ and γ' phases, as defined according to equation (2.1)

$$\delta = 2 \cdot \left[\frac{a_{\gamma'} - a_{\gamma}}{a_{\gamma'} + a_{\gamma}}\right] \quad [39] \ (2.1)$$

Where a_{γ} and $a_{\gamma'}$ are the lattice parameters of the γ and γ' phases, respectively. The lattice misfit is described as positive if $a_{\gamma'} > a_{\gamma}$ and negative if the converse is true. In Nickel-based alloys, a lattice value between 0 and 0.2 percent produces a spherical precipitate; between 0.5 and 1.0 percent, a cuboidal precipitate; above 1.25 percent, a plate-like precipitate [3]. Size and morphology of the Ni-based γ'-precipitate is also important to understand their properties [40]. In first case, there is an increase in hardening brought about by increased amounts of a precipitates. In addition, it is well known that controlling the precipitation of the γ'-size during the aging time it is possible to increase the hardening until the particle reaches a critical size (0.25 to 0.5 μm) that is a function of time and temperature. Before the age-hardening peak is reached during precipitation, the dislocation movement mode changes from a cutting mode to a bypassing mode, causing loss of hardness and strength [2, 13, 41].

The morphology of the precipitate in Ni-based also can be modified through a coarsening process that can take place at high temperature [42]. The yield strength is also increased with temperature in the range of 196 to 800 °C. This relationship between yield strength and temperature is dependent on the element content in the γ' phase, the alloying elements as titanium or niobium [43]. Volume fraction of the γ' phase is also important for determining strength and creep properties of the alloy and for determining the manufacturing processes of the particular component [7].

2.5. The importance of heat treatments

All superalloys require the application of heat for some period of time to the prepare solid material for a subsequent processing step, chemical processing or microstructural changes.

Heat treatment is the processing step required for the generation of optimal properties in superalloys for many applications. It is possible to improve the mechanical properties and eliminate residual stress, by allowing atom movements to redistribute existing alloy elements [44]; heat treatment is also used to obtain the desired grain boundary distribution with a combination of small and large γ' precipitates for the best strength behavior at high temperatures. Grain boundary carbides can have the control of creep response and fracture behavior by modifying heat treatments [45]. In as-cast superalloys, solution heat treatments can reduce or eliminate the elemental segregation, dissolve phases and/or produce new ones, owing to precipitation from solid solution [13, 46].

It is important to note that some common heat treatments for cast superalloys are solution, full aging for precipitation (age) hardening. In this case, it is important to apply the correct heat treatments in order to obtain the desired γ/γ' dual phase microstructure. The heat treatment has different purposes. The standard heat treatment consists in a solution treatment followed by an aging that can be explained due to the demands of strengthen the desired superalloy by precipitation of one or more phases. The size and distribution of the precipitates can be adjusted by the aging temperature, time and cooling rate. To obtain optimum properties in precipitation-strengthened superalloys, the solution heat treatment should dissolve the γ'-phase into the γ matrix between the γ' solvus and solidus temperatures, called "solutioning window" [46, 47], following by quenching or furnace cooling. A substantial time is required to obtain a uniform distribution of alloying element through diffusion [48].

During the aging, the alloy is heated at γ' sub-solvus temperature to produce the fine and uniform γ' precipitates by diffusion into the γ matrix. After this, the material is rapidly quenched to suppress the formation of the γ'-phase. In this process, the elevated temperature increases the solid-state diffusion and achieve a more uniform distribution of elements by reducing of compositional gradients. The resulted microstructure by heat treatments do not produce a perfect dual phase. It is existing some secondary phases surrounded the cuboidal matrix, that may provide better mechanical response in terms of creep strength. In any case, the aging temperature and times are chosen depending on the expected applications. Desirable creep and stress rupture request demand high aging temperature to produce coarse γ' precipitates. Tang *et al.* [49] reported

that γ' precipitates coarse with the increasing exposure time during heat treatments. Furthermore, for good strength and fatigue resistance it is necessary lower aging temperature to produce homogeneous γ' precipitates [50]. The morphology of the γ' can be modify by changing heat treatments parameters. Xue *et al.* [51] reported the effect of aging temperature on the morphology transition of the γ' phase in a Ni-Co base superalloy. It is shown that the interfacial energy and coherent strain energy determine the morphological evolution in high and low aging temperatures.

2.6. Role of alloying elements in superalloys

One of the most important goal in superalloy development is to achieve an alloy with optimal mechanical properties at high temperature while providing sufficient environmental resistance. The effects of the various alloying elements used in nickel and cobalt superalloys are listed in Table. 2.2.

Table. 2.2 Effect of the major alloying elements in nickel and cobalt-based superalloys [40].

Element	***Nickel-based***	***Cobalt-based***
Cr	• Improves hot corrosion and oxidation resistance • $M_{23}C_6$ and M_7C_3 carbide precipitation • Moderate solid-solution hardening • Moderate increase in γ' volume fraction • Promote tcp phases	• $M_{23}C_6$ and M_7C_3 carbide precipitation • Improves hot corrosion and oxidation resistance • Promote close-packed (tcp) phases
Al	• Moderate solid-solution hardening • γ' precipitation • Improves oxidation resistance	• Improves oxidation resistance • Forms intermetallic β-(CoAl)
Ti	• Moderate solid-solution hardening • γ' precipitation • TiC carbide precipitation	• TiC carbide precipitation • Formation of Co_3Ti intermetallic • Formation of Ni_3Ti with sufficient Ni • Reduces surface stability
Mo	• High solid-solution hardening • Moderate increase in γ' volume fraction • Increase density • Promote tcp phases (σ,μ)	• Solid Solution hardening • Formation of Co3Mo intermetallic • Promote tcp phases
W	• High solid-solution hardening • Moderate increase in γ' volume fraction • M_6C carbide formation • Increases density • Promote tcp phases (σ,μ)	• Solid-solution hardening • Formation of Co_3W intermetallic • Promotes tcp phases

Ta	• High solid-solution hardening • TaC carbide precipitation • Large increase in γ' volume fraction	• MC and M_6C carbide precipitation • Formation of Co_2Ta intermetallic • Reduces surface stability
Nb	• High solid-solution hardening • Large increase in γ' volume fraction • NbC carbide formation • Promote γ' formation • γ'' precipitation • δ-Ni_3Nb precipitation	• MC and M_6C carbide precipitation • Formation of Co_2Nb intermetallic • Reduces surface stability
Re	• Moderate solid-solution hardening • Retards coarsening • Increases γ/γ' lattice mismatch	
Fe	• Decrease oxidation resistance • Promotes tcp phases (σ, laves) • Improves workability	• Improves workability
Co	• Raises γ' solvus temperature • Moderate increase in γ' volume fraction (some alloys)	Not applicable
Ni	Not applicable	• fcc stabilizer • Decreases hot corrosion resistance
C	• Carbides formation • Moderate solid-solution hardening	• Carbide formation • Decreases ductility
B	• Moderate solid-solution hardening • Borides formation • Improves grain-boundary strength	• Improves creep strength and ductility • Borides formation
Zr	• Moderate solid-solution hardening • Inhibits carbide coarsening • Improves grain-boundary strength • Improves creep strength and ductility	• MC carbide formation • Improves creep strength and ductility • Reduces surface stability
Hf	• Improves creep strength and ductility • Improves grain-boundary strength • HfC formation • Promotes eutectic γ/γ' formation	

The microstructure of superalloys is influence on the alloying elements at high temperature application, being necessary to ensure the stability of fcc lattice, controlling the strength of the matrix, precipitation of carbides particles and feature of the precipitate.

Regarding to alloying elements in cobalt-based superalloys, it should be taking in account that Nb, Cr, Mo, Ni, W and Ta are solid solution strengtheners. It is also known that this alloy

is primarily strengthened by carbide precipitation. The addition of Ta, Ti, Zr, Mo and W can form primary carbides of M_7C_3 and MC during solidification. These primary carbides are metastable, and their decomposition induces secondary carbides precipitation, pinning dislocations and harden the alloy matrix, contributing to strength. Al, Mo, Ti, W and Ta are hardening precipitates. Al and Cr improve the corrosion and oxidation resistance, which is much high compared to nickel alloys. B and Zr increase the rupture strength and creep properties.

The increasing thermal stability of γ' precipitate is a key role. It is clear that this temperature is strongly increased by adding Nb, Ta and Ti, slightly by adding Sc, V, Cr, Fe, Ni, Hf, Zr and Mo but Re does not influence it at all. In addition, grain boundaries are important parameters, and specially to resist creep at high temperatures. Small additions of B and Zr, can increase the plasticity of the grain boundary by preventing carbide precipitation on the boundaries and pushes carbon atoms into the grain.

2.7. Processing of γ/γ' Cobalt-based alloys

Processing is crucial whilst alloying metals are useful, others such as oxygen can deteriorate the structure. The cobalt-based alloys have been conventionally processed by ingot metallurgy for the development of this new family of superalloys. Vacuum melting is therefore commonly used to give strict control over the elemental make-up of the superalloy. It is also critical to specify the composition in order to avoid possible undesired secondary phases.

In case of other families of alloys, as nickel-based superalloys or γ-TiAl intermetallics, for high temperature applications, powder metallurgy powder metallurgy route has been widely used to develop new materials as well as better performance in some cases [2].

2.7.1. Arc Melting casting route in Cobalt-based alloys

Casting is the operation of pouring molten metal into a mould and allowing it to solidify. The arc melting casting technique is widely used for the fabrication of ingots by applying a potential different between a tungsten electrode in a water-cooled copper crucible, which forms an electric arc between both. The electric arc can reach temperatures up to 3000 °C, thus allows to melt high-melting materials. The resulting ingot can be produced faster as there is not thermal shock due to high temperature gradient between the crucible. In addition, a magnetic stirrer allows the homogenization of the material.

From the discovery of Sato, recent research works on the development of a new class of Cobalt-based alloys including mechanical testing, structural stability and oxidation resistance. As it was mentioned below, serious doubt about the thermal stability of the ternary $L1_2$ has been studied. Some works indicated that γ'-solvus temperature is quite low (<1000 °C), compared to Ni-Al system [1, 52, 53]. However, significant advances have been reported in two areas. It has been showed that adding -Ta and -Ti to Co-Al-W increases considerably the γ'-solvus temperature about ~100 °C [5]. Pyczak *et al.* [54] also demonstrated that increasing the W-content increases the γ' solvus temperature ~20 °C per 1% increase in W. However, W-addition increase the mass density, which is harmful to the aeronautical applications,

For this case, Makineni *et al.* described a light Co-based alloy by substituting W with Mo and Nb [55], or Mo and Ta [56]. But, the γ' solvus temperature decreases significantly without W. Recently, Lass *et al.* [57] combined the enhanced γ' stability of Ni, Ta and Ti, with the decrease mass density of W-free, creating a new hybrid alloy with benefits of both alternatives. An overview of the main cobalt-based compositions used in different works is shown in Table. 2.3

Table. 2.3. Main cast cobalt-based compositions since ternary system Co-Al-W discovery

Main Composition (at. %)	Reference
Co–9Al–7.5W	[1]
Co–7Al–8W–4Ti–1Ta Co – 7Al–7W–4Ti–2Ta	[5]
Co–8.5Al–xW (x = 8, 9, 11)	[54]
Co–9Al–9W Co–9Al–10W (+2-4Ta + 2-4Ti-2-4Mo-2-4Nb)	[8, 29, 58–60]
Co – (8.8-9.4)Al – (9-10.7)W (+2Ta – 2Re – 4.5Cr)	[9]
Co – 10Al – 13W Co – 10Al – 12W	[52]

Another important point on the development of novel Co-Al-W ternary superalloys is their superior yield strength at room temperature and high service temperatures (up to 900 °C) compared to those of nickel-based alloys, as can be shown in Fig. 2.10 [1, 10]

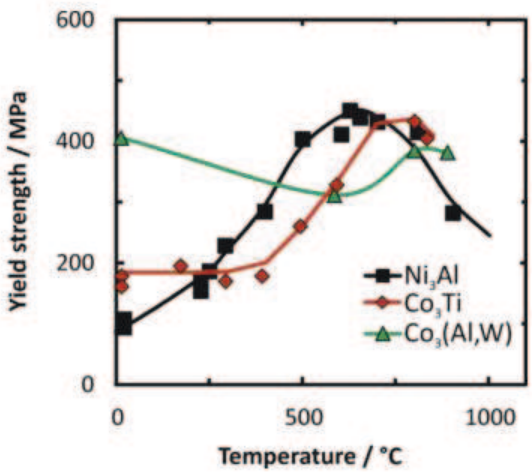

Fig. 2.10 Flow stress of the intermetallic phases Ni_3Al [61], Co_3Ti [62] and $Co_3(Al,W)$ [24] as a function of temperature.

It has to be considered that conventional Ni and Co-based alloys exhibit an anomalous positive temperature dependence above 600 °C. In order to explore this potential mechanical property, Suzuki *et al.* [8] and Suzuki and Pollock [9] reported that Co-Al-W system with Ta-containing exhibit strength comparable to a commercial polycrystalline MAR-M-247 Ni-base alloys at 900 °C. Miura *et al.* [52] also reported that Cobalt-based alloys shows a weak positive temperature dependence of the 0.2 % flow stress at the temperature range around 723 °C. Even at room temperature, the Co-Al-W ternary alloy shows ductile deformation, higher than 10 % plastic strain in compression. Tanaka *et al.* [29] shows stacking faults in the γ'-phase after creep deformation of single crystal of Co-Al-W alloys at 1000 °C and 137 MPa. The same stacking faults has been observed during creep test of nickel-based alloys at 750 °C and 650 MPa in the [0 0 1] orientation [63–65]. Compressive creep tests show how cobalt-based alloys suffer from intergranular fracture at higher temperatures, but it can be improved with addition of boron element, being comparable to polycrystalline nickel-based alloys [7, 66]. Single-crystal tensile creep test at 900 °C has indicated that cobalt-based alloys perform comparably to single-crystal nickel-based alloys with respect to minimum creep rate and creep-rupture lives [29, 67].

2.7.2. Powder Metallurgy route

The MA technique was developed and studied by John Benjamin (INCO, International Ni Co) in an effort to combine the strengthening mechanism by oxide dispersion strengthened with precipitation hardening of γ'-phase [68–70]. Since the mid-70s, the aerospace industry has used superalloy components by using powder metallurgy techniques [71]. Hot Isostatic Pressing (HIP)

has been the most developed technique for this industry. As it is well known, one of the main advantages of HIP process is the ability to manufacture efficient components to the near-net shape reducing machining time and cost [72].

PM can be divided in three major stages [16]: (i) production of powders, (ii) compaction and shaping of the powders (iii) consolidation and fusing under high temperature and pression. The production of powders is usually obtained by mechanical alloying (MA) or gas atomization (GA) techniques, where the quality of the powders is measured by particles size, particles size distribution and shape.

(GA) is a technique that produce powder by pouring molten superalloy through a narrow hole to produce a liquid stream. High-pressure argon gas is blown into the metal and produce fine spherical powder. Mechanical alloying (MA) is a deformation process, defined as a method to merge elemental powders, obtaining the desired chemical composition, as well as, more homogeneous and refined final microstructures [73]. The MA process involves repeated fracturing and rewelding of a mixture of elemental powders in a high energy dry ball mill, as can be seen in a schematic view of the fundament of the milling process in Fig. 2.11.

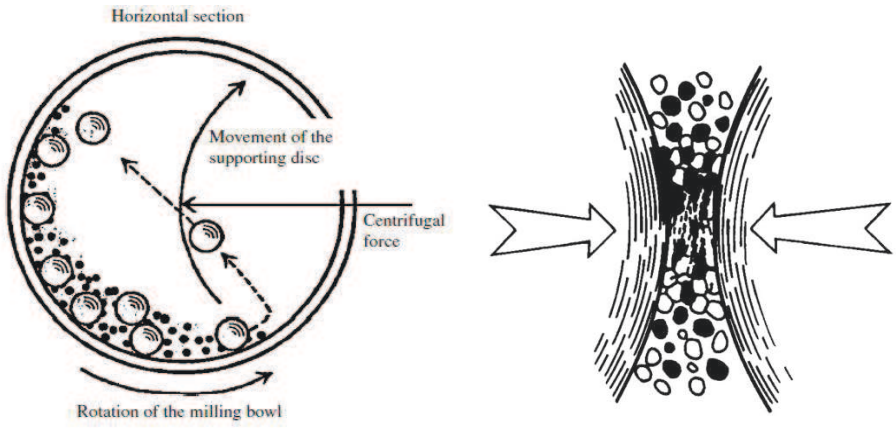

Fig. 2.11 Schematic view of motion of the ball and powder mixture (left) and the sketch showing formation of mechanically alloy superalloy powder particles in a ball mill (right) [13].

Microstructurally, the mechanical alloying process can be divided into four stages: a) initial b) intermediate c) final d) competition stage [74].

a) At the early stage, the powders particle is flattened by the compressive forces due to the collision of the balls. Micro-forging leads to changes in the shapes of the particles, being impacted repeatedly by the milling balls with high kinetic energy.

b) At the Intermediate stage exists significant changes in comparison with initial stage. Cold welding and fracturing are now significant with some dissolution, but the chemical composition of the alloyed powder is still not homogeneous.

c) At the Final stage, it can be seen that the refinement and reduction of the particle size is evident, showing a homogeneous microstructure.

d) At the Completion stage of the mechanical alloying process, the powder particles possess an extremely deformed metastable structure.

Powders are mixed and then placed in a high-energy ball mill. The intensive milling process repeatedly fractures and then rewelds the powder particles. During each collision with the grinding balls, the particles are plastically deformed to the extent that the surface oxides are broken, exposing clean metal surfaces [50,75]. On subsequent impacts, the clean surfaces are welded together. This cold-welding process increases the size of the particles, while at the same time additional impacts are fracturing particles and reducing their size [50,76] .

Oxide Dispersion Strengthened (ODS) can be also used to obtain powder metallurgy superalloys starting from elemental alloy powders and yttrium oxide by using the mechanical alloying (MA) process [77]. The ternary Co-Al-W ODS alloys exhibit a complex microstructural evolution during heat treatment L. Zhang *et al.* [78] explain the microstructural formation mechanism of cobalt-based ODS alloys as follow:

- Mechanical Alloying (MA) induce the formation of the solid solution supersaturated with Al and W due to the solubility of Al and W elements in cobalt matrix is too low at room temperature [79, 80].
- Liquid phase is formed during the sintering that migrates along the prior powder metallurgy under pressure. The W-rich precipitates do not contribute to the formation of liquid phase and their distribution confines to the interior of MA powder particles and constitutes the precipitation free area. This supersaturated solid solution is a non-equilibrium state, which during aging heat treatments promotes the formation of the γ' phase through the following reaction: $\gamma + CoAl + Co_3Al \rightarrow \gamma'$ [81].

After (MA) mechanical alloying or Oxide Dispersion Strengthened (ODS), the resulted powders must be consolidated under specific conditions that develop coarse grains during a secondary recrystallization heat treatment. For this purpose, MA powders are consolidated by field assisted sintering techniques (FAST) at high temperature, applying simultaneously pressure

and temperature, a continuous alternative current of low frequency heats the materials by Joule effect [82–84].

FAST samples are then heat treated to optimize grain structure and promote the desired γ/γ' dual phase microstructure. Heat treatments include solution/aging and precipitation hardening. The precipitation hardening treatments are varied and often have multiple aging cycles to optimize properties depending of their applications, as shown in the previous paragraph 2.5.

Focusing on recent Cobalt ODS works produced by Mechanical Alloying (MA) and Spark Plasma Sintering (SPS), Takezawa *et al.* [85] produced a Co-3Al-1.5Y_2O_3-1.2Hf (wt.%) with a significant improvement of tensile strength of 125 MPa at 1000 °C which is 60 MPa higher than that of the oxide particle free Co-3Al alloy. Cui [86] reported an Co-20Cr-20Ni-10W-2Y_2O_3 Cobalt-based alloy, with a density over 99% and compression strength and elongation of 1982 MPa and 23%, respectively. Yu *et al.* [87] studied the tensile properties of Co-20Cr-20Ni-5Al-2.4Hf-1.5Y_2O_3 ODS alloy, that exhibits a tensile strength of 2.85 GPa at room temperature but a reduction of 100 MPa at 1000 °C. Sasaki *et al.* [88] also described that Co-3Al-1.5Y_2O_3-1.2Hf (wt.%) were able to provide high hardness with outstanding microstructure stability after aging at 1000 °C for 240h, owing the pinning of grain boundaries by the dispersed oxide particles. Yu *et al.* [89] also investigated the beneficial effect of Cr and Y_2O_3 on the oxidation behavior at 900 °C of Co-20Cr-10Al ODS superalloy. Zhang *et al.* investigated the evolution of Y_2O_3 during mechanical alloying and subsequent annealing and the influence of alloying element on particle size of Co-1.5Y_2O_3 [90]. Sasaki *et al.* [88] studied the detailed microstructure and thermal stability of the microstructure and hardness of the Co-3Al-1.5Y_2O_3-1.2Hf (wt. %) ODS alloy.

Considerable research work has been undertaken to develop the ternary Co-Al-W ODS base alloy. In 2011, a family of novel Co-Al-W base ODS alloy exhibiting the dispersion of γ' precipitates and extremely fine oxides was synthesized [91]. In 2012, the influence of microstructural characteristic and compression parameters on high-temperature hot deformation behavior of the Co-Al-W ODS alloy was examined [78]. Another study was performed to investigate the effect of Ni on the microstructure and mechanical properties of the Co-Ni-Al-W base ODS [92].

2.8. Dynamic behavior of materials: High Strain Rate

In the aerospace industry, there are a wide range of conditions where materials are exposed and tested. The response of materials under type of loading boundary conditions differs from the quasi-static loading being necessary to test this kind of materials at high strain rates. Ice or bird impact are example of high strain rate at 10^2 - 10^4 s^{-1}, being necessary to apply other techniques than conventional servo hydraulic machines.

Strain rate can be defined as the rate of change in strain over time, in s^{-1}, as can be shown in the following term (equation 2.2):

$$\dot{\varepsilon} = \frac{d\epsilon}{dt} \approx \frac{\Delta\varepsilon}{\Delta t} \quad (2.2)$$

Where Δε is the variation in strain during the time Δt. In this case, high strain rate tests are usually performed to study the strain rate sensibility of materials. The most common device is the compression Split Hopkinson Pressure Bar (SHPB).

The effect of high strain rates on superalloys was studied by D.P. Moon and J. E. Campbell [93]. It is evident that the structure of the alloy can affect the properties, such as, precipitation hardening, aging, recrystallization, grain growth of other combination of them. Fig. 2.12 show the effect of the strain rate in an Inconel X. At room temperature (RT), the yield and ultimate strength are not affected or are increased slightly as the strain rate is increased. At high temperature, increasing the strain rate causes substantial increases in the yield and ultimate strength, as can be seen at 871 °C. The elastic modulus is constant regardless of strain rate.

Moreover, the high-strain deformation of fcc metal, has been studied by Follansbee [94] in compression using the SHPB. It has been showed that the inherent rate sensibility of the fcc materials between 10^{-3} and 10^4 s^{-1}, where the flow stress at constant strain varies linearly with strain rate, is controlled by the thermal activated interactions of dislocations with obstacles, indicating that the strain-rate sensitivity of these metals must be due to the strain-strain rate sensibility of substructure evolution. Many impact phenomena lead to deformation at strain rates exceeding 10^3 s^{-1}. It should be taken into account that test results are only valid at strain rates approaching or exceeding 10^4 s^{-1} if certain precaution is taken.

Gray *et al.* [95] compared the high strain rate mechanical behavior and the deformation substructure evolution in a range of materials. In the case of fcc metals, a schematic representation of the characteristic strain-hardening is shown in Fig. 2.13. It is clear that the strong dependency

of strain hardening with decreasing temperature and/or increasing strain rate is due to the suppression of dynamic recovery processes.

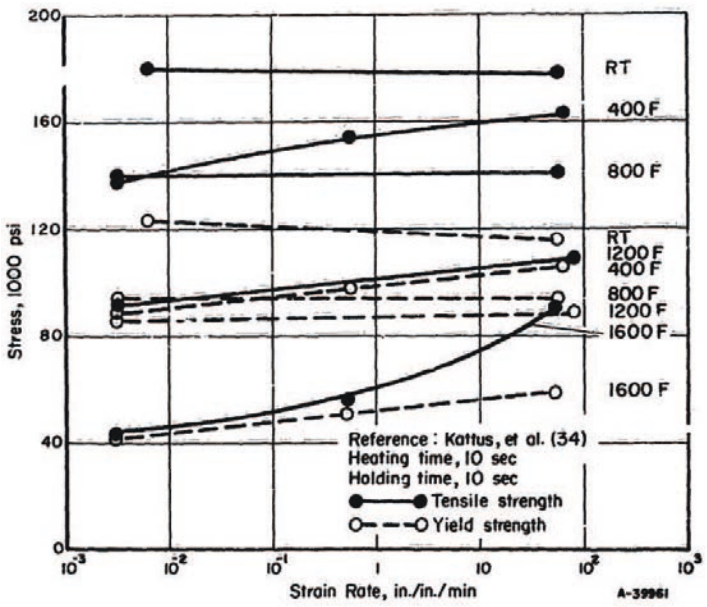

Fig. 2.12 Effect of the strain rate and the temperature vs Stress in an Inconel X [93].

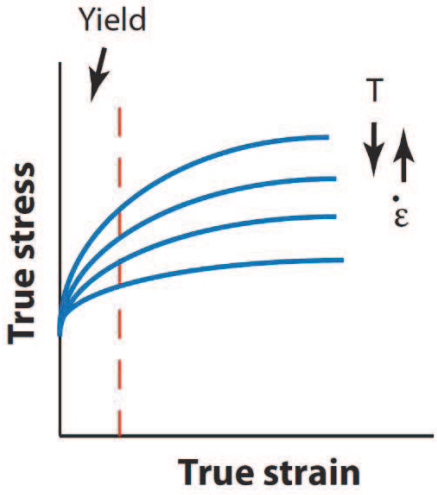

Fig. 2.13 Schematic of the influence of temperature and strain rate on the yield and strain-hardening response [95].

2.8.1. Split Hopkinson Pressure Bar

The Split Hopkinson Pressure Bar system is one of the most important experimental techniques to investigate the mechanical properties of materials at high strain rates, from 10^2 s^{-1} to 10^4 s^{-1}. It was developed by Bertram Hopkinson [96] to measure the pressure-time relation produced by the impact of a bullet or an explosion at the end of a cylindrical rod. Previously, his father, John Hopkinson, studied in 1872 the rupture of iron wires by a blow [97, 98]. In November 1913, Bertram Hopkinson, developed an experimental set up to determine the pressure-time relation on a rod due to an impact [99]. In this method, the pressure to be measured is applied normally to one end (the "pressure" end) of a cylindrical steel bar; the magnitude of the pressure is deduced from measurement of the momentum trapped in detachable end-pieces wrung to the other end (the "measuring" end) of the bar.

In 1949, Kolsky developed a procedure, called "Kolsky or Split Hopkinson pressure bar", to determine the stress-strain relation of materials when stress is applied for times of the order of 20 microseconds. The device was a variation of the Hopkinson pressure bar, and detonators were used to generate large transient stresses [100]. The actual set-up is based on determining the forces that act on a specimen situated between two bars by measuring the stress or strain waves of the bars, as shown in Fig. 2.14.

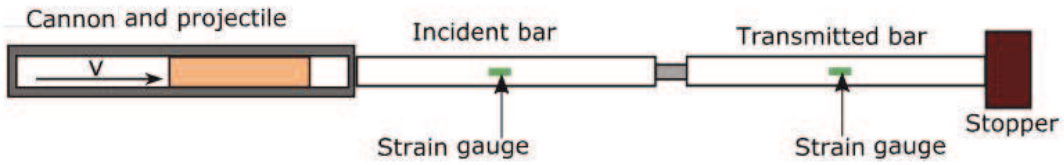

Fig. 2.14 Schematic representation of the Kolsky or Split Hopkinson Pressure Bar device [101].

3. Experimental procedure

The main objetive of this work is to obtain a novel cobalt-based superalloy by Powder Metallurgy (PM) technology. With this aim, thermodynamic design and powder route manufacturing were carried out to obtain the cobalt-based specimens, that were subsequently characterized and tested by different mechanical systems. Given the complexity of the entire work, starting from the simulation and fabrication of the cobalt-based superalloy, the effect of the heat treatments and mechanical response are reviewed in each chapter with a description of the process. It should be taken in account that casting route has been also developed to provide like-for-like comparisons of both routes. Thus, this chapter introduces the materials and processing that has been used and provides a theoretical overview of the instrument utilized and the corresponding characterization used in this thesis. A schematic of PM processing sequence is shown in Fig. 3.1.

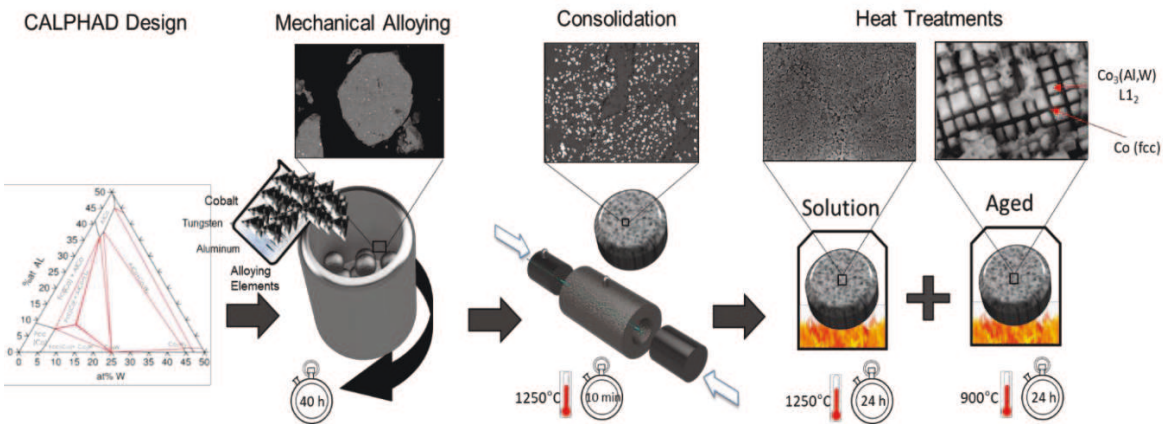

Fig. 3.1 Schematic of powder metallurgy processing sequence in the production of cobalt-based superalloys designed for this research.

3.1. Experimental outline

For the development of this research thesis, it has been necessary several experimental techniques that are summarize in Fig. 3.2.

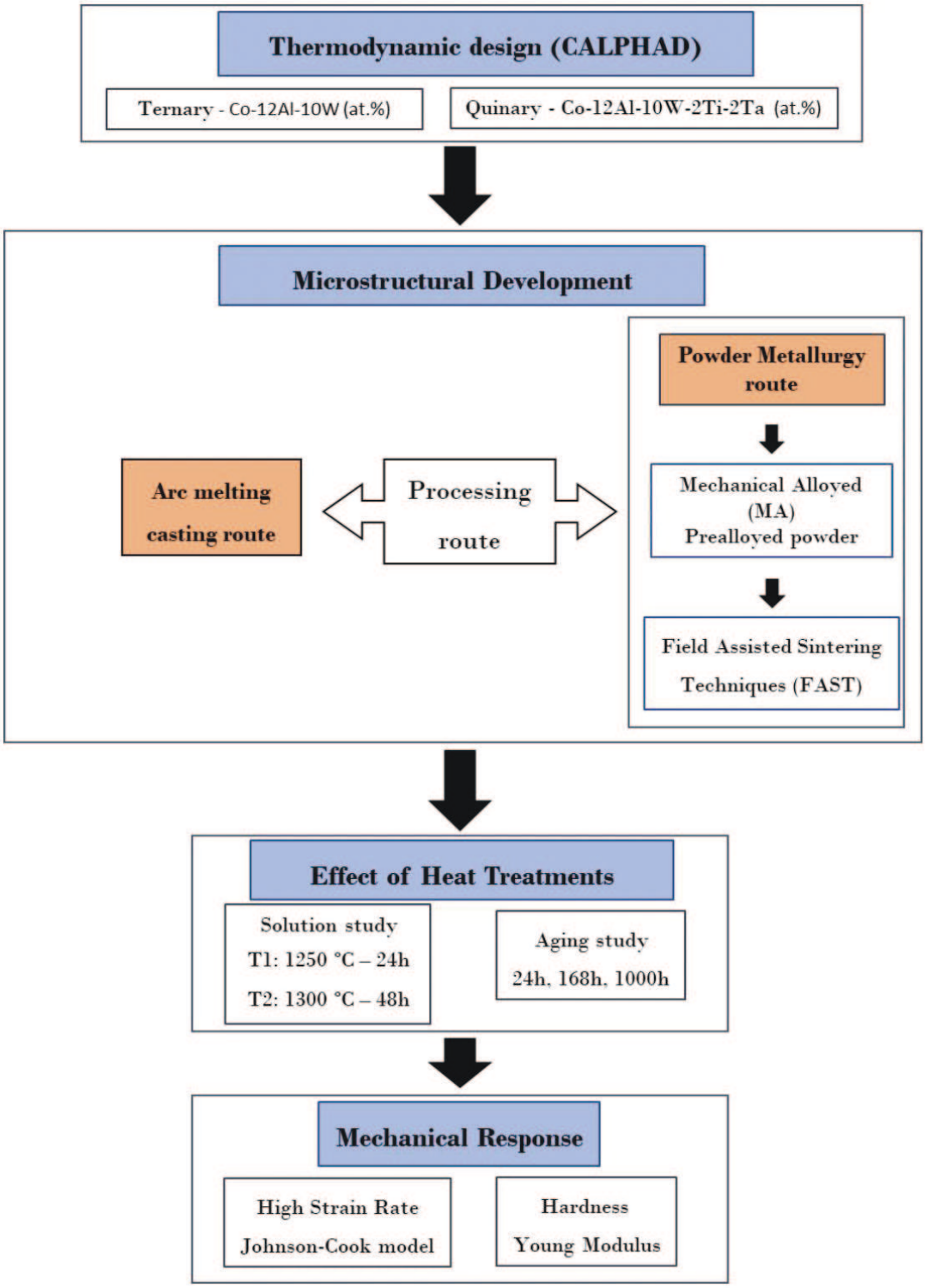

Fig. 3.2 Materials and experimental methods utilized during this research work

3.2. Materials

The composition of the Cobalt-based superalloys of this research have been designed after thermodynamic calculation as Co-12Al-10W and Co-12Al-10W-2Ti-2Ta (at. %), also known as ternary (T) and quinary (Q) alloys, respectively. The design of the Cobalt-based alloys will be discussed in Chapter 4. The MA process was carried out under static Ar atmosphere (refilled during the milling). The elemental powders used in this work are shown in Table. 3.1.

Table. 3.1. Reference of the elemental powders used in this work

Element	Reference	Supplier
Cobalt	Co6160	Eurotungstene (France)
Tungsten	W4105	Eurotungstene (France)
Aluminum	Al54Ns	SultzerMetco (Switzerland)
Titanium	-Ta (99,98%)	Aesar Karlsruhe (Germany)
Tantalum	CPTi grade 4	(GfE Metalle und Materialien GmbH, Germany).

3.3. Thermodynamic design

Thermodynamic modeling (ThermoCalc 5®) was used to design the desired cobalt-based superalloy by using the data base offered by *Cui et al.* [1]. This method, called CALculation PHAse Diagram (CALPHAD), helps to obtain a more precise point of view of the ternary phase diagram by using thermodynamic properties of each phase described through the Gibbs free energy, applying a mathematical model containing adjustable parameters. This is accomplished by considering multiple physical and chemical properties of the system in the thermodynamic model, i.e. crystallography, type of bonding, order-disorder transitions and magnetic properties [102].

Once the prediction of the cobalt-based thermodynamic model had been obtained, it was possible to verify the feasibility of the different phases contained in the Co-Al-W ternary system at different temperatures (see: Fig. 3.3).

After designing the optimal composition (see Chapter 4), two different routes were followed to compare the advantages and inconvenient of both possibilities.

- Route 1 - Powder metallurgy route: Mechanical milling + consolidation by field assisted sintering techniques (FAST) + heat treatments
- Route 2 - Arc casting melting route*:* Arc casting melting + heat treatments.

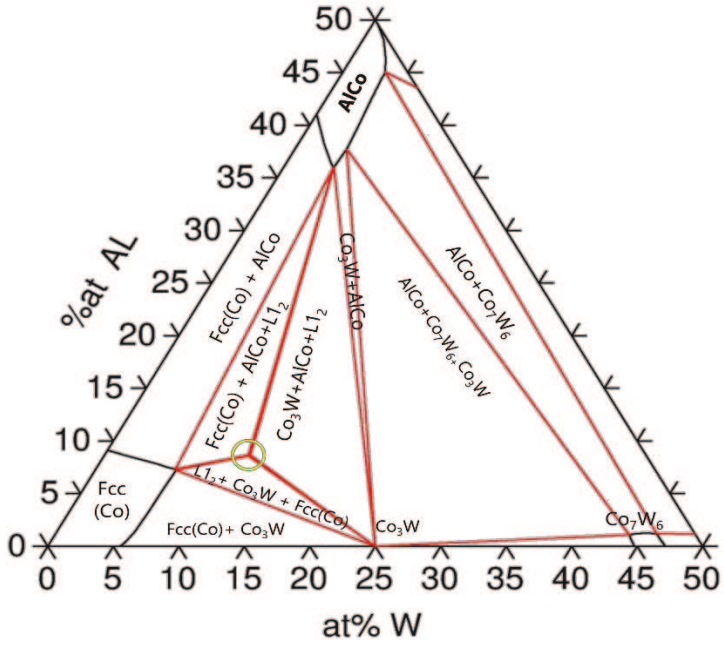

Fig. 3.3 Isothermal section of Co-Al-W ternary system at 900 °C. Selected Co-Al-W composition is marked as a yellow circle.

3.4. Arc-melting casting processing route

The ternary and quinary cobalt-based superalloys were processed by arc-melting casting technology using the selected elemental powders described in Table. 3.1. These superalloys were cast in an Arc 200 furnace, (Arcast Inc.) at the Institute of Materials of Madrid (IMDEA, Madrid, Spain). This equipment offers the ability to melt, cast and rapidly solidify metal alloys at over 3000 °C. The melting furnace is placed in a stainless-steel vacuum (~10^5 Pa) chamber with a crucible of copper water cooled. The as-cast specimens were identified as T-AC and Q-AC, for ternary and quinary composition, respectively.

3.5. Powder metallurgy processing route

The alloys were processed by alloying using the elemental powders described in Table. 3.1. MA was carried out in a planetary ball mill (Planetary Pulverisette 6, FRITSCH), using hard metal Co-WC vessel and balls at a speed of 300 rpm with a ball to powder weight ratio of 10:1 following the finding of Carton *et al.* [103]. The MA process was carried out under static Ar

atmosphere refilled during each technical stop to maintain an inert atmosphere during the milling step. Previously, the powders were mechanically blended for 30 min in a turbula mixer. Once the desired composition of Co-Al-W (Ternary) and Co-Al-W-Ti-Ta (Quinary) were achieved by MA, the milled powders were consolidated by FAST in a Gleeble 3800 equipment (Dynamic System Inc. USA), applying simultaneously pressure and temperature. For doing that, a DC voltage of low frequency heats the material by Joule effect.

Prior to consolidation, the equipment allows a dilatometry mode to optimize the final thermal cycle. This process involves the identification of the major dimensional changes of the material with the temperature.

The milled powder was set into a cylindrical graphite die of 10 mm diameter for the consolidation. Following previous work of Junceda *et al.* [104], the cylindrical space was film-coated with tungsten to avoid carbide contamination during the sintering. The graphite die was gripped at a load of 5 MPa inside the vacuum chamber. When the temperature achieved 800 °C, the pressure was increased up to 80 MPa (the heating and cooling rates were, respectively, 100 °C min^{-1} and approximately 3 °C min^{-1}). The temperatures were recorded with a thermocouple placed, respectively, in a punch and the center of the graphite die. The optimal conditions are illustrated in Fig. 3.4, with a temperature of 1250 °C during 10 min with a heating rate of 100 °C min^{-1}, and cooling rate was 3 °C min^{-1}.

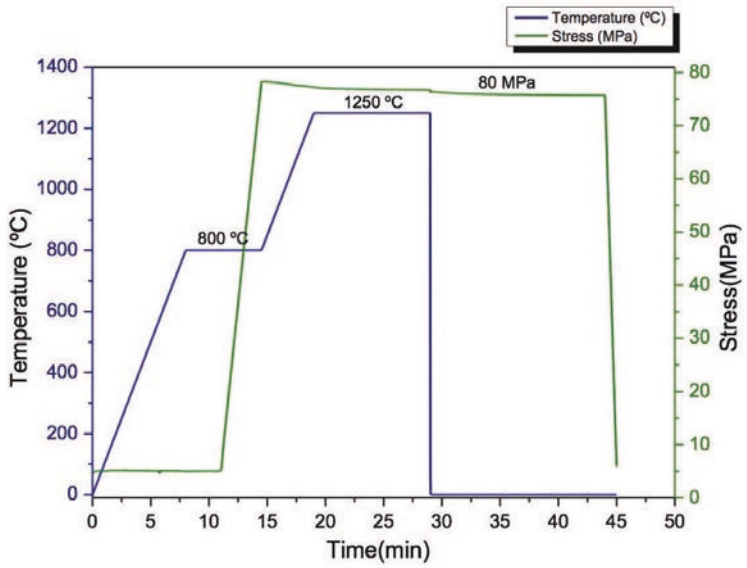

Fig. 3.4 Schematic of the optimal consolidate cycle for cobalt-based PM alloys

The consolidated samples were cylinders of 10 mm diameter and 4 mm height. The density of the as consolidated specimens was measured with an AccuPyc II 1340 Pycnometer, using helium inert gas. This technique is non-destructive as it uses the gas displacement method to measure volume. The powder metallurgy specimens are identified as: T-PM and Q-PM, for ternary and quinary composition, respectively. A summary of the powder metallurgy route it is shown in Fig. 3.5.

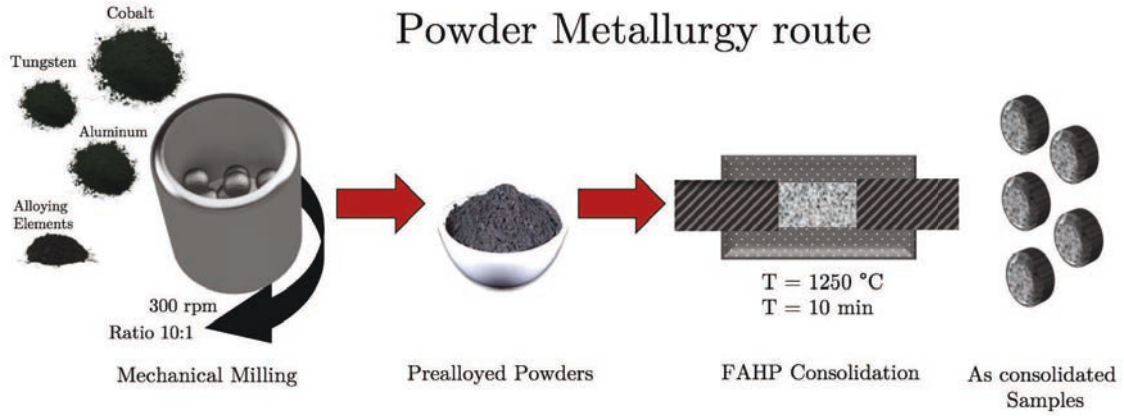

Fig. 3.5 Schematic of the powder metallurgy route designed in the production of cobalt-based samples

3.6. Heat treatments design

As it is well known from literature review in Chapter 2, it is essential to design an appropriate heat treatment in order to precipitate the γ'-phase into the γ-fcc matrix. For this purpose, Differential Thermal Analysis (DTA) was performed in a Setsys Evolution thermogravimetric analyzer TGA & DTA/DSC (Setaram), to determine the phase transformation temperatures, such as, solvus temperature, melting point temperature and Curie temperature of the cobalt-based alloy from room temperature up to 1550 °C with a step rate of 5 °C min^{-1}.

With the aim of obtaining the dual phase γ/γ' microstructure, two different routes were proposed according to previous works and the revealed phase transformation temperatures. Several studies on ternary Co-Al-W system have used a solution heat treatment at 1250 °C for 24 h followed by an aging treatment range of 900 - 1000 °C for many different times [10, 29, 47, 105, 106]. In many of the studies, authors concluded the need of homogenizing at 1300 °C and aging at 900 °C when alloying elements are included of the ternary cobalt system, [7, 8, 59, 107–110]. There is not a general agreement between the authors according to the time. For this case, a long-term aging treatment study has been performed in chapter 5.

To optimize the design of the precipitation of the γ'-phase; T1 correspond to a 1250 °C for 24 h and T2 to 1300 °C for 48h. Both heat treatments were performed in a vacuum furnace (~10^4-10^5 Pa), where the heating and the cooling rate was always programmed to be 5 °C min^{-1}. Afterwards the samples were wrapped in molybdenum foil and encapsulated in purged quartz tubes filled with argon atmosphere to avoid possible oxidation. The specimens were annealed at 900 °C for 24, 168 and 1000 h in a muffle furnace, and subsequently quenched in water to room temperature, to analyze the effect of the aging time on the microstructure. A summary of the required heat treatments is shown in Table. 3.2.

Table. 3.2. Summary of heat treatments parameters performed for cobalt-based alloys

Alloy		Solution heat treatment	Aging heat treatment
Ternary	T1	1250 °C – 24 h	900 °C – 24, 168, 1000 h
		furnace cooled	Water quenched
	T2	1300 °C – 48 h	900 °C – 24, 168, 1000 h
		furnace cooled	Water quenched
Quinary	T1	1250 °C – 24 h	900 °C – 24, 168, 1000 h
		furnace cooled	Water quenched
	T2	1300 °C – 48 h	900 °C – 24, 168, 1000 h
		furnace cooled	Water quenched

3.7. Materials characterization

The microstructural characterization of the cobalt-based samples was carried out by using several techniques described below.

3.7.1. Measurement of particle size distribution

Powder size distribution was characterized by using a Mastersizer 2000 (Malvern, United Kingdom), to discriminate the particle size, considering the d_{50} parameter. PM powders usually are produced in a range of specified particle size, which ensure uniform heating and melting during the consolidation process. To measure the particle size distribution, it is important to prepare and disperse the sample in correct concentration to avoid possible incorrect analysis. The data can be displayed in various ways once the information has been analyzed. Usually the display shows a histogram of the result, with band percentages. Each bar in the graph represents a size band of particles and the height of the bar represents the percentage of the sample that is within that band.

The statistic of the distribution are computed from the result using de derived diameters D(m,n). The common value used to discriminate the particle size is described below:

- **D(v,0.5)** is the size in microns at which 50% of the sample is smaller and 50% is larger. The value is also known as the Mass Median Diameter (MMD) or the median of the volume fraction
- **D(v,0.1)** is the size of particle below which 10% of the sample lies
- **D(v,0.9)** is the size of particle below which 90% of the sample lies

3.7.2. X-ray diffraction (XRD)

X-ray diffraction (XRD) was performed to identify the phases present in the cobalt-based microstructure. X-ray patterns were collected on a X'Pert Philips using Cu Kα excitation line (λ =1,542 Å) obtained by an X-ray tube consisting on a Cu anode and a W filament excited with a 40-mA current and 40 kV of voltage. The angular range spread over the region between 30° and 100° in 2Theta (2θ) with a step size of 0,02° and step time of 2,4 seconds per step.

The resulted data were compared with the X'Pert HighScore software and the standards patterns of the PCPDFWIN database. In addition, this software has been also required to calculate by Scherrer Method, the crystallite size and the microstrain from the most intensity peaks of the indexed patterns.

The misfit parameter (δ) of the cobalt-based alloy after heat treatments was calculated using X-ray diffraction patterns and the equation 3.1. The (111)-reflection peak recorded at room temperature, allows to calculate the a_γ and $a_{\gamma'}$ parameters. This peak has an asymmetric reflection due to the existing sub-peaks coming from the γ-phase, with it is lower than another sub peak of γ'-phase (see: Fig. 3.6).

$$\delta = \frac{2\left(a_{\gamma'} - a_\gamma\right)}{\left(a_{\gamma'} + a_\gamma\right)} \text{ [39] } (3.1)$$

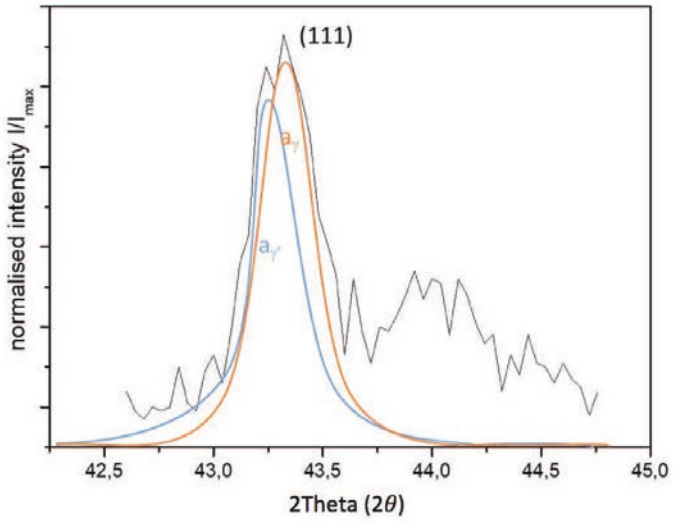

Fig. 3.6 XRD (111)-reflections showing the existing sub-peaks of the γ/γ'dual phase microstructure

For cobalt-based alloys, the lattice parameters of the γ-phase are larger than γ'-phase. The magnitude and sign of the misfit also influences the development of microstructure under the influence of a stress at elevated temperatures as it was discussed in Chapter 2.

For the qualitative analysis of the diffractograms and to obtain the values crystalline size (*L)* and micro deformation (με), the Scherrer method was chosen by means of a specific calculator software. This method uses the Scherrer equation 3.2.

$$\beta = \frac{\kappa \cdot \lambda_{\alpha}}{L \cdot \cos\theta} \ (3.2) \ [111]$$

Where κ is the Scherrer constant = 0.9 and λ=0.154 nm. β is the peak width. L is the crystallite size (volume-weighed domain size in the direction parallel to the diffraction vector).

The full width at half maximum (FWHM) is the width of the diffraction peak, in radians, at a height half-way between background and the peak maximum (β_{sample}). It can be calculated by subtracting the experimental value obtained by X'Pert Data Viewer for the width peak instrument aberrations ($\beta_{instrumental}$), as shown in equation 3.3.

$$\beta_{sample} = \beta_{experimental} - \beta_{instrumental} \ (3.3)$$

3.7.3. Metallurgical sample preparation

A good specimen preparation is essential if the true microstructure is to be observed, identified and measured. Microstructural characterization requires a good surface finishing of the specimens to avoid possible errors and to carry out all the experimentations. For this reason, all samples obtained from both routes (powder metallurgy and cast), have been grinded with sandpaper up to 1200 grade, followed by polishing with diamond abrasive suspension of 3 and 1 µm, respectively. For cobalt-based superalloys, polishing down to 1 µm may yield a surface suitable for routine examination. All samples were previously mounted in resin with the main purpose of good handling due to their small size.

To reveal the γ' structure after the heat treatments, all the cobalt-based specimens were chemically etched via immersion in Carapella's solution (2 ml hydrochloric acid; 5 g ferric chloride; 99 ml ethanol). This etchant dissolves the cobalt γ matrix leaving the γ' structure intact. The samples were immersed in a glass beaker containing etchant during at least 5 seconds, then rinsed with ethanol and dried.

3.7.4. Scanning electron microscopy (SEM)

Microstructure analysis was also performed using scanning electron microscopy (SEM). This microscope allows the analysis and the examination of the microstructure morphology and chemical composition characterization. Accelerated electron in a SEM carry significant quantities of kinetic energy, and this energy is dissipated as variety of signals produced by electron-sample interactions when the incident electrons are decelerated in the solid sample. The signals generated by a SEM can include, secondary electrons (SE) to analyze surface topography and backscattered electrons (BSE) to examine composition; diffracted backscattered electrons (EBSD) used to determine crystal structures and orientations of mineral; characteristic X-Rays for elemental analysis, visible light (cathodoluminescence), and heat [112].

In this case, SEM analysis was carried out in a FE-SEM (FEI TENEO) scanning electron microscope and a HITACHI SU8083. The chemical composition of the surfaces was analyzed with semi-quantitative elements analysis by EDAX, energy disperse spectroscopy (EDS) detector.

3.7.5. Image Analysis

Image analysis was carried out to calculate various properties during SEM microscopy, (i.e. volume fraction, porosity, cuboidal size). Image analysis was characterized on the sets of micrographs collected by SEM and analyzed using ImageJ® software.

The volume fraction of the γ/γ' dual phase was studied using SEM micrographs. By using histogram measurements, it is possible to recognize perfectly what fraction the area of the micrographs is black and white (see: Fig. 3.7). At least 2 μm^2 were studied in different random micrographs regions to calculate the average volume fraction of both cobalt-based compositions.

It is possible to determine the average size of the γ' cuboidal matrix by using at least 5 micrograph zones. The distance between the flat sides of the cuboidal particles was measured in both directions. The total porosity was also measured by SEM micrographs, with respect to micrograph area giving a total area porosity (%).

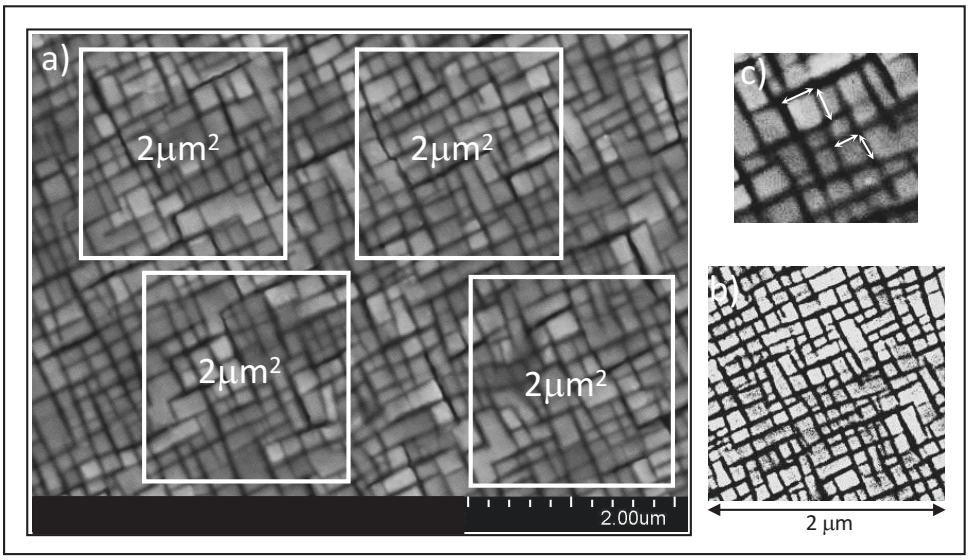

Fig. 3.7 a) Cobalt-based micrograph with measure random regions b) Volume fraction measurement c) Cuboidal size measurement

3.7.6. Transmission electron microscopy (TEM)

By means of transmission electron microscopy (TEM) it is possible to visualize very fine γ' precipitates within a sample of the ternary and quinary cobalt-alloys.

TEM analysis was performed at IMDEA Materials Institute using a Talos™ F200X, FEI) at 200 kV. TEM foils were first thinned mechanically by grinding down the material to a thickness of ~100 μm, then punching 3 mm diameter disks, and finally thinning then electrolytically in an

electropolisher Tenupol-5 (Struers) with an electrolyte A3 (Struers) of 60 pct perchloric acid in methanol and 2-butoxyethanol electrolyte with a voltage of 19 V at – 30 °C.

3.8. Mechanical behavior

3.8.1. Microhardness testing

The microhardness test is referred to the hardness testing of materials where low load from 0.1 to 1 kg is applied. In this test, a diamond pyramid indenter with specific geometry is impressed into the surface of the test specimen using a known applied force chosen with respect to the material. The hardness number is calculated measuring the surface area made by indenter divided by the applied force. A Vickers method can be applied for microindentation hardness testing.

In this study, the Vickers hardness test (HV) was measured using Zwick Roell microhardness tested equipped with Vickers diamond indenter. The load of 200 g was applied for 15 seconds at room temperature. The average microhardness value has been determined for averaging over at least five indentations over the γ/γ' dual phase microstructure.

3.8.2. Nanoindentation testing

Nanoindentation technique was carried out to determine the hardness (H) and the elastic modulus (E) of the cobalt-based superalloy. This testing is popular static method to measure the elastic modulus when the volume of material is limited. Both mechanical properties have been measured by using load and depth sensing indentation, used to obtain a cycle of loading and unloading, (see: Fig. 3.8). In typical test, force and depth are recorded as load is applied from zero to some maximum and then from maximum fore back to zero. The surface roughness of the sample should not be more that 10 % of the indentation depth [113]. For this purpose, the cobalt-based alloys were metallography polished as shown in paragraph 3.7.3, to produce the smooth surface needed for nanoindentation testing.

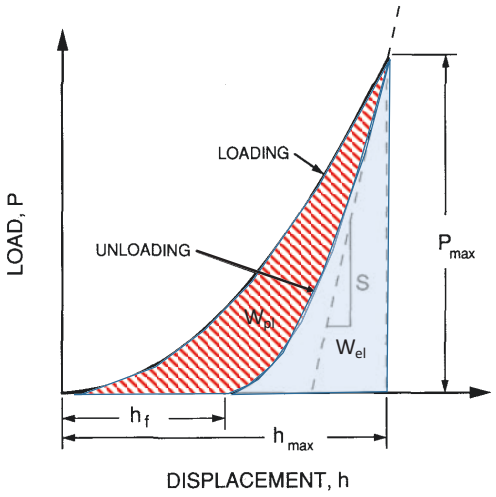

Fig. 3.8 A schematic illustration of load vs indenter displacement data for an indentation experiment [114].

In this case, the experiment was carried out by using an MTS Nano-indenter XP with a maximum load of 360 nm and strain rate of 0.05 s^{-1}. Hardness and elastic moduli were obtained by using an indentation depth between 500 nm and 1250 nm. Both values were determined from the unloading part of the force-depth curves with a minimum of 30 repetitions on each sample, according to the Oliver-Pharr method [115]. Yan *et al.* [116] reported that Oliver-Pharr method can be applied to measure the elastic modulus of the particle with sufficient accuracy if the indentation depth is smaller than the particle-dominated depth. If deformation phenomenon of "pile-up" occurs, the elastic modulus and hardness can be overestimated if Oliver-Pharr method is applied.

3.9. High strain rate testing

The high strain rate testing was carried out by using a Split Hopkinson Pressure Bar (SHPB) designed by F. Gálvez *et al.* [117] to include a furnace and to perform high temperature tests. The SHPB consists of a projectile which is placed inside a cannon, two elastic bars, called incident and transmitter bars, with strain gauges and a stopper (see: Fig. 3.9). This equipment is equipped on two Rene41 nickel superalloy bars of 19 mm diameter and 1-m long which allow to remain elastic even at high temperature with a yield strength greater than 800 MPa at 800 °C and over 450 MPa at 900 °C. This system is equipped with a high temperature furnace controlled by using three thermocouples. The bars are refrigerated to maintain the strain gages of the bars at room temperature by means of a water-cooling system. The strain rate was kept constant at 10^3 s^{-1} during the tests. The powder metallurgy specimens used in these experiments were cut by using a wire cutting machine with a geometry of 2x2x4 mm.

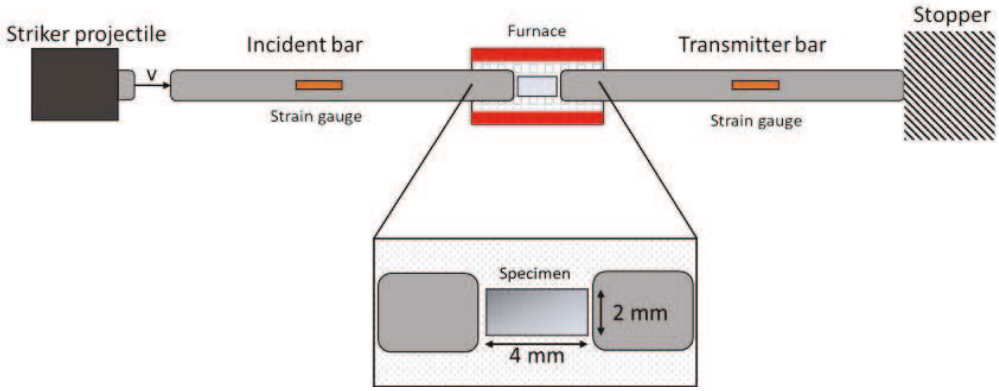

Fig. 3.9 Schematic of the Split Hopkinson Pressure bar (SHPB) device equipped with high temperature furnace.

It is well known that a stress wave is a wave that creates a disturbance in a material and travels along it. To obtain a correct analysis and to fit a stress-strain curve from the resulting waves of the incident and transmitted bars, different tests were carried out from room temperature up to 850 °C. The results of the materials test have been used to fit a Johnson-Cook material strength model due to it faithfully reproduces well the behavior of the cobalt-based superalloys at high temperatures, high strain rates and large deformations simultaneously.

3.9.1. Theory of the Split Hopkinson Pressure Bar

The SHPB is based on the wave propagation in the bars.

$$\frac{\partial^2 u}{\partial x^2} = \frac{1}{c_b^2}\frac{\partial^2 u}{\partial t^2} \quad (3.4)$$

The displacements of the bar ends are given as:

$$u_1 = f(x - c_b t) + g(x + c_b t) = u_i + u_r \quad (3.5)$$

$$u_2 = h\,(x - c_t t) = u_t \quad (3.6)$$

Parameters f, g and h are functions calling the incident, reflected and transmitted waves. C_b is the longitudinal wave speed in the bar and u_1 and u_2 are displacements in the incident and transmitter bars; u_i, u_r and u_t are the incident, reflected and transmitted displacement and the corresponding strains are: ε_i, ε_r and ε_t.

$\varepsilon_1 = \varepsilon_i + \varepsilon_r$ (3.7)

$\varepsilon_2 = \varepsilon_t$ (3.8)

Differentiating Equation 3.5 and 3.6 with respect to time results in:

$\dot{u}_1 = c_b(-f' + g') = c_b(-\varepsilon_i + \varepsilon_r)$ (3.9)

$\dot{u}_2 = -c_b\varepsilon_t$ (3.10)

The force F_1 and F_2 can be written as:

$F_1 = AE(\varepsilon_i + \varepsilon_r)$ (3.11)

$F_2 = AE(\varepsilon_t)$ (3.12)

A is the cross section of the bars and E is the elastic modulus of the bar material. The equilibrium of both forces should be equal:

$\varepsilon_t = \varepsilon_i + \varepsilon_r$ (3.13)

The strain rate can be written as:

$\dot{\varepsilon} = \frac{\dot{u}_1 - \dot{u}_2}{l_s}$ (3.14)

Using equations 3.9, 3.10, 3.13 and 3.14, the strain rate can be written as:

$\dot{\varepsilon} = \frac{2C_b\varepsilon_r}{l_s}$ (3.15)

Using equation 3.10 and knowing that force is the product of stress and area:

$\sigma = \frac{EA\,\varepsilon_t}{A_S}$ (3.16)

A_s is the initial area of the specimen. Finally, the true stress and true strain is:

$\sigma = \sigma(1 + \varepsilon)$ (3.17)

$\varepsilon = \ln(1 + \varepsilon)$ (3.18)

When stress and strain are positive in tension and negative in compression.

3.10. Johnson-Cook model

The Johnson-Cook model was proposed by Johnson and Cook [118, 119], for any application with variables of strain rate and thermal softening due to the simple form. It also important for ballistic application due to the high strain rate phenomena and to describe the stress and strain relation of metallic materials under conditions of large deformation and high temperature.

3.10.1. Theoretical aspect

The hardening of the equivalent stress is modelled by a constitutive relation composed of three terms: plastic strain hardening, plastic strain rate hardening and thermal softening. In addition, the effects of the three terms are considered totally independent. The original Johnson-Cook model can be expressed as,

$$\sigma = (A + B\,\varepsilon^{n})(1 + C\,ln\,\dot{\varepsilon}^{*})(1 + T^{*m}) \quad (3.19)$$

Where:

σ is the Von Mises flow stress (MPa),

A is the yield stress (MPa) at reference temperature and strain rate,

B is the coefficient of strain (MPa),

n is the strain hardening exponent,

ε is the plastic strain,

$\dot{\varepsilon}^{*} = {\dot{\varepsilon}}/{\dot{\varepsilon}_{ref}}$ is the dimensionless strain rate,

$\dot{\varepsilon}$ is the strain rate (s^{-1}), and $\dot{\varepsilon}_{ref}$ the reference strain rate (s^{-1}),

T^{*} is the relative temperature, expressed as:

$$T^{*m} = \frac{T - T_{ref}}{T_{m} - T_{ref}} \quad (3.20)$$

T is the absolute temperature (K),

T_{m} is the melting temperature (K),

T_{ref} is the reference temperature ($T > T_{ref}$) (K),

Determination of constant B and n:

$$\sigma = A + B\varepsilon^n \quad (3.21)$$

$$ln(\sigma - A) = ln\, B + n\, ln\, \varepsilon \quad (3.22)$$

Determination of constant C

$$\sigma = (A + B\varepsilon^n)(1 + C\ ln\, \dot{\varepsilon}^*) \quad (3.23)$$

$$\frac{\sigma}{A+B\ \varepsilon^n} - 1 = C\ ln\, \dot{\varepsilon} \quad (3.24)$$

Determination of constant m:

$$\sigma = (A + B\varepsilon^n)(1 + T^{*m}) \quad (3.25)$$

$$ln\left(1 - \frac{\sigma}{A+B\ \varepsilon^n}\right) = m\, ln\, T^* \quad (3.26)$$

4. Microstructural Development

The main purpose of this chapter is to develop a cobalt-based superalloy composition to obtain γ/γ' dual phase microstructure when it is processed by PM route. The dual phase microstructure consists of rafted γ'-cuboidal ($L1_2$) precipitates embedded in a continuous γ-Co matrix. With this aim, a thermodynamical design by CALPHAD (CALculation of PHAse Diagrams) method were done to determine an optimal composition where the γ/γ' dual phase microstructure may exist in a temperature range of 800-1000 °C. In addition, considered some previous works of this kind, another composition with 2 (at. %) of –Ta and –Ti, were designed. Mechanical alloying (MA) was used at room temperature up to 40 h milling to achieve the desired compositions. Characterization of the powders show how this kind of process may produce a prealloyed composition, optimal to consolidate by field assisted hot pressing (FAHP).

4.1. Thermodynamic design

Thermodynamic calculation, called as CALPHAD method, provides a more precise view of the ternary phase diagram and design the optimal composition of the cobalt-based γ/γ' dual phase microstructure. A ternary diagram assessment of Co-Al-W is show in Fig. 4.1.

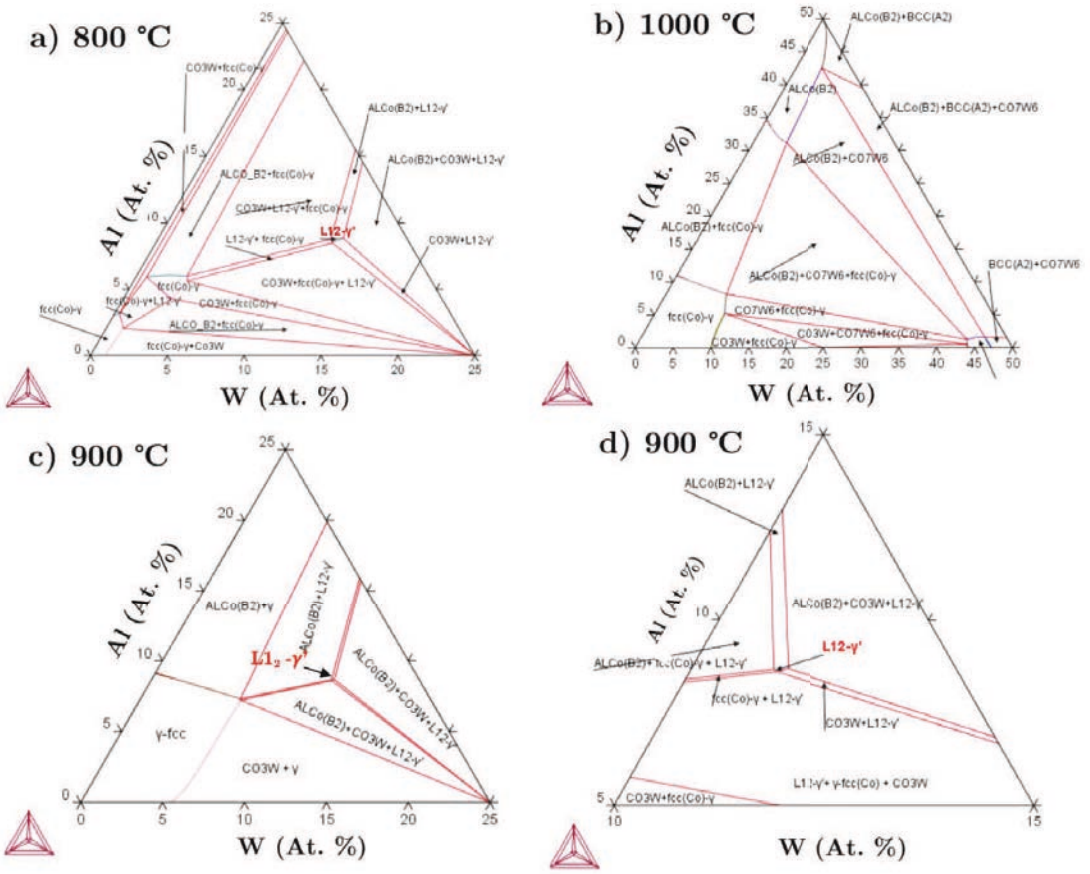

Fig. 4.1 Isothermal section of Co-Al-W ternary system at a) 800 °C, b) 1000 °C and c) 900 °C, respectively. Zoom of the most interested area is shown in d) 900 °C.

The use of CALPHAD (CALculation of PHAse Diagrams) allows new alloys to be prepared by using preliminary databases from other published researchers. Although there is only a limited thermodynamic description of the phase stability of the γ' phase in the case of cobalt-based superalloys, it is possible to predict the ternary compound of Co-Al-W with the data bases provided by Cui *et al.* [120], Yang *et al.* [121], and Zhu *et al.* [109]. It should be noted that in the three studies the metastable γ'-phase was described as a stable one.

Current research shows that it is necessary to reassess the thermodynamic description of the scheme due to the metastable condition of the γ'-phase in the Co-Al-W system [122]. Some studies claim that ordered metastable $L1_2$ phase exists in binary Co-X alloys, with stoichiometry Co_3X

(X = Ti, Al, Nb, Ta, W), but these phases are not stable at high temperatures (ie, >600 °C), [23, 123–125]. Co-Nb, Co-Ta and Co-W binary alloys can form metastable $L1_2$ (Co_3Nb, Co_3Ta and Co_3W) with martensite plates in the fcc Co matrix at the early stage of heat treatment. Co-Ti binary system, Co_3Ti has a $L1_2$ order structure, but the precipitates have large misfit that lowers thermal stability at high temperature [126].

The phase diagram was determined by Thermocalc software® at 800, 900 and 1000 °C (see: Fig. 4.1a) b) c)). It was found that γ' was only stable at 800 °C and 900 °C. In the Fig. 4.1c) and d) it is possible to see the constituent phases in the Co rich portion at 900 °C, with Cobalt solid solution γ-(fcc Co), the β-phase (AlCo), χ-phase (Co_3W), μ-phase (Co_7W_6), and the ternary compound γ'-Co_3(Al,W) phase $L1_2$. Considering these constituents at 900 °C isothermal section, the composition has been chosen with Co (bal), 12 Al (at. %) and 10 W (at. %).

Aluminum and W are the primary γ'($L1_2$) former in the ternary Co system. The addition of W and Al with proper proportion in Cobalt stabilizes the γ' structure with stoichiometry Co_3(Al,W) that are stable up to 900 °C. It is widely known that larger amount of W increases the γ'-solvus temperature. Suzuki and Pollock [127] reported that γ'-solvus temperature are 1000 °C in 9W and 1033 °C in 11W, respectively. Pyczak *et al.* [54] demonstrated that increasing the W-content increases by about 20 °C per 1% increase in W, while increasing the γ'-volume fraction, thereby improving creep strength. However, W-content has a negative impact on the bulk alloy mass density, an important aspect for aerospace applications. Alloying addition, such as Ti and Ta, improve solvus temperature, stability and mechanical properties at high temperatures [5, 128]. Suzuki and Pollock, also reported that the addition of Ta increase the solvus temperature up to 1080 °C [127]. A higher content of Al was selected in order to compensate for losses during consolidation of future heat treatments. It is important to considered that intermetallic Co-Al is a potential hardening phase [23].

4.2. Compositional and microstructural analysis of the powders

The milled powders were obtained by MA methods. This process of high-energy milling stimulates modifications in the cobalt lattice due to the operating conditions of plastic deformation, fracture, welding mechanisms, and the increase of alloying elements in the gamma cobalt phase. The starting powder of cobalt is a mixture of the fcc and hcp allotropes. At room temperature cobalt may present as fcc and hcp since the energy to transform it is too low. XRD patterns of the ternary cobalt milled up to 0.5 h can confirms the mixture of the two allotropes

(see: Fig. 4.2). This could be due to the continued impact of the balls trapping the powder in between them which causes an increase of the temperature. The force of the impact plastically deforms the powder particles leading to work hardening and fracture. Lizárraga *et al.* [129] reported that hcp phase is the ground state of cobalt and it is shown that as the temperature increases favor fcc because bring the energy of the fcc phase closer to that of the hcp phase.

As milling time progresses, evolution of the phases became clear in the XRD patterns, showing a transformation from the common elemental peak's patterns to the gamma cobalt phase enriched with alloying elements and the W-phase. In general, it is appreciated that Al-content is included in the cobalt lattice, but further consideration also needs to be given to solid solution of W content due to it is not successfully included in the resulted prealloyed powder.

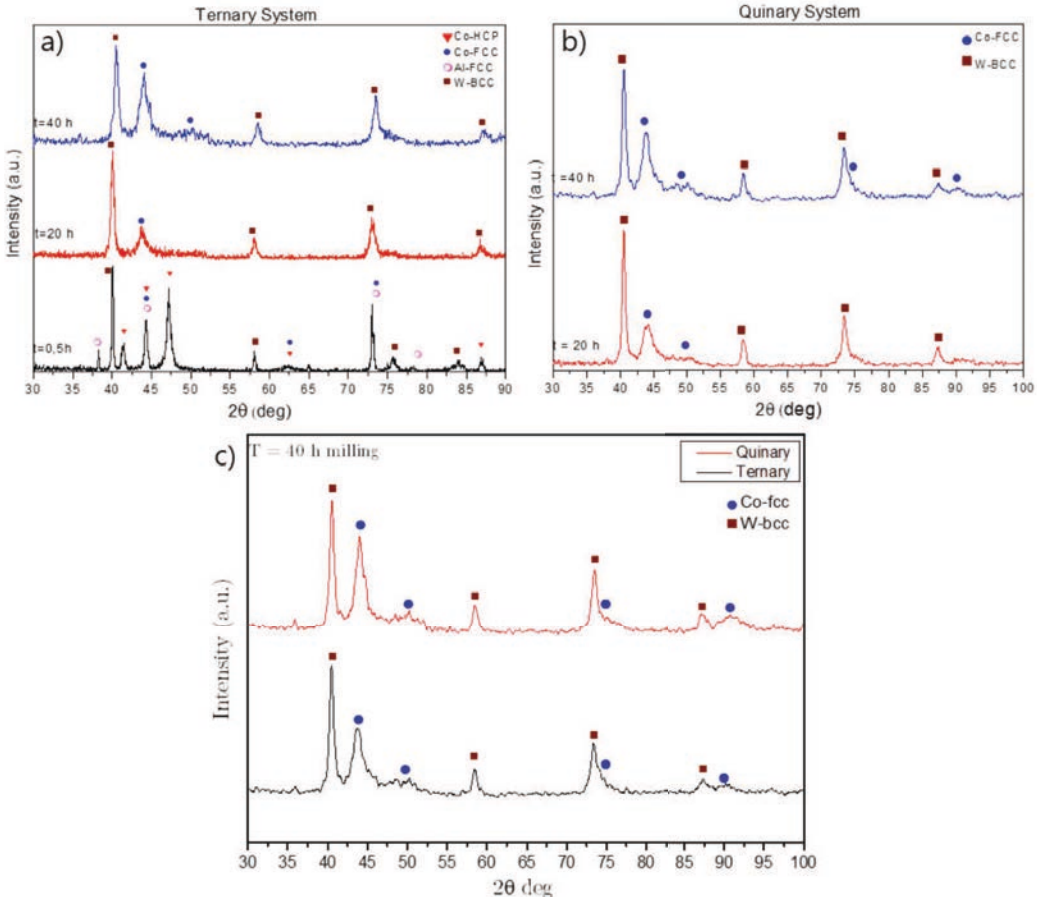

Fig. 4.2 XRD patterns showing the transformation from elemental powders to γ-Co fcc and W-phases with increasing milling time for a) ternary, b) quinary and c) comparison of both Co alloys after 40 h milling.

The crystallite size and lattice microstrain are two crystallographic parameters sensitive to milling changes. The amount of defects generated during the milling leads to a high-dislocation density, developing subgrains recombined into the original grain. Therefore, both crystallite

coherence and crystallite size decrease. The high density of dislocations, alloying processes and increase in lattice distortions produced during the milling increase the microstrain [73]. As a result of these changes, a small displacement for 2θ angle and broadening of the Bragg peaks can be produced by lattice expansion due to dissolution of the Al and W into cobalt matrix. On the other hand, this change on the lattice parameter can be correlated to the defects in the crystal lattice disturbing the lattice structure around the vacancies and finally resulting in a distorted crystal lattice [130]. The evolution of the structural parameters of the cobalt materials obtained in the most intensity peak ((1 1 1) plane of the γ-Co phase) at different milling times is shown in Fig. 4.3.

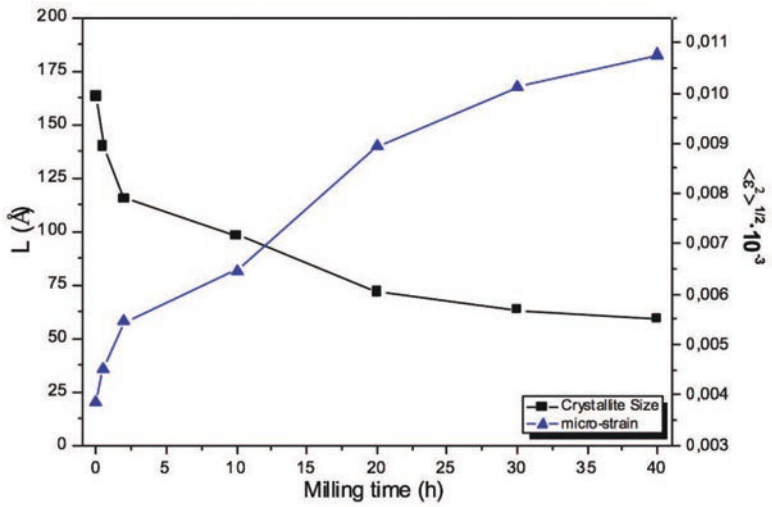

Fig. 4.3 Evolution of crystallite size and microstrain with milling time of the most intensity peak (1 1 1) of fcc-Co Co-Al-W ternary superalloy

A relationship between the normalized minimum grain size and the activation energy of self-diffusion has been calculated by F. A. Mohamed and Y. Xun in [76]. The minimum crystallite size attainable in MA is the result of a balance between the defect density induced by the high-energy milling and the recovery of the microstructure by thermal processes that took place during milling [75]. In the case of ternary Co-12Al-10W alloy, their calculations showed a minimum crystallite size of 56 Å. After the MA process, ternary alloy reached 75 Å and for quinary alloy <L> 54 Å.

These were an indication that steady state, or a point sufficiently close to it, had been reached. For consolidation by Field Assisted Hot Pressing, there was no need to increase significantly the hardness of the powder. During MA, a heavy deformation is introduced into the particles by the presence of crystal defects, such as, dislocations, vacancies, stacking faults, and increased number of grain boundaries. For this, a high number of defect concentration helps the kinetics of diffusion and thereby improve the sintering of the powder.

Particle size distribution is often obtained by the technique of sieving. By measuring the particle size and the weight percentage a histogram can be constructed. In MA powders, this histogram is generally Gaussian (log-normal); a bell curve is obtained when the frequency is plotter on a linear scale against the logarithm of the particle size [73]. Fig. 4.4 shows the powder particle size distribution of the ternary and quinary alloys. The average particle was centered at slightly greater sizes in the case of quinary addition. Furthermore, measurements revealed some differences regarding the d_{50} factor. For quinary, a higher parameter was also found (d_{50}=55.87 μm); and for ternary it was d_{50} = 44.80 μm. In addition, the particle sizes measured at d_{10} factor of the total powder volume were, respectively, d_{10}= 19.80 μm for ternary alloy, and d_{10}=28.16 μm for quinary alloy. The powder of both alloys was sufficiently fine, maintaining an adequate distribution to ensure good packaging and one that was necessary for the subsequent consolidation. It must be considered that under equal conditions of milling, good progress has been made in ternary than quinary system with finer and better distribution powder. It seems that the addition of alloying elements causes a delay on the milling evolution.

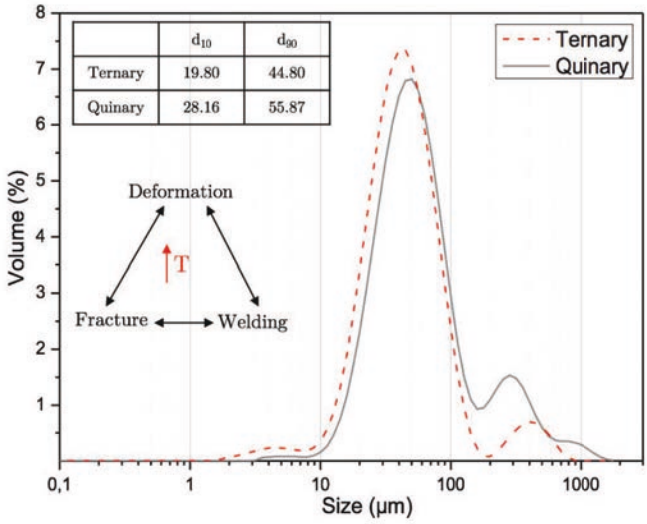

Fig. 4.4 Particle size distribution of ternary and quinary system powders

The SEM analysis of MA powder confirmed the phases identified by X-ray in Fig. 4.2. The matrix is the Co γ-phase (fcc) and the white precipitates were W-phase (bcc). Fig. 4.5 shows a typical evolution when a ductile material is considered together with a hard-and-brittle one [73, 131]. The particles are predominantly equiaxial; even in the case of the hardness of W elemental powder, the brighter signals underwent plastic deformation and were integrated during the ball collision with the welded particles. This observation led to an incomplete W dissolution in the Co γ-phase. The intrinsic properties of this element limited the possibility of a total alloying. It is

worth mentioning that there is a small amount of MA particles in an intermediate stage (the red arrow marks the fracture) coexisting after 40 hours of milling with equiaxial MA particles that belonged to a steady state of alloying. The intermediate MA particles could decrease the densification ability during the consolidation step.

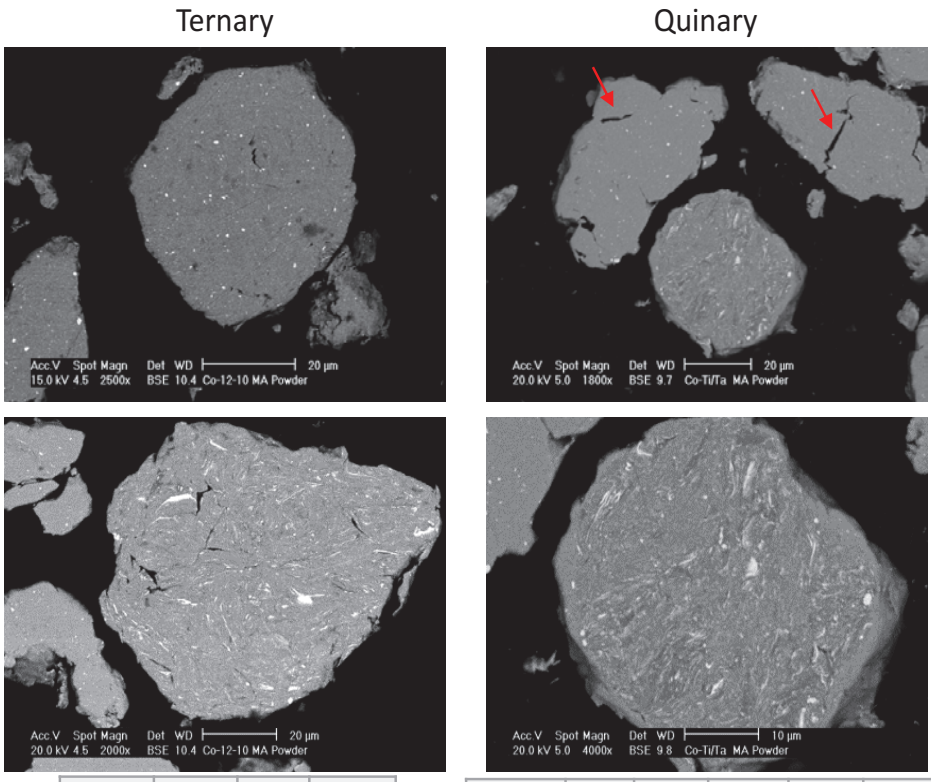

Elem	Co	Al	W
At(%)	79.58	8.35	12.08

Elem	Co	Al	W	Ti	Ta
At(%)	73.4	11.7	14.01	0.48	0.41

Fig. 4.5 SEM micrographs of MA powders after 40h milling, white areas correspond to free-W undissolved. EDS results show some general particle measurements

4.3. Thermal analysis of the prealloyed powders

Differential thermal analysis (DTA) was conducted for ternary and quinary powder to identify the critical temperatures and phases during the further heat treatments. The DTA of both materials are shown in Fig. 4.6a), where are identified the Curie temperature, the γ' solvus temperature and the melting point. It should be mentioned that the critical temperatures do not matches due to the degree of homogenization is lower during heating. Once the material has melted, the composition is more homogeneous.

Considering the Curie temperature (T_c), the thermal behavior was similar for both alloys. It should be considered that T_c is about 1115 °C for pure cobalt. This temperature can be influenced depending on the amount of alloying elements and plastic deformation. McAlister reported in

[132] that the T_c is about 800 °C when the Al addition is 10 at. % being closer to the Curie temperature of both alloys with an aluminum content of 12 at % (~ 710 °C). The dependence on the tungsten content in the morphology of the γ'-phase and Curie temperature was reported by Davidov *et al.* [133]. In this case, an amount of W causes a decrease of the T_c ~ 780 °C. It is clear that alloying elements produces a decrease in the T_c due to the difficulty in maintain aligned the magnetic moments of the material. However, the effect of γ'-stabilizers is clearly seen when is considered the solvus temperature and the melting point [134]. Thanks to the presence of Ti/Ta alloying elements an increase of ~ 90 °C is promoted, enhancing the stability of γ' field. In addition, $T_{melting}$ decreases with the addition of alloying elements as -Ta and -Ti. When compared with the T_{solvus} of both compositions there was an increase close to 90 °C, when -Ti and -Ta (2 %.at) elements are included in the Co-Al-W. This was a main purpose of the research given that previously works had mentioned that the addition of -Ti, -Ni and especially -Ta increase the solvus temperature [5, 12, 59].

In order to certify the relationship between the experimental DTAs results, a binary diagram of the ternary Co-Al-W was designed as shown in Fig. 4.6b) with the corresponding composition which is marked with red line. It is possible to see how the peaks from melting to solidification in DTA are in accordance with the phases in the binary diagram. The precipitation of the γ'-phase is not clear in the diagram, but A. Tomaszewska *et al.* [135] investigated the γ' range precipitation of Co-9Al-9W with a temperature of 1005 °C. For quinary alloys, DTA results was compared with A. Epishin *et al.* work [136] where γ' temperature is 1114 °C.

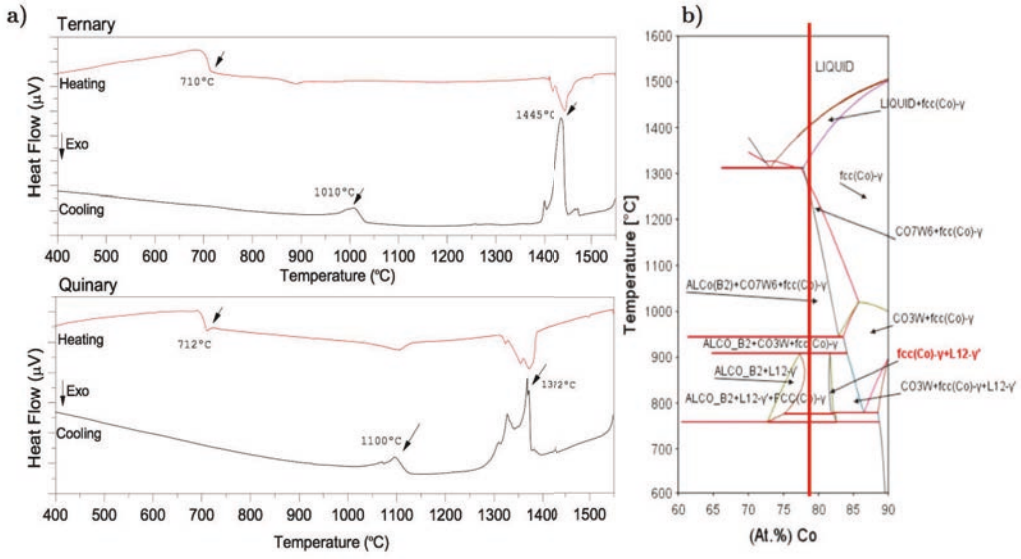

Fig. 4.6 a) Thermal analysis (DTA) for ternary (above) and quinary (below) alloys; b) Binary diagram of ternary alloy Co-Al-W with the corresponding composition marked with the red line.

4.4. Consolidation by field assisted hot pressing

In order to identify the shrinkage evolution with the T, ternary and quinary milled powders were study under the dilatometric mode recording the dimensional change at low pressure (5 MPa) with T, Fig. 4.7a. As can be seen from the ternary results, there were two major shrinkages: i' on the T_{range} = 543-1173 °C with $dL/\Delta L = 2 \cdot 10^{-4}$ (%) and ii' on the T_{range} = 1173-1302 °C with $dL/\Delta L = 1{,}3 \cdot 10^{-4}$ (%). For the quinary system, there were three major shrinkages: i on the T_{range} = 616-785 °C with $dL/\Delta L = 2{,}3 \cdot 10^{-3}$ (%), ii on the T_{range} = 785-1082 °C with $dL/\Delta L = 3{,}8 \cdot 10^{-4}$ (%) and iii on the T_{range} = 1082-1288 °C with $dL/\Delta L = 7{,}9 \cdot 10^{-3}$ (%).

It is clear that the quinary system has better shrinkage as T increases, when -Ti and -Ta elements are added to the alloying system there is a sintering activation. Considering this, the FAHP cycle was designed, applying the maximum pressure once the sample has reached 800 °C and heating up to 1250 °C for 10 minutes, (see: Fig. 4.7b). In both cases, sintered samples reached 99% of relative density with values of 9.47 g/cm^3 for ternary system and 9.94 g/cm^3 for the quinary (measured by He pycnometer).

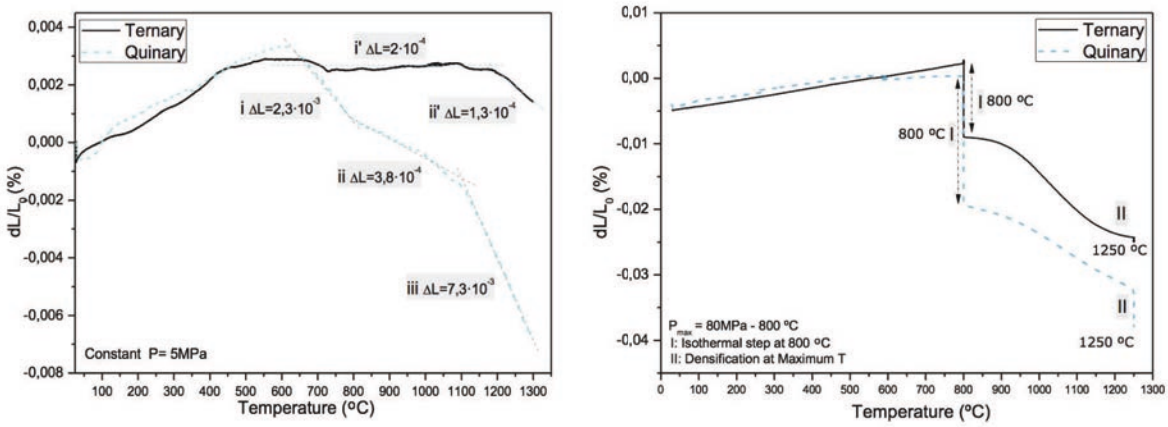

Fig. 4.7 a) Dimensional change dilatometry for ternary and quinary system vs temperature placed on the punch; b) Dimensional change undergone consolidation by FAHP

Once consolidation by FAHP had been completed, the microstructural characterization of both as-consolidated materials was studied by X-Ray diffraction and SEM. Both compositions revealed a good densification (Fig. 4.8), with a γ-Cobalt as matrix and high population of fine spherical particles identified as secondary precipitates. The white and grey precipitates in the ternary alloy is identified by EDX and XRD as η-phase (Co_6W_6C), χ-phase DO_{19}(Co_3W). In the quinary alloy, in addition to the abovementioned phases, another secondary phase was detected, μ-phase (Co_7W_6) (see: Fig. 4.9). EDS measurements on this alloy have shown how –Ti and –Ta

elements exhibited a partitioning behavior since –Ti was associated with Al-rich precipitates and –Ta with W-rich precipitates.

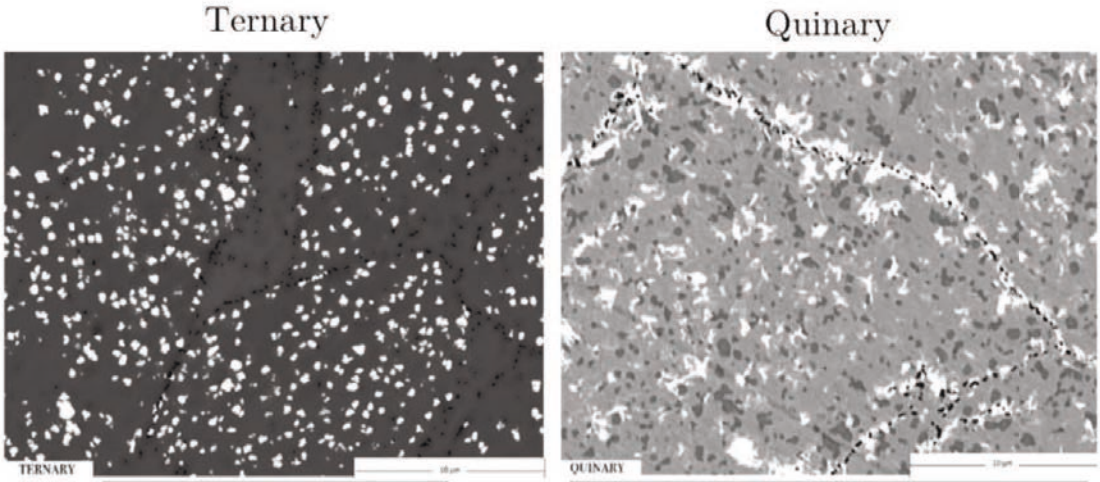

Elem	Co	Al	W
At(%)	78.63	13.66	7.71

Elem	Co	Al	W	Ti	Ta
At(%)	75.49	11.65	9.03	2.14	1.69

Fig. 4.8 Backscatter scanning electron microscopy micrographs of as-consolidated microstructure for ternary (left) and quinary (right) system. General measure of composition by EDS.

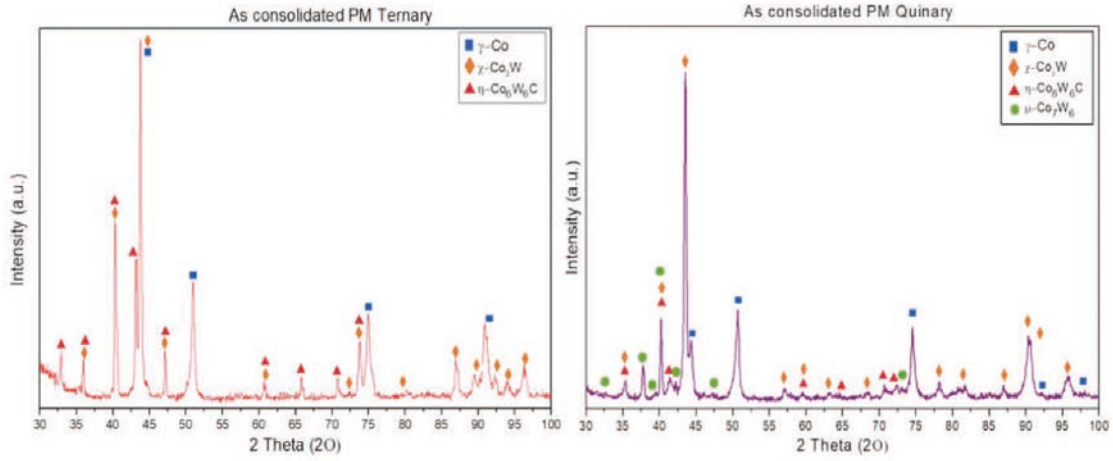

Fig. 4.9 X-ray diffraction patterns of as-consolidated microstructure for ternary (left) and quinary alloys (right)

4.5. Consolidation by Arc melting casting route

The Co-Al-W (Ternary) and Co-Al-W-Ti-Ta (Quinary) alloys were also processed by arc melting casting route in order to compare the results with the ones of powder metallurgy route. The micrographs of the Fig. 4.10, corresponding to the both as cast cobalt-based compositions, with the presence of the γ-Co matrix and bright spots of secondary phases.

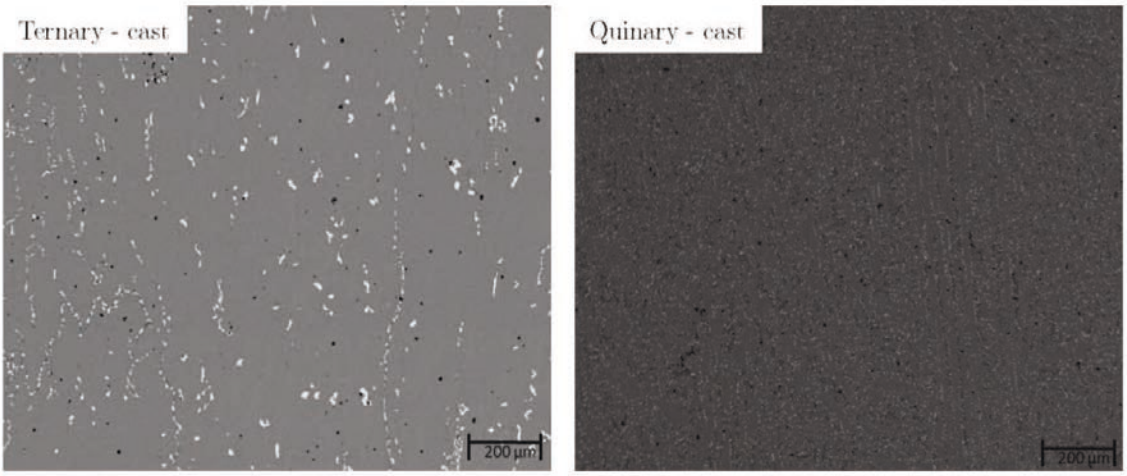

Fig. 4.10 Backscatter scanning electron microscopy micrographs of as-cast microstructure for ternary (left) and quinary (right) alloys.

The thermal behavior of as-cast alloys is shown in DTA diagrams (see: Fig. 4.11). If compared with previous PM DTA diagrams (see: Fig. 4.6), it can be observed how temperatures remain in a similar range. As discussed above in 4.3, Curie temperature can be identified at the same range that PM samples in both compositions, (T_c= 710 ± 5 °C). Focusing on derivative cooling heat flow, for ternary system, as cast γ'-solvus temperature is in line with PM samples with two inflexion points at 1000-1050 °C. This temperature also matches with previous work of as-cast Co-9Al-9W in [135]. For quinary alloys, γ'-solvus is always about 100 °C above in both routes and also matches with quaternary alloy with 2 (at.%) of Ta [136]. Taking these values as a reference, the as-cast specimens were solution treated at 1250 °C during 24 h in the vacuum furnace with a heating/cooled rate of 5 °C/min. The microstructures obtained following the heat treatments are described below.

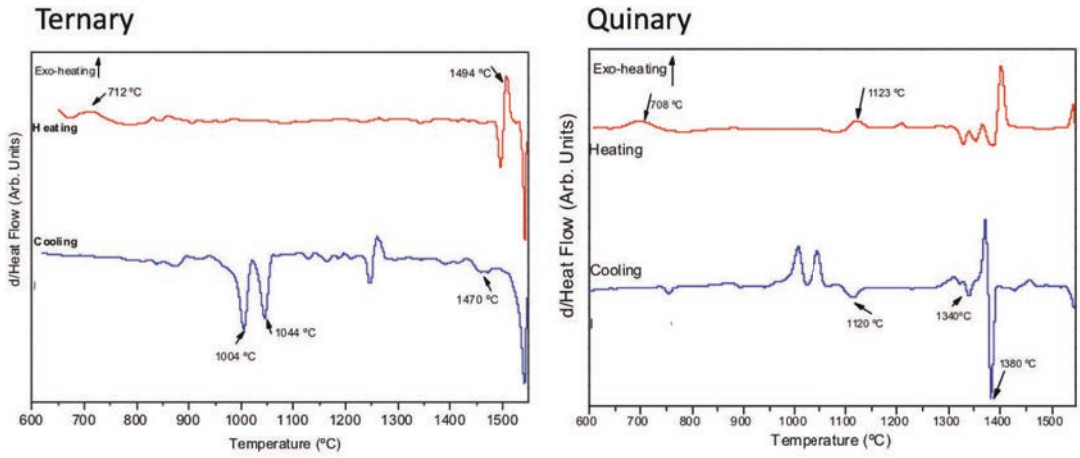

Fig. 4.11 First derivative of the differential thermal analysis (DTA) for ternary (left) and quinary (right) as-cast alloys

4.6. First approach of dual phase microstructure

It is a well-known fact that heat treatments have taken in account to achieve the γ/γ' dual phase microstructure. After obtaining full density specimens by powder metallurgy and arc melting casting route, solubilization and aging heat treatments were used as it was described in chapter 3.6.

As it was mentioned in chapter 2.3 the solution heat treatment should dissolve the γ'-phase into the γ matrix between the solutioning window. In this case, a temperature of 1250 °C was chosen for solution heat treatment since the solidification range is above this temperature. In contrast, a temperature of 900 °C was determinate for aging due to it has to be at γ' sub-solvus temperature to produce the fine and uniform γ' precipitates by diffusion into the γ matrix.

The microstructure of the both specimens after solubilization heat treatments were formed by the γ/γ' dual phase, as evidenced in the XRD patterns (see: Fig. 4.12). It should be apparent that, these most intensity peaks of the $L1_2$-phase and γ-Co appear in all the systems at the same diffraction angle. Compared to previous XRD specimens without heat treatments, it is significant the intensity decreases of the secondary peaks, in benefit of the appearance of the desired γ/γ' intensity peaks.

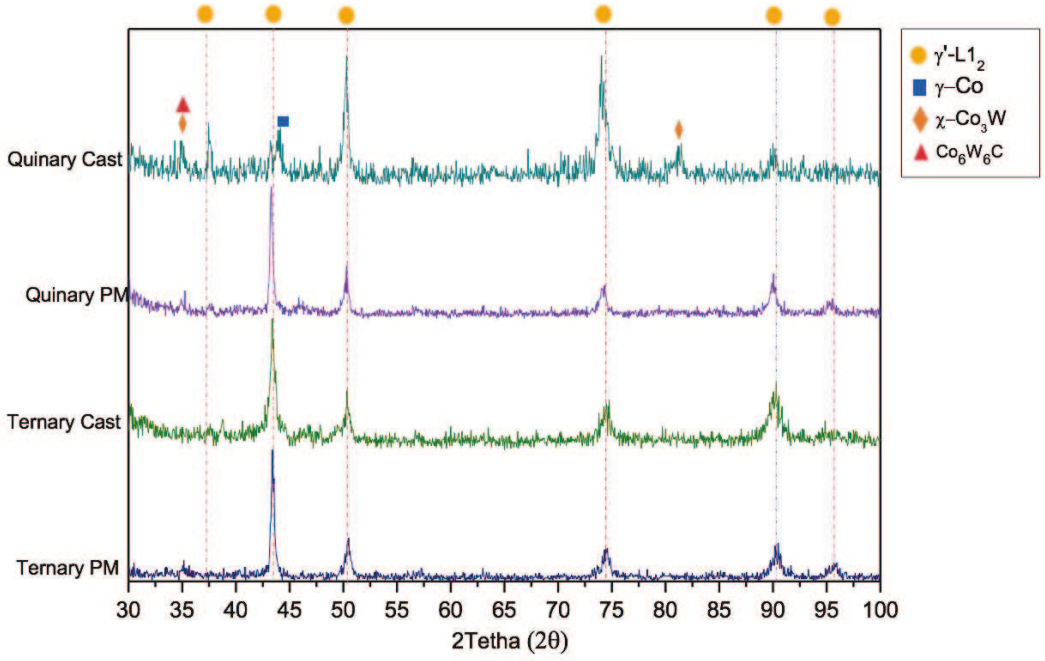

Fig. 4.12 XRD patterns of ternary and quinary alloys after solubilization of 1250 °C – 24h. Vertical lines show the indexed γ/γ' dual phase

Micrographs of cobalt-based alloys with a specific measure of energy dispersive X-Ray spectroscopy (EDS) of the cuboidal cobalt matrix are shown in Fig. 4.13. To achieve a correct view of the cuboidal matrix, all the samples were etched with Carapella's solution for 5 seconds, removing a residual coating which blocked the cuboids. Based on the complexity of the PM samples, it could be required more time to reveal the dual phase. On the other hand, it can be observed the irregular cuboids density, so it is essential to carry out aging treatments to help the development of improved and refined cuboids.

The composition of the cobalt-based superalloys developed by powder metallurgy and casting route after heat treatment is given in Table. 4.1. As can be seen from the table, both routes achieve the same nominal composition measured in the cuboidal matrix, with a cobalt content range from 80-83 (at. %).

Table. 4.1 Compositions of the cobalt-based dual phase determined by energy dispersive X-Ray spectroscopy (EDS).

(At. %)	Co	Al	W	Ti	Ta
PM-Ternary	81,96	11,85	6,20	-	-
PM-Quinary	80,79	10,13	6,23	1,90	0,95
Cast-Ternary	81,74	11,91	6,35	-	-
Cast-Quinary	83,39	8,35	5,44	1,86	0,95

For quinary PM alloy, it could be observed how the cuboidal morphology exhibited a greater degree of roughness, due to the etching time, being necessary a period of time longer that allows to show the cuboidal matrix. However, it can be confirmed the presence of the desired γ/γ' dual phase in all the specimens of casting route (see: Fig. 4.14).

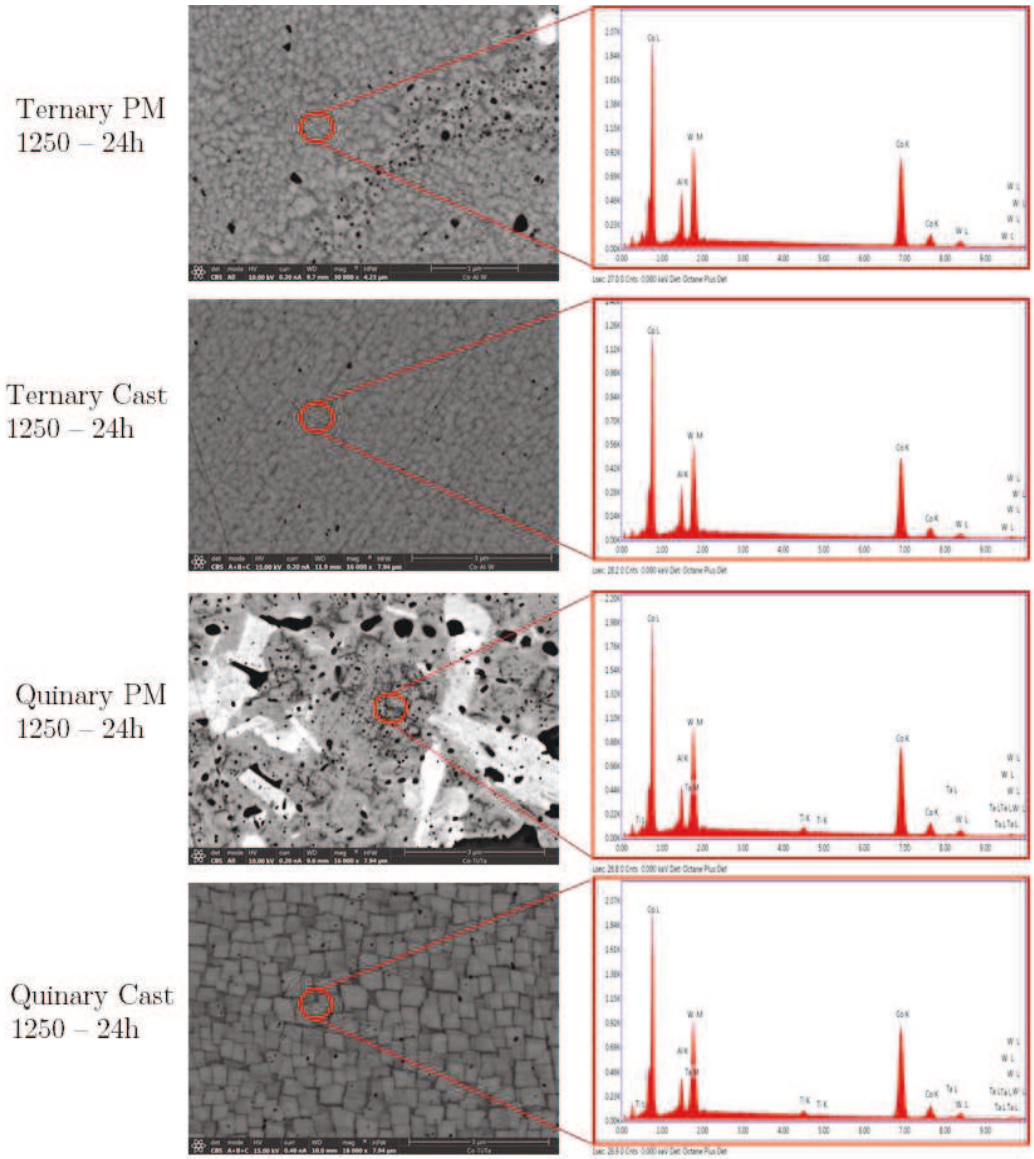

Fig. 4.13 SEM micrographs and EDS maps of the cobalt-based dual phase matrix.

Micrographs of cobalt-based alloys after 24h aged at 900 °C are presented in Fig. 4.15. As in the previous case of the solubilized specimens, it was necessary to remove the surface layer by deep etching during 5 seconds in order to reveal with good resolution the γ/γ' dual phase microstructure. The ternary compound exhibited fine cuboidal γ' precipitates of a smaller size than the quinary cuboidal matrix.

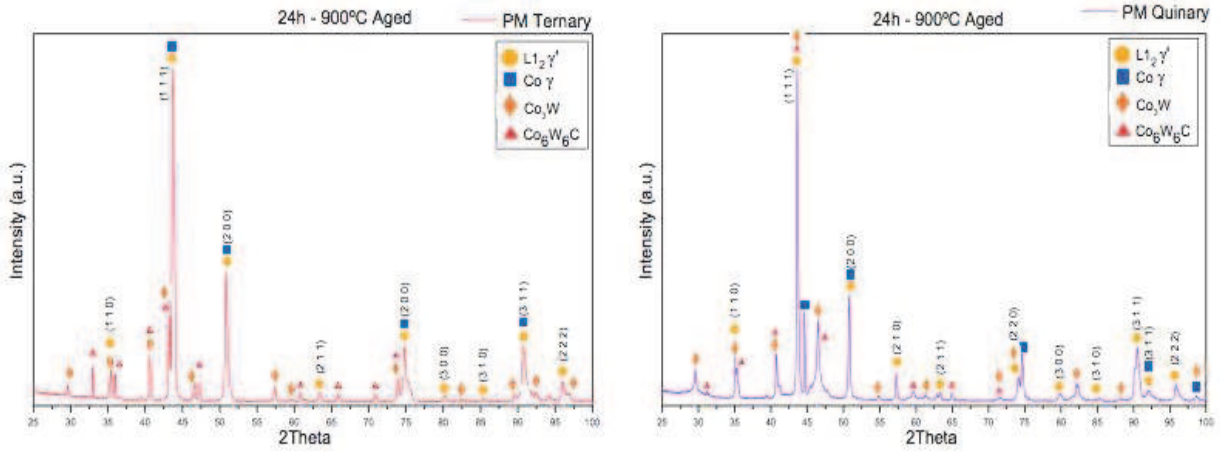

Fig. 4.14 XRD patterns of ternary (left) and quinary (right) alloys after aging heat treatment of 900 °C – 24h. Miller indices (hkl) of the γ'-L12 phase are also identified for both alloys.

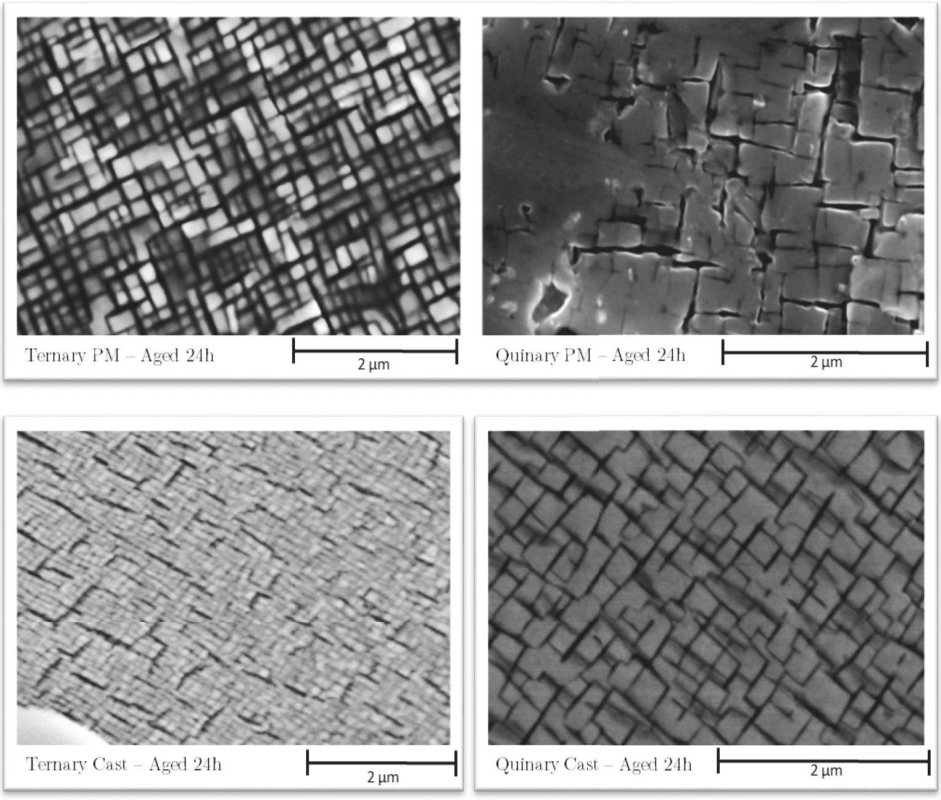

Fig. 4.15 Micrographs of the ternary (left) and quinary (right) alloys for PM (above) and Cast (below) routes

4.7. Remarks

Cobalt-based ternary and quinary superalloys can be produced following a PM route. The earlier mentioned mechanical alloying (MA) may produce powders with an almost constant composition. The consolidation was carried out by field-assisted hot pressing (FAHP), where simultaneous pressure and a continuous alternating current were applied to achieve the desired full-density specimen. Thus, the chapter offers the following conclusions:

- Milled powder obtained by MA depends on the relationship between crystallite size and microstrain.

  However, when W is included in MA-powders, it is not possible to incorporate it totally as solid solution. There is a part of W% that will remain as free element into the particles.
- PM Ternary and quinary cobalt-based powders can be consolidated by FAHP at 1250 °C. The consolidated specimens have shown a good densification (~ 99%) and a fine microstructure.
- In order to achieve the objective of promoting the γ/γ' dual phase, additional heat treatments have been considered (thermal solution up to 1250 °C for 24 hours and further aging at 900 °C to promote the γ' precipitation).
- Cast route was also investigated. It is clear that γ/γ' dual phase can appear by applying same heat treatments in both routes. Further experiments will be discussed in chapter 5 to see the possibilities of PM samples in relation to cast samples.

5. Effect of the heat treatments

The aim of this chapter is focused on the effect of the heat treatments on the evolution of the γ/γ' dual-phase, once Cobalt-based superalloy has been processed by powder metallurgy (PM) route. As can be seen in Chapter 4, it has been assumed that to reach γ/γ' dual phase microstructure, the starting elemental powders have to be processed by mechanical alloying (MA) and consolidated by field assisted sintering techniques (FAST). Additional cast manufacturing was also carried out to compare the resulting microstructures for both routes.

The development of the γ'-phase requires specific heat treatments. Various solvus heat treatments with different cycles were tested, designing, in this case, two routes: 1250 °C for 24 h (T1) and 1300 °C for 48 h (T2). A specific long-term aging study has been performed at 900 °C for different times: 24, 168 and 1000 h, respectively. The grain growth and γ'-volume fraction was studied to select the optimum solvus and to obtain a homogeneous coarse grain microstructure. Finally, a comparison made with all the heat treatments show how the volume fraction of γ'-phase rapidly increases with the first 24 h aging time, stabilizing after up to 1000 h aged. This is an indication of the good stability of the microstructure, and therefore it is anticipated to exhibit good creep behavior. It has been seen that longer aging times lead to a larger mean size of cuboids.

5.1. Design of heat treatments

As it was mentioned in section 2.5. it is important to apply the correct heat treatment by knowing the γ'-solvus temperature of both compositions due to γ' precipitation is predominantly controlled by the cooling rate [2]. PM alloys are usually heat treated above their γ' solvus temperature to achieve a significantly coarser grain size and a homogeneous microstructure. The specimens are then rapidly quenched to eliminate the formation of the γ' phase. It is important to know that mechanical properties are dependent of the cooling path. Higher thermal gradients can induce surface stresses during quenching. Instead, for aging treatment, a temperature of 900 °C was chosen regarding previous thermodynamic design where γ' is stable.

With the aim to reach the desired γ/γ' two-phase in the sintering samples, two solution heat treatments cycles were designed. Regarding the γ' solvus of ternary (~ 1000 °C) and quinary (~ 1100 °C), a solution heat treatment at 1250 °C for 24h (T1) and 1300 °C for 48h (T2), as shown in Fig. 5.1. Considering the γ'-phase solvus temperature and the solvus temperature of the both alloys, there is a heat treatment window of at least 200 °C. These heat treatments temperatures are discussed based on the phase transformation temperatures, previously determined by Differential Thermal Analysis (DTA) (see: Fig. 4.6).

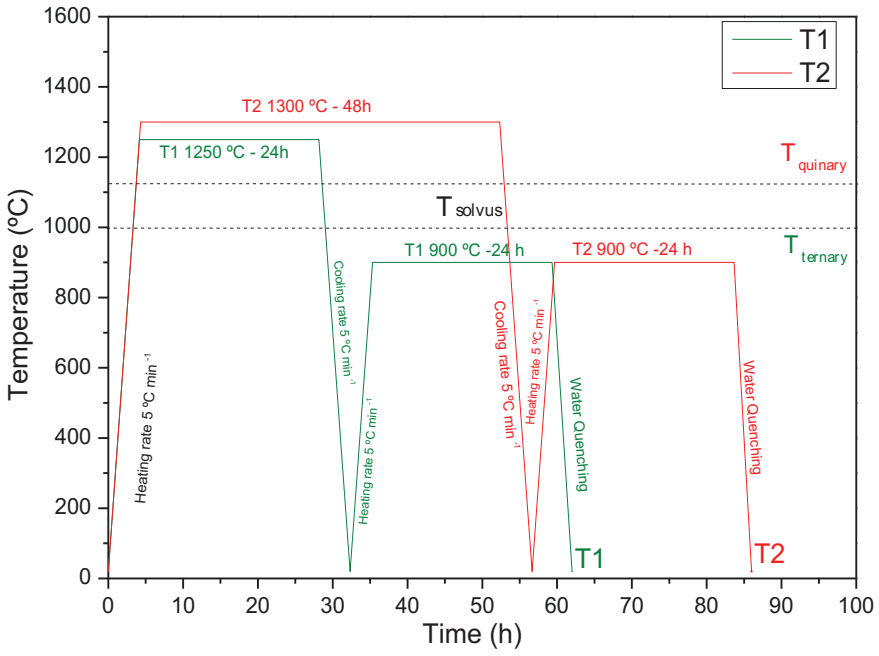

Fig. 5.1 Scheme of the design of heat treatments

5.2. Microstructural characterization

5.2.1. As-Cast and FAHP cobalt-based alloys

Micrographs of the as-consolidated PM samples and as-cast alloys are presented in Fig. 5.2, with a heterogeneous microstructure depending on the selected composition and route. Focusing on PM samples (left micrographs), it can be seen that the densification is complete, with a full density close to ~ 99 %. It can be seen the presence of heterogeneous secondary phases, as β (dark-contrast precipitates), and W-rich precipitates as χ-Co_3W (bright-contrast precipitates) or η-Co_6W_6C, dispersed into the γ-Co matrix

Table. 5.1 show an EDS analysis giving an overall view of the microstructure. In all samples, it has been possible to affirm that the results of the calculated cobalt alloy composition are in line with the theoretical one. It has to be pointed out that in ternary alloys, (see: Fig. 5.2a,b), there are fewer secondary precipitates than with addition of -Ti and -Ta alloys (see: Fig. 5.2c,d).

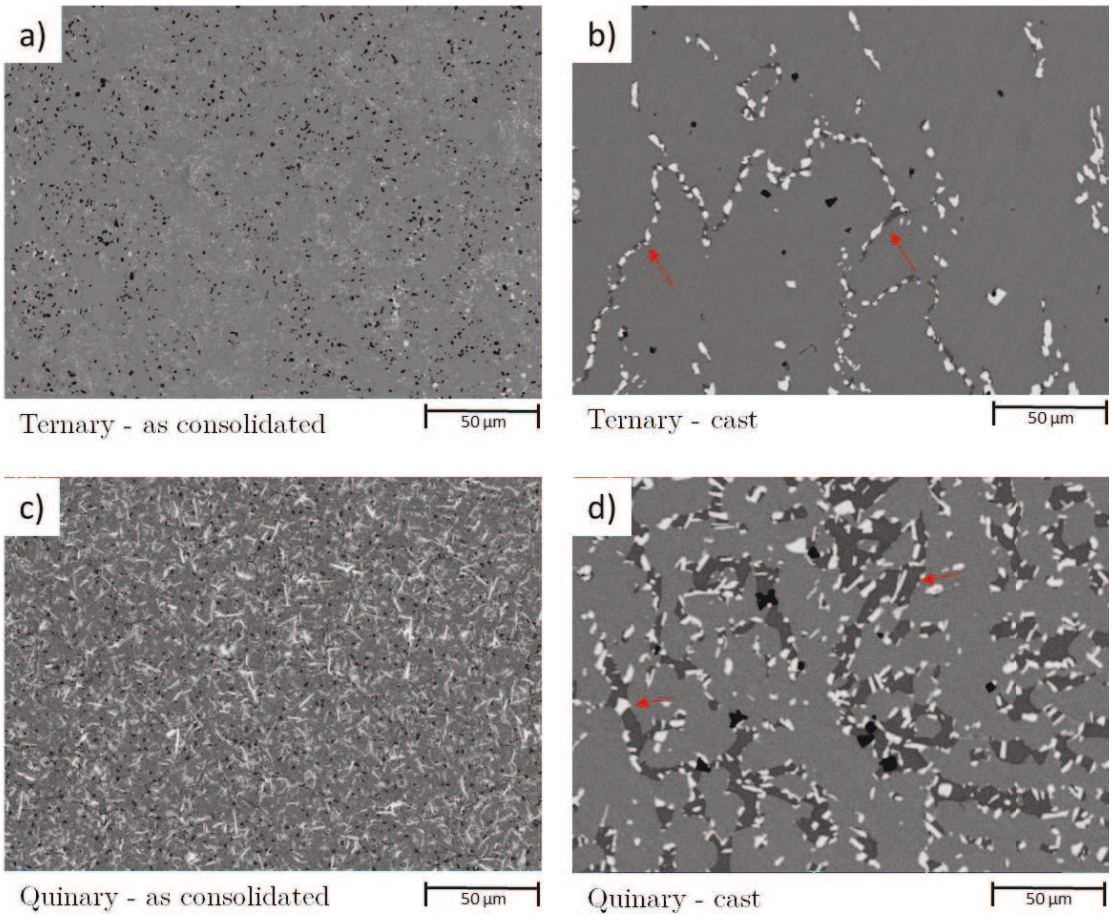

Fig. 5.2 Microstructure of the ternary (above) and quinary (below) alloys for PM (left) and cast (right) route

Table. 5.1 EDS Chemical composition of the overall microstructure under study (in at. %)

Sample	Co (at.%)	Al (at.%)	W (at.%)	Ti (at.%)	Ta (at.%)
Ternary-PM	78,63	13,63	7,71	-	-
Quinary-PM	75.49	11.65	9.03	2.14	1.69
Ternary-cast	81.34	11.53	7.13		
Quinary-cast	77.28	10.17	8.46	1.92	2.17

Previous works confirms these phases. Sato *et al.* reported in [1] that in the ternary system, the γ'-phase is stable at 900 °C, but further investigations showed that $Co_3(Al,W)$ is metastable at 1000 °C [52, 137], decomposing into either γ'-phase co-existing with γ-Co (A1) and secondary phases as (B2) β-phase (CoAl), $D0_{19}$ χ-Co_3W and μ-Co_7W_6 phases. Kobayashi *et al.* [53] showed that γ' is also metastable for long aging time at 900 °C, decomposing into γ, CoAl and Co_3W after 2000h.

On the other hand, microstructural observation of the as-cast samples show how secondary phases are located in the grain boundaries which consists of mostly globular W-rich precipitates and a small fraction of the β phase at the edge of the Co_3W (marked with red arrows). This type of as-cast cobalt-based alloys exhibit similar microstructures to other achieved by J. Zhu *et al.* [109].

XRD patterns corresponding to the as-consolidated PM and as cast alloys can validate the presence of γ-Co, χ-Co_3W and η-Co_6W_6C phases after consolidation, (see: Fig. 5.3).

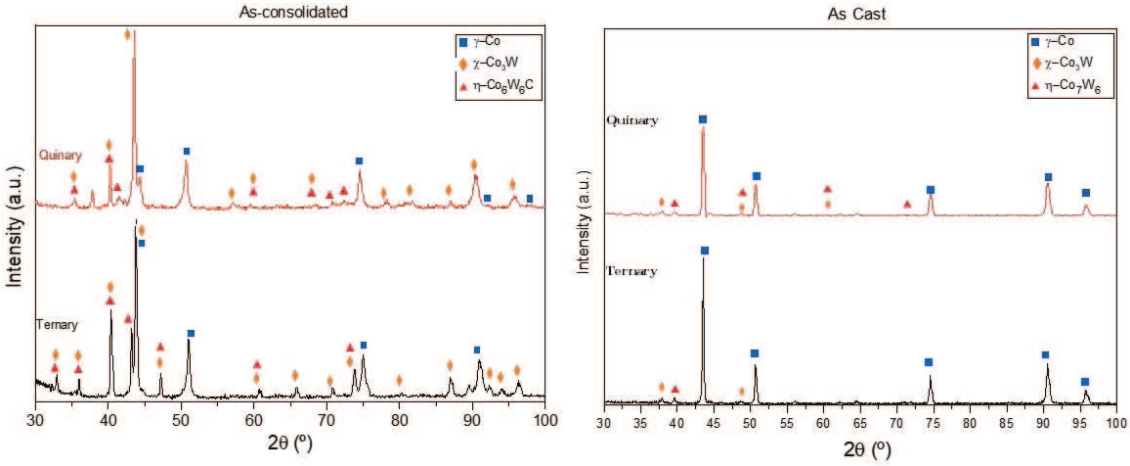

Fig. 5.3 XRD patterns corresponding to the PM (left) and cast (right) alloys.

The effect of the secondary precipitates can be directly traced to the Vickers microhardness, where a greater increase of these W-rich and carbides precipitates in the cobalt matrix causes a greater hardness in the microstructure, as can be seen in Fig. 5.4.

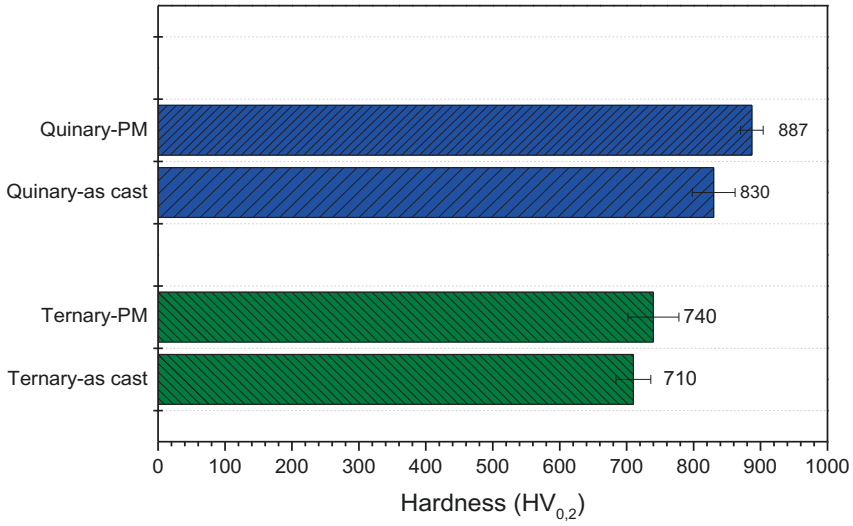

Fig. 5.4 Microhardness of as-consolidated and cast ternary and quinary alloys

5.2.2. As-cast and FAHP cobalt alloys after solubilization

5.2.2.1. Casting route

Two different solution heat treatments have been designed, (T1, 1250 °C/24 h) and (T2, 1300 °C/48 h), following Fig. 5.1. As mentioned below, casting route has been studied in the same conditions than powder metallurgy route in order to compare the resulting microstructure.

Fig. 5.5 and Fig. 5.6 show the resulting BSE-SEM micrographs for ternary system after T1 and T2 solution treatments, respectively. In both general microstructures, (see: Fig. 5.5a and Fig. 5.6a), it is possible to recognize the γ/γ' dual phase microstructures and the secondary precipitates. Focusing on the free precipitates areas, (see: Fig. 5.5b and Fig. 5.6b), it can be seen the cuboidal shape of the γ'-phase. Chemical composition of the cobalt matrix is listed in Table. 5.2. It can be observed how ternary system with T1 possess 5 at. % more of cobalt element than T2 treatment, which is closer to the theoretical composition of cobalt-based superalloy.

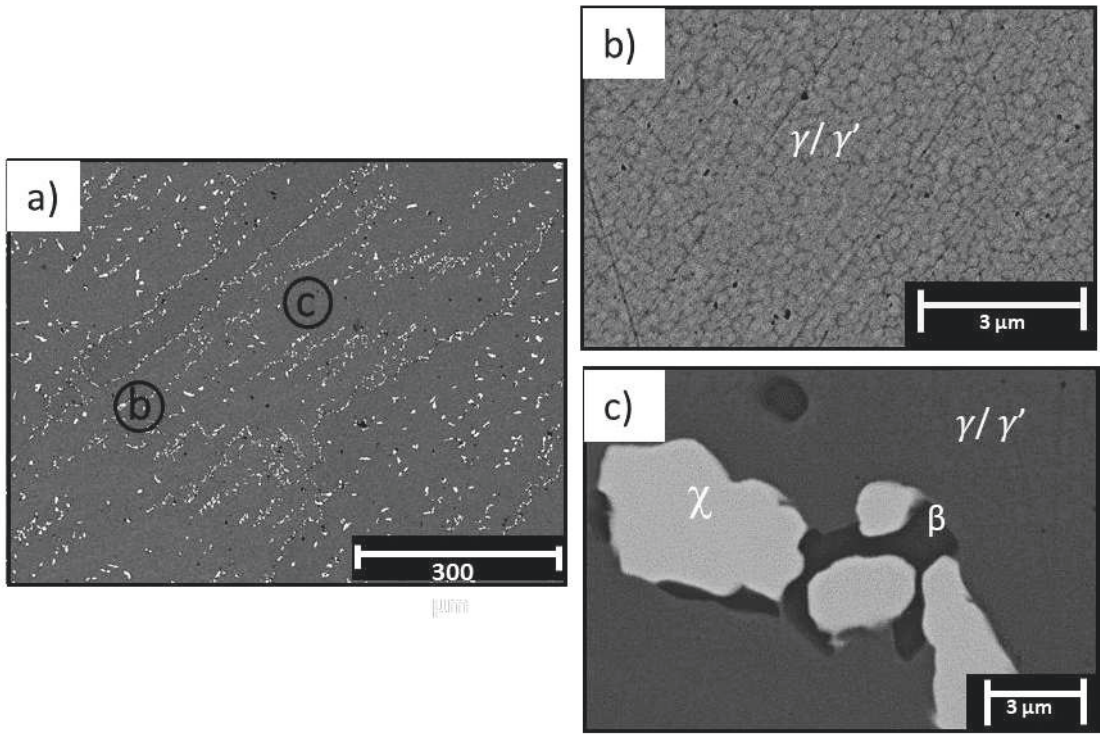

Fig. 5.5 BSE-SEM micrographs of ternary cast alloy after T1 solution heat treatments

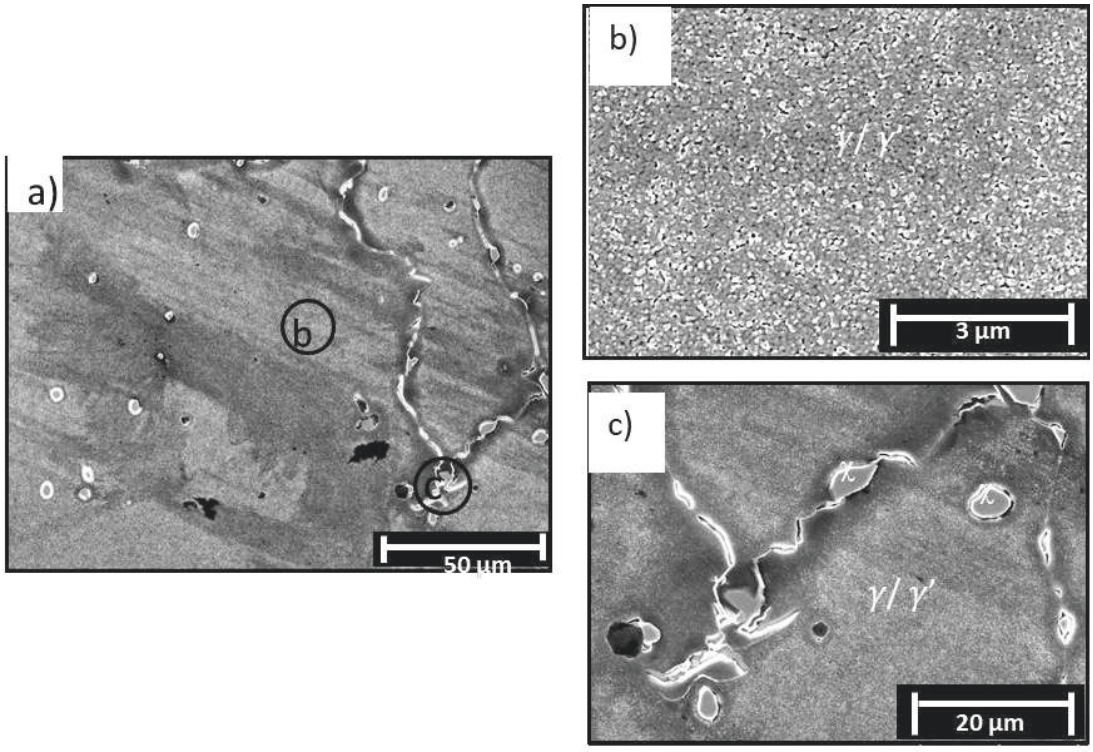

Fig. 5.6 BSE-SEM micrographs of ternary cast alloy after T2 solution heat treatments

If it looks closely at the secondary precipitates, in Fig. 5.5c it is possible to identify bright-contrast precipitates (χ-phase), surrounded by small amount of dark-contrast pools precipitates (β-phase). Fig. 5.6c also shows small volume fraction of secondary phases located in small pools at the grain boundary. These phases can be confirmed by using XRD (Fig. 5.7). In both heat treatments for ternary alloy, it can be checked the most intensity peaks of the dual phase, γ-Co and γ'-$L1_2$. Other peaks have been identified as W-rich phases (Co_3W and Co_6W_6C).

Table. 5.2 chemical composition of the cast dual phase region under study measured by EDS

Sample	Co (at.%)	Al (at.%)	W (at.%)	Ti (at.%)	Ta (at.%)
Ternary-cast (T1)	81.74	11.91	6.35	-	-
Quinary-cast (T1)	83.39	8.35	5.44	1.86	0.95
Ternary-cast (T2)	76.22	12.22	11.56	-	-
Quinary-cast (T2)	75.39	8.68	11.75	1.55	2.63

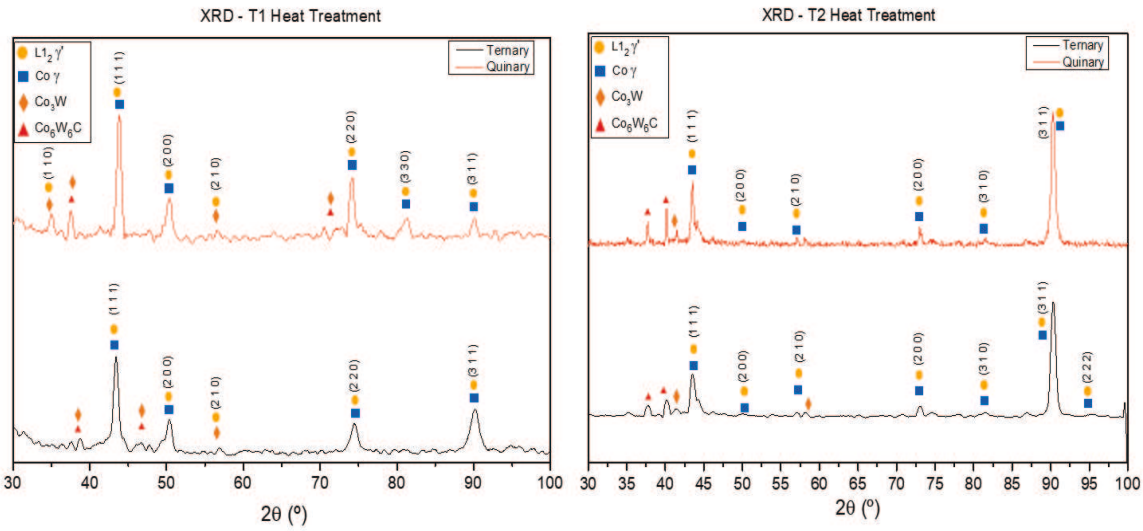

Fig. 5.7 Indexed XRD patterns of T-cast and Q-cast alloys after T1 and T2 heat treatments

For quinary alloys, same procedure has been followed. Fig. 5.8 and Fig. 5.9 present the BSE-SEM micrographs after T1 and T2 solution heat treatments, respectively. The general micrographs present different configurations and morphologies of the secondary precipitates, as can be seen in Fig. 5.8a and Fig. 5.9a. In the case of the γ/γ' dual phase matrix, the cuboidal shape it is clearer in the case of T1 (see: in Fig. 5.8b, Fig. 5.9b). The chemical composition by EDS measurements show larger amount of cobalt element (< 8 % at.) in the case of T1 (see: Table. 5.2).

The secondary precipitates show different morphologies, as can be shown in Fig. 5.8c and Fig. 5.9c. In the case of T2 precipitates, it presents M_6C carbides with a typical Widmanstätten patterns. These eutectic carbides can be induced from liquid phase due to the -Ti and -Ta elements additions into the cobalt-based composition [43]. Jiang *et al.* [138] reported that M_7C_3 and MC are a metastable phases and decompose easily into $M_{23}C_6$ and M_6C carbides at high temperature. In the case of primary MC carbide, the M mainly contains -Ti and –Ta elements [43, 139]. For this reason, -W and –Ti elements are prior to be released from MC carbide and -Ta remain in MC carbide during heat treatments. The low diffusivity of W is due to the high possibility for the border region to reach the composition close to the M_6C carbide. It is clear that cobalt-based alloys are out of equilibrium, and heat treatments can induce carbide degeneration. The decomposition when MC carbide reacting with the matrix is: MC + Matrix → M_6C [43].

It should be noted that residual MC carbide enriched –Ta becomes more stable at high temperature. At high temperatures the primary carbide decomposes into M_6C carbide from temperature higher than 1140 °C and dissolves into the matrix partially at or above 1260 °C [138]. This can be confirmed due to the existence of greater quantities of -Ta elements in the quinary T2 microstructure (see: Table. 5.2).

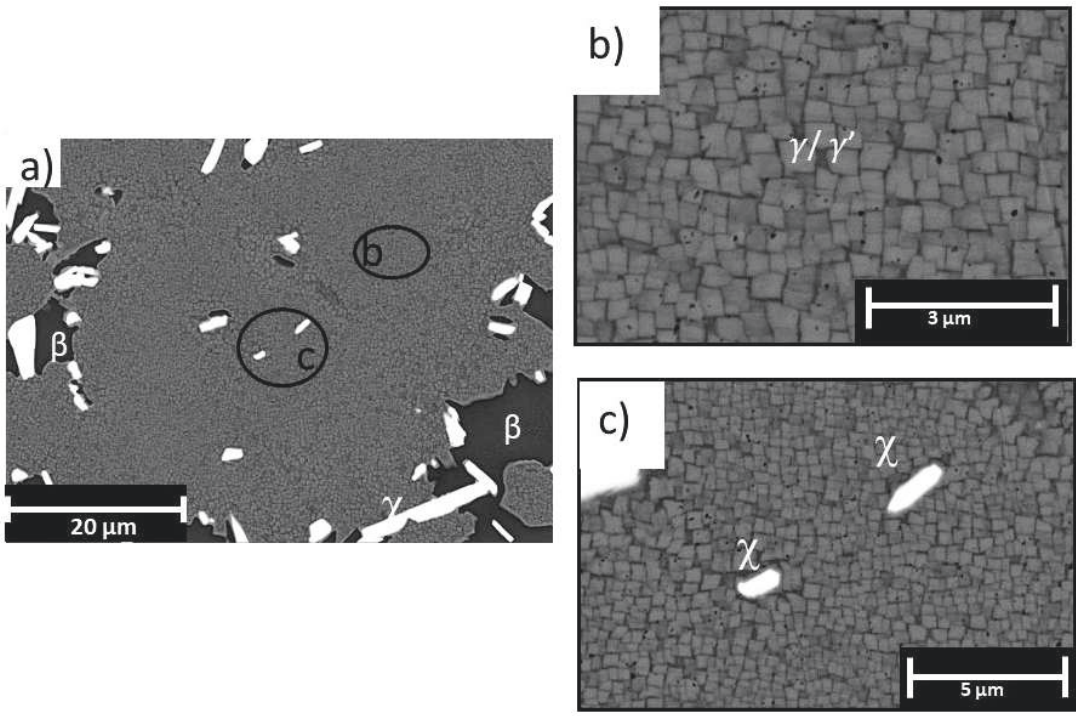

Fig. 5.8 BSE-SEM micrographs of quinary cast alloys compounds after T1 solution heat treatments

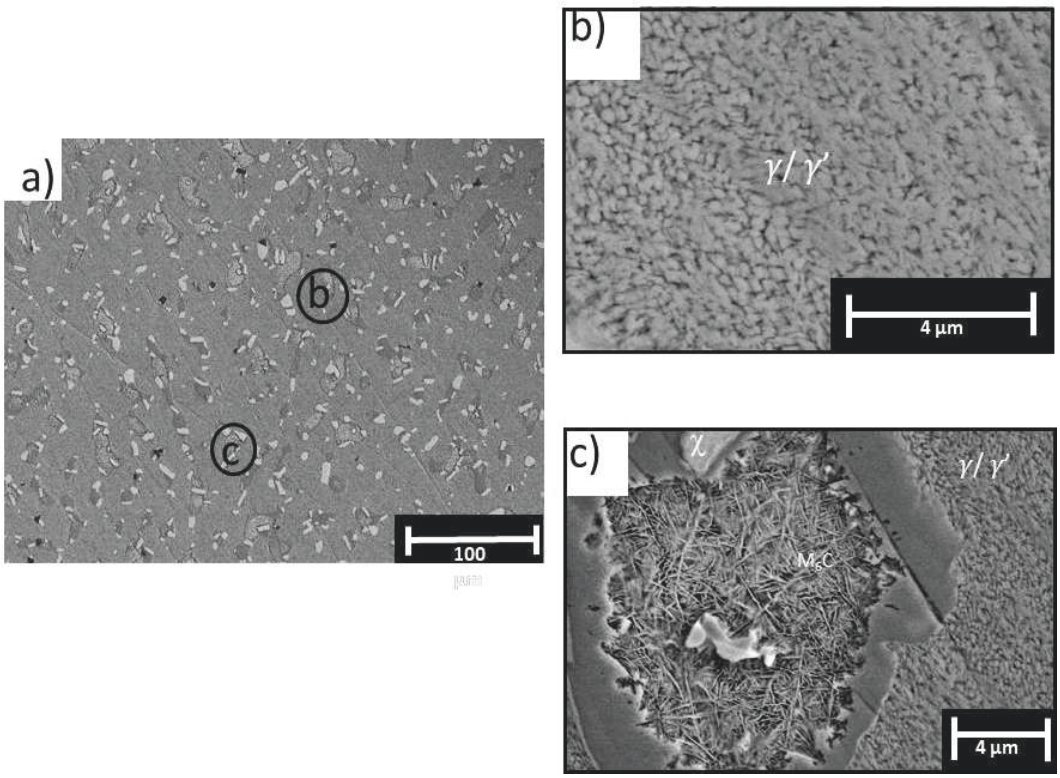

Fig. 5.9 BSE-SEM micrographs of quinary cast alloys compounds after T2 solution heat treatments

Table. 5.3 presents the recorded (1 1 1) reflection peaks of both alloys after T1 and T2 solution treatments. As can be seen, misfit values (δ) are similar for all alloys except to quinary T2 result, with a value of 0.24 – 0.22 for ternary, and 0.23 – 0.17 for quinary system. It should be noted that higher values of misfit have better cube edge as explained by Reed *et al.* [2].

Table. 5.3 Recorded (111)-reflections of ternary and quinary cast alloys after solution heat treatments.

Alloy		Misfit δ
Ternary	$T1_{(1250\text{-}24h)}$	0.24
	$T2_{(1300\text{-}48h)}$	0.22
Quinary	$T1_{(1250\text{-}24h)}$	0.23
	$T2_{(1300\text{-}48h)}$	0.17

The volume fraction of the γ/γ' dual phase is calculated from BSE-SEM micrographs, as shown in Fig. 5.10. For all cases, the volume fraction of the γ'-phases achieve more than 60 %, being slightly higher in the case of ternary alloys. Zenk *et al.* [140] suggested that the reason of this decrease is the comparatively high solubility of Ti in cobalt at elevated temperatures.

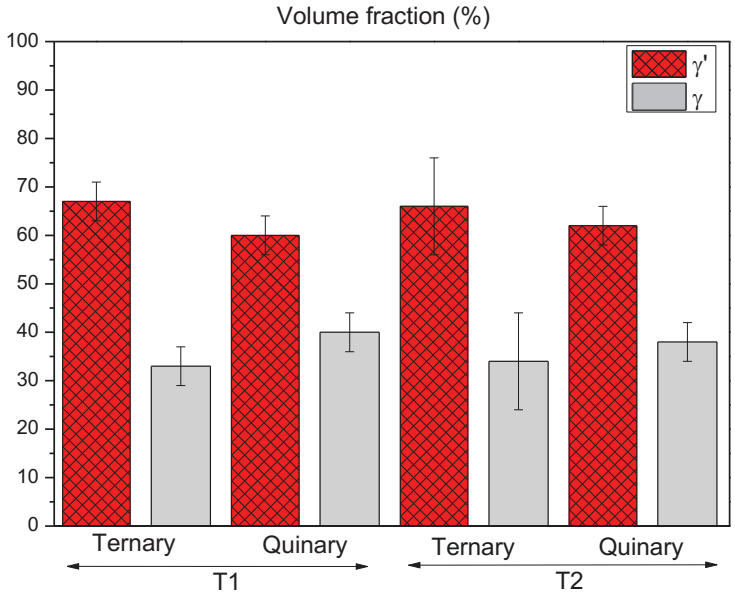

Fig. 5.10 Volume fraction values for ternary and quinary cast alloys after solution heat treatments

The cuboidal size has been calculated in both cases (see: Table. 5.4). It should be noted that ternary alloys cause that particle size becomes more cuboidal than quinary alloys, which are more elongated. This could be explained by Reed *et al.* [141], due to the faster precipitate growth in –Ti rich alloys, caused by their lower overall content of W element, being a slow diffusing element in superalloys. Zenk *et al.* [142], show how the shape of the γ' precipitates also changes from cubic to an elongated and frayed morphology with increasing –Ti element. In any case, no particle size is greater than 200 nm, with a cube edge length of 120 – 160 nm for ternary, and 150 – 190 nm for quinary, respectively.

Table. 5.4 Average cuboidal size for ternary and quinary cast alloys after solution heat treatments.

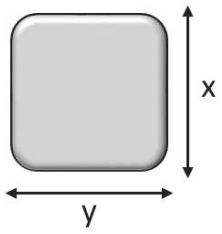		Size (nm)	
Alloy		x	y
Ternary	$T1_{(1250\text{-}24h)}$	164 ± 10	157 ± 10
	$T2_{(1300\text{-}48h)}$	121 ± 15	122 ± 10
Quinary	$T1_{(1250\text{-}24h)}$	157 ± 30	192 ± 10
	$T2_{(1300\text{-}48h)}$	196 ± 10	157 ± 10

5.2.2.2. Powder Metallurgy route

The resulting PM ternary microstructures after applying T1 and T2 solution heat treatments are shown in Fig. 5.11a and Fig. 5.12a. By comparing the two BSE-SEM micrographs, it can see the high amount of secondary precipitates dispersed throughout the matrix. Fig. 5.11b and Fig. 5.12b shows the γ/γ' dual phase with almost cuboidal shape. By using EDS measurements, it is possible to see some similarity in terms of chemical composition of the cobalt matrix for both alloys, (see: Table. 5.5).

Regarding secondary precipitation, in ternary alloy under T1 (see: Fig. 5.11c), there are W-rich phases in form of bright spots, and some black spots located at the grain boundary. These particles that appear dark in BSE images, suggesting they possess lower electron density, can confirm by EDS that they were the intermetallic β_2-phase (CoAl). For ternary T2 (see: Fig. 5.11c) these phases are more distributed in the grain boundaries. By using XRD, it is possible to identify the most intensity peaks of the dual phase γ'-$L1_2$ and γ-Co, as well as W-rich phases, Co_3W and Co_6W_6C, (see: Fig. 5.15).

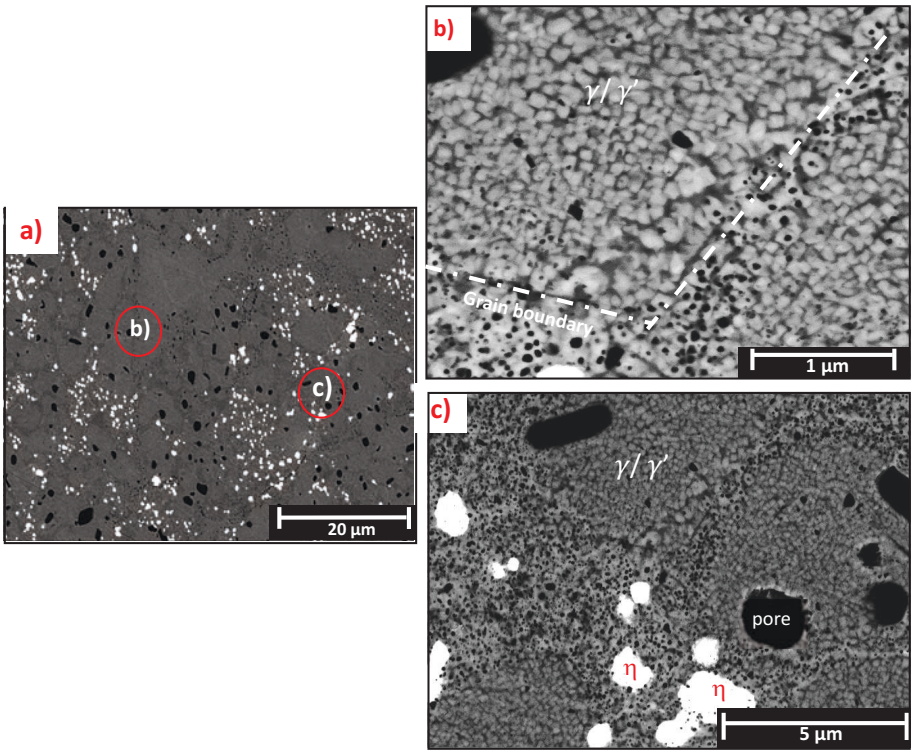

Fig. 5.11 SEM micrographs of ternary PM alloy after T1 solution heat treatment

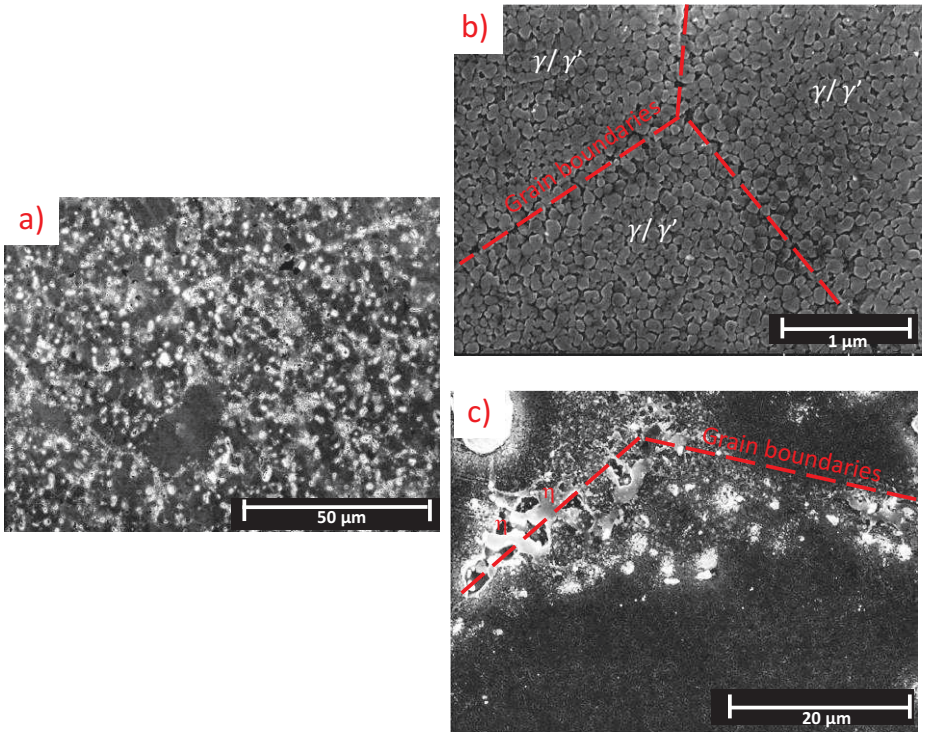

Fig. 5.12 SEM micrographs of ternary PM alloy after T2 solution heat treatment

Table. 5.5 Chemical composition of the cuboidal PM microstructure under study measured by EDX in FE-SEM

Sample	Co (at.%)	Al (at.%)	W (at.%)	Ti (at.%)	Ta (at.%)
Ternary-PM (T1)	81,96	11,85	5,08	-	-
Quinary-PM (T1)	80,79	10,13	6,23	1,90	0,95
Ternary -PM (T2)	78.32	10.92	10.76	-	-
Quinary.PM (T2)	80.28	10.58	5.67	2.35	1.12

In the case of quinary alloys, the resulting microstructures after applying T1 and T2 solution heat treatments are more complex than for ternary alloys, with higher amount of different secondary precipitates (see: Fig. 5.13a and Fig. 5.14a). In addition, it is possible to reach the dual phase matrix, as can be seen in Fig. 5.13b and Fig. 5.14b. The chemical composition measured by EDS shows how quinary alloy T2 has more amount of -Ta in the cuboidal microstructure than quinary T1 (see: Table. 5.5). In addition, it can be see a large volume of W-rich secondary precipitate (bright stick) and black spots located in the grain boundary (see: Fig. 5.13c and Fig. 5.14c). XRD patterns for quinary alloys show the most intensity peaks of the dual phase and W-rich phases, such as Co_3W and Co_6W_6C (see: Fig. 5.15).

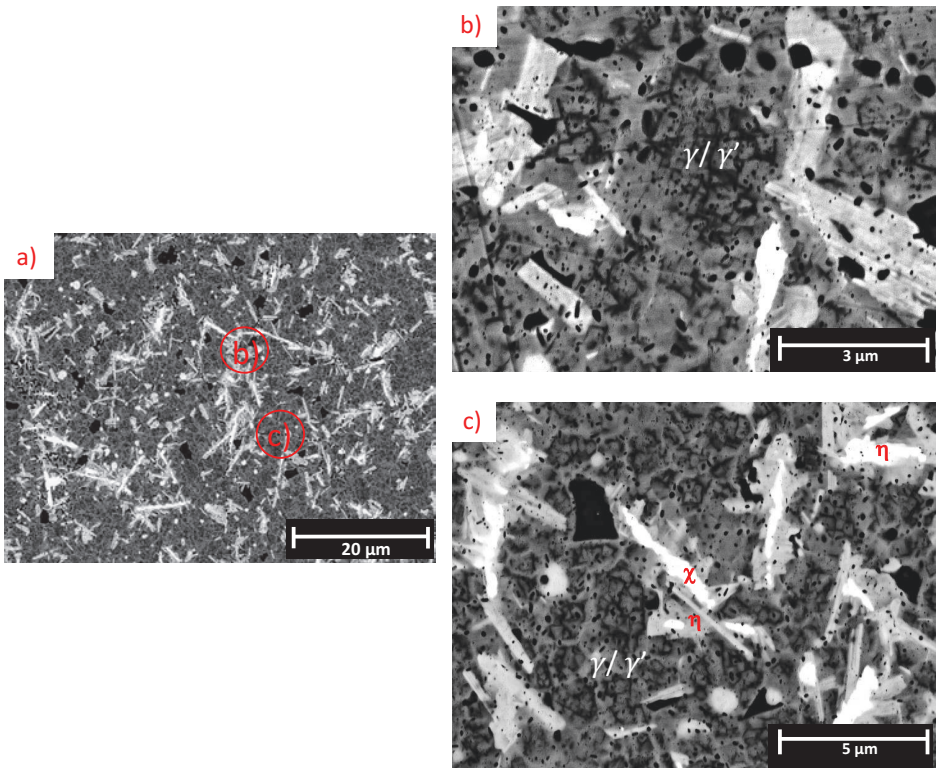

Fig. 5.13 SEM micrographs of quinary PM alloy after T1 solution heat treatment

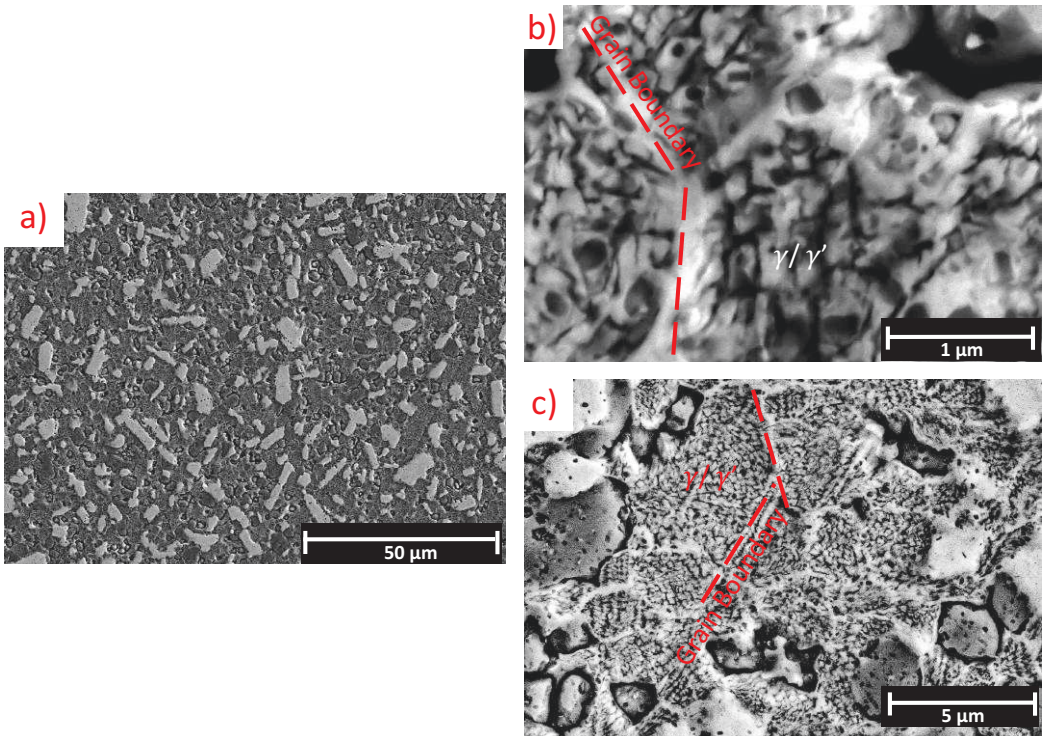

Fig. 5.14 SEM micrographs of quinary PM alloy after T2 solution heat treatment

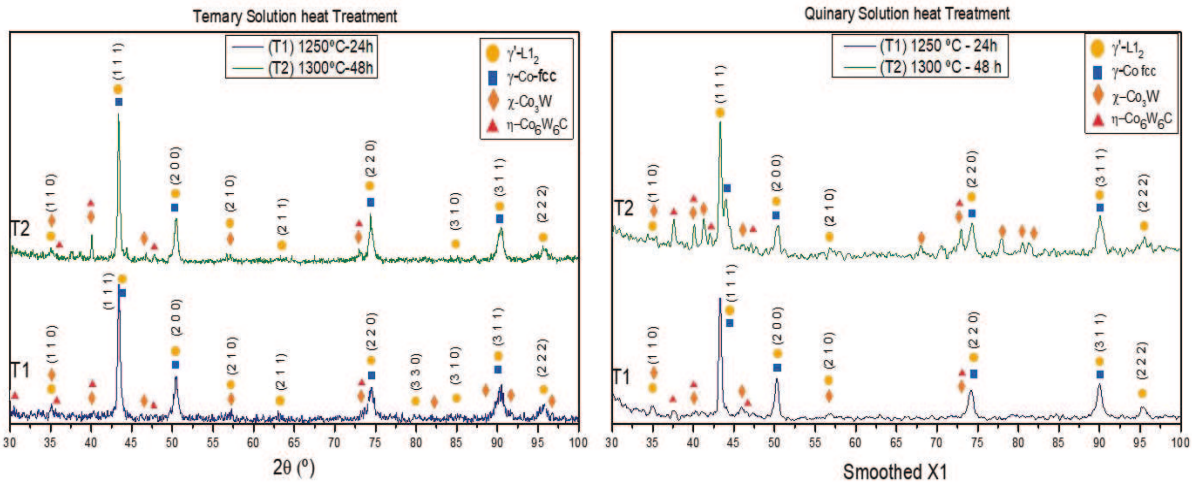

Fig. 5.15 Indexed XRD pattern of ternary and quinary PM cobalt-based alloys after solution heat treatments

The calculated γ/γ' lattice misfit ratio for both alloys after T1 and T2 solution heat treatments show how the δ parameter is higher for ternary alloys than the quinary one (see: Table. 5.6). Povstugar *et al.* [59] suggest that is variation is due -Ti and -Ta additions are found to strongly partition to the γ' phase, needing less energy than the ternary system to achieve the

ternary A_3B structure ($L1_2$ type). If it compares T1 and T2 treatments, for T2, it usually obtains better value of misfit than T1 in both specimens.

Table. 5.6 Recorded (111)-reflections of ternary and quinary PM alloys after solution heat treatments

Alloy		Misfit δ
Ternary	$T1_{(1250\text{-}24h)}$	0.33
	$T2_{(1300\text{-}48h)}$	0.37
Quinary	$T1_{(1250\text{-}24h)}$	0.29
	$T2_{(1300\text{-}48h)}$	0.30

The appropriate outcome for solution heat treatment may be to apply T2 heat treatment for both cobalt-based alloys. Moreover, the volume fraction obtained is quite similar in all cases, having a value around 60 ~ 65 %. It is ternary T1 that achieves the greatest value of volume fraction (see: Fig. 5.16).

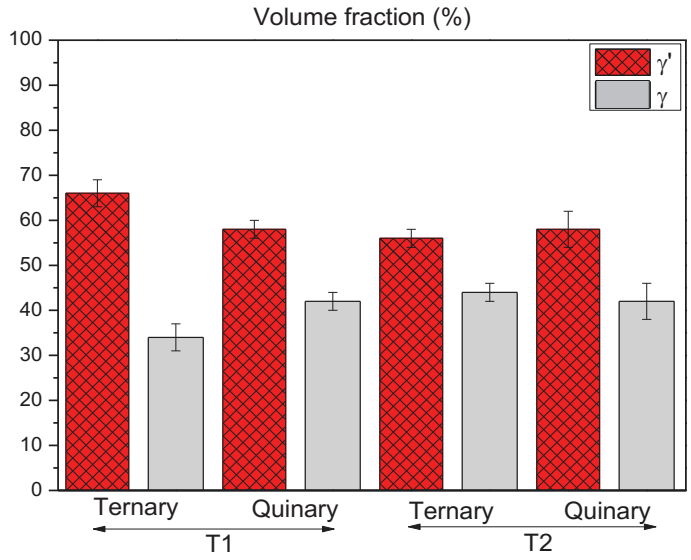

Fig. 5.16 Volume fraction values for ternary and quinary PM alloys after solution heat treatments

Recent studies have demonstrated that a higher fraction of γ'-phase influences the hardness and creep resistance [143, 144]. Ti and -Ta additions are linked to the change in hardness due to can be ascribe to the substitution of Al and W atoms by Ti and/or Ta [59]. Fig. 5.17 can show how a higher misfit value offers a higher hardness, being in this case better to apply T2 heat treatment for both alloys. For T1, it is clear that it is not recommendable for quinary alloys. The

cuboidal size it was also calculated for ternary and quinary alloys, as shown in Table. 5.7. In general, all the alloys possess the cuboidal shape with a similar average size, (60 nm), except for the ternary T1, which is larger than the rest (110 nm).

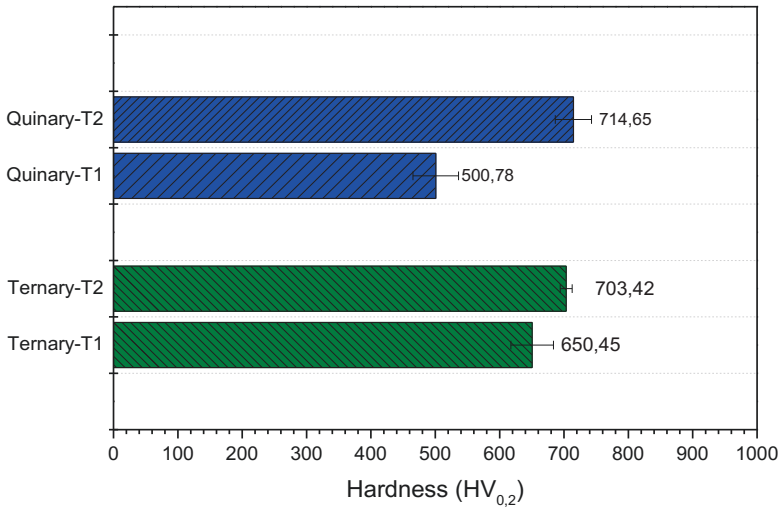

Fig. 5.17 Microhardness of ternary and quinary PM alloys after solution heat treatments

Table. 5.7 Average cuboidal size for ternary and quinary PM alloys after solution heat treatments.

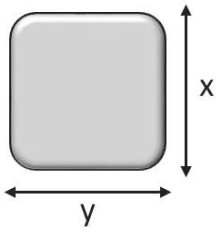

Alloy		Size (nm)	
		x	y
Ternary	$T1_{(1250\text{-}24h)}$	110 ± 20	110 ± 20
	$T2_{(1300\text{-}48h)}$	80 ± 20	80 ± 30
Quinary	$T1_{(1250\text{-}24h)}$	60 ± 30	60 ± 30
	$T2_{(1300\text{-}48h)}$	60 ± 20	60 ± 10

5.2.3. Effect of Aging treatment

The aging heat treatments are fundamental in superalloys to increase and distribute homogeneously the size of the of γ' precipitates in the γ microstructure [1]. For this reason, all the samples were homogenized at temperatures between their γ' solvus and solidus temperatures, and then aged at temperatures below the γ' solvus temperatures (see: Fig. 5.18). The relationship between aging time and γ/γ' microstructure has been studied at 900 °C for cast and powder metallurgy route. It was proposed a long-term aging heat treatment with three fixed steps at 24, 168 and 1000 hours where the specimen was rapidly water quenched to analyze the resulting microstructure.

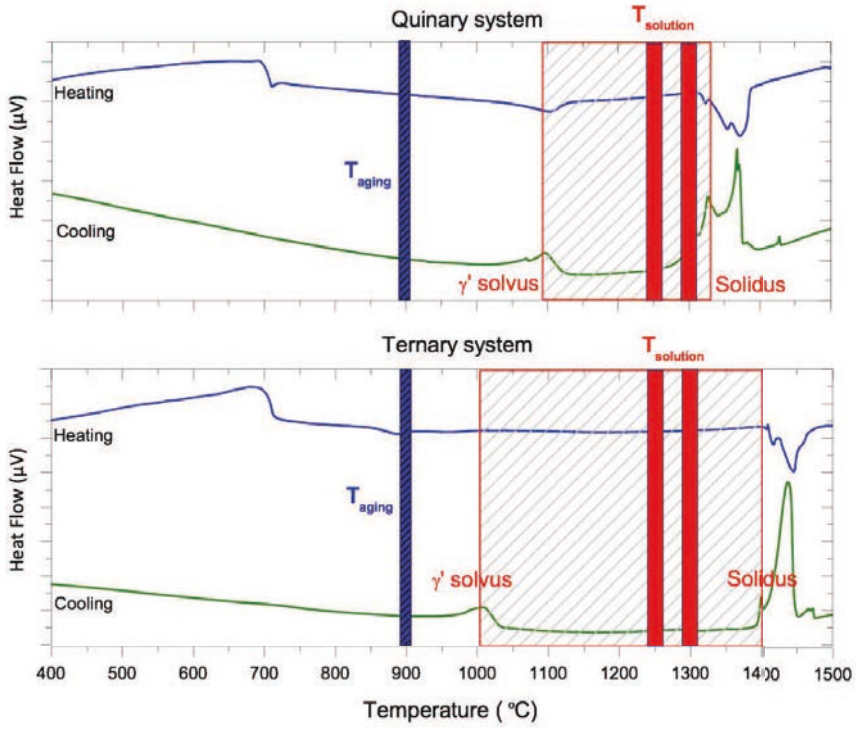

Fig. 5.18 Schematic of the ranges proposed to apply the heat treatments

5.2.3.1. Aged cast Alloys

Once heat treatments have been done and focusing on the dual phase microstructure, it is important to know the evolution of the cuboidal microstructure after long term aging up to 1000 h at 900 °C. It can be seen that two-phase microstructure almost preserves their chemical compositions for longer aging exposure, (see: Fig. 5.8).

Fig. 5.19 shows the evolution of the microstructures of the both cast alloys after aging heat treatments. After first 24 h aging, ternary and quinary alloys exhibit cuboidal γ' precipitates with about 120 -160 nm and 210 - 370 nm cube edge length, respectively (see: Table. 5.9). It is clear that the addition of the -Ti and -Ta elements led to an increase in the γ' volume fraction and the cuboidal size due to these elements can occupied Al or W sites in the $Co_3(Al,W)$ [145]. Bauer *et al.* [7] shows how addition of 2 at.% -Ta, as well as -Ti on the ternary alloy produced a substantial increase in the γ' volume fraction from 60 % to about 82 %, as can be seen in the studied quinary cast alloys after 24 h aging heat treatments. In contrast to other studies with same heat treatments, ternary alloys show an increase of the γ' volume fraction from 60 - 65 % to 77 - 80 %. (see: Fig. 5.20). It should be noted that it was reported that alloys with γ' volume fractions of more than 60 % offered an improved strength compared with lower ones [67, 110].

Table. 5.8 Chemical composition of the cuboidal cast microstructure under study measured by EDX in FE-SEM after aging heat treatments

Time (h)	Sample	Co (at.%)	Al (at.%)	W (at.%)	Ti (at.%)	Ta (at.%)
24	T-cast (T1)	74.79	10.52	14.69	-	-
24	Q-cast (T1)	74.05	8.57	12.88	2.83	1.67
24	T-cast (T2)	76.79	9.64	13.4	-	-
24	Q-cast (T2)	78.2	9.81	9	1.62	1.35
168	T-cast (T1)	74.95	14.79	10.27	-	-
168	Q-cast (T1)	79.88	8.50	8.87	1.50	1.27
168	T-cast (T1)	81.82	9.80	8.38	-	-
168	Q-cast (T2)	81.06	8.62	7.40	1.80	1.12
1000	T-cast (T1)	72.63	6.79	20.58	-	-
1000	Q-cast (T1)	83.39	8.35	5.44	1.86	0.95
1000	T-cast (T2)	80.09	9.42	10.49	-	-
1000	Q-cast (T2)	75.04	9.34	11.87	1.78	1.97

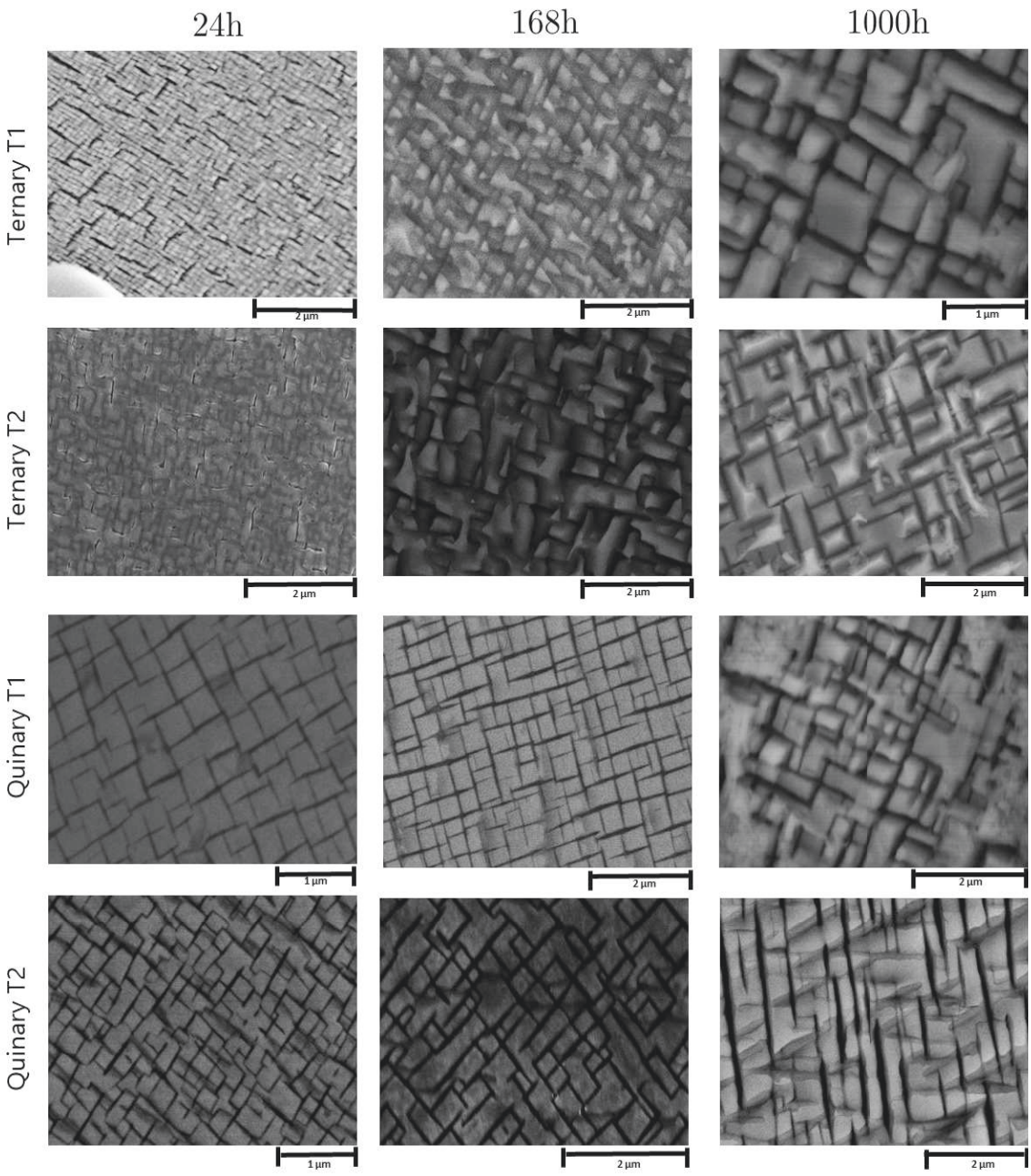

Fig. 5.19 BSE-SEM micrographs of the ternary and quinary cast alloys after 24h aged

By increasing the aging time up to 168 h, γ' cuboidal size increase in both cases, up to 240-290 nm for ternary and 220 - 340 nm for quinary, respectively. The γ' volume fraction remains constant, with an average of about 80 %. After 1000 h aging heat treatments, the cuboidal size of ternary alloys grows up to 350 - 450 nm, and 390 - 440 nm for quinary alloys. Kobayashi *et al.* [81] suggest that the small change in the volume fraction after 1000 h can induce that γ' phase is metastable and the γ-Co, β-CoAl and χ-Co_3W are in equilibrium in the ternary and quinary alloy. In any case, the morphology of the γ' precipitates remained cuboidal in all samples.

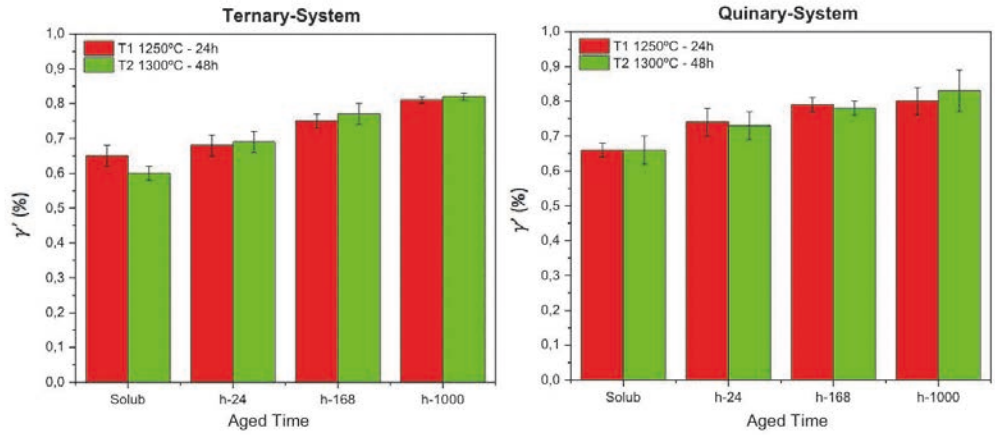

Fig. 5.20 γ' volume fraction values for ternary (left) and quinary (right) cast alloys after long term aging heat treatments

Table. 5.9 Average cuboidal size for ternary and quinary cast alloys after aging heat treatments

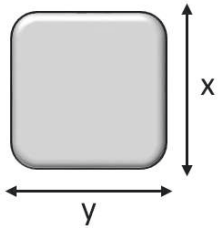		Size (nm)	
Alloy		x	y
Ternary	$T1_{(24h)}$	120 ± 10	110 ± 10
	$T2_{(24h)}$	160 ± 10	150 ± 10
	$T1_{(168h)}$	240 ± 30	280 ± 20
	$T2_{(168h)}$	280 ± 40	290 ± 30
	$T1_{(1000h)}$	400 ± 80	450 ± 60
	$T2_{(1000h)}$	350 ± 40	370 ± 50
Quinary	$T1_{(24h)}$	350 ± 50	370 ± 50
	$T2_{(24h)}$	210 ± 30	220 ± 20
	$T1_{(168h)}$	340 ± 20	330 ± 30
	$T2_{(168h)}$	220 ± 30	250 ± 30
	$T1_{(1000h)}$	410 ± 40	390 ± 50
	$T2_{(1000h)}$	440 ± 20	400 ± 20

The evolution of the Vickers microhardness with long term aging of both Cobalt-based alloys reveal the good stability of the cast microstructures (see: Fig. 5.21). After first 24 h, it can be seen an average hardness of 500 HV, being higher in the case of quinary alloys due to the higher amount of W-rich secondary precipitates around the cuboidal microstructure. Long term aging

time (900 °C up to 1000 h) allows to explore the good stability and Vickers hardness of the microstructure, achieving an average value of 320 - 400 HV for ternary alloys, and 430 - 520 HV for quinary ones, respectively. The decrease of the Vickers hardness may indicate that the peak aging condition can be stopped at 24 h. By comparing these results with Lass *et al.* study [146], with a similar composition of Ni (10 at. %), -Ti (4 at. %) and -Ta (1 % at. %), can be comparable with quinary alloys, achieving ~ 410 HV after first 24 h, increasing up to ~ 420 HV after 168 h, and a final stabilization of ~ 425 HV after 1000 h.

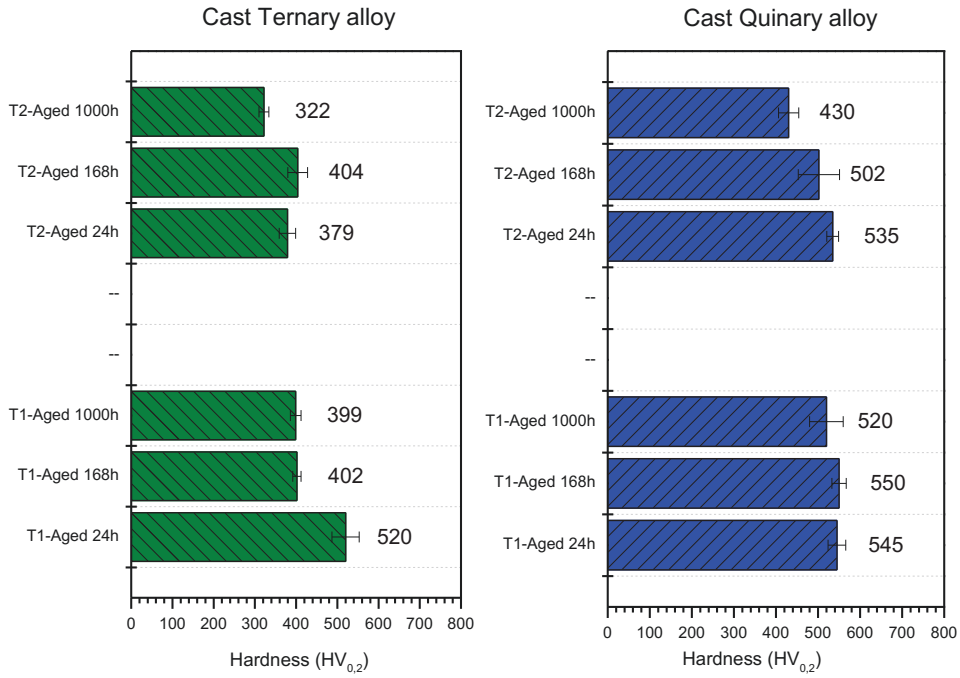

Fig. 5.21 Microhardness of ternary and quinary cast aged specimens after 24, 168 and 1000 h, respectively

5.2.3.2. Aged PM alloys

TEM analysis can show the distribution of γ' precipitates with a mean size of about 87 x 74 ± 10 nm (see: Fig. 5.22). Unlike other research's analysis, no evidence of secondary nanocubic γ' precipitates has been found between the primary γ' precipitation of cobalt-based alloy [147].

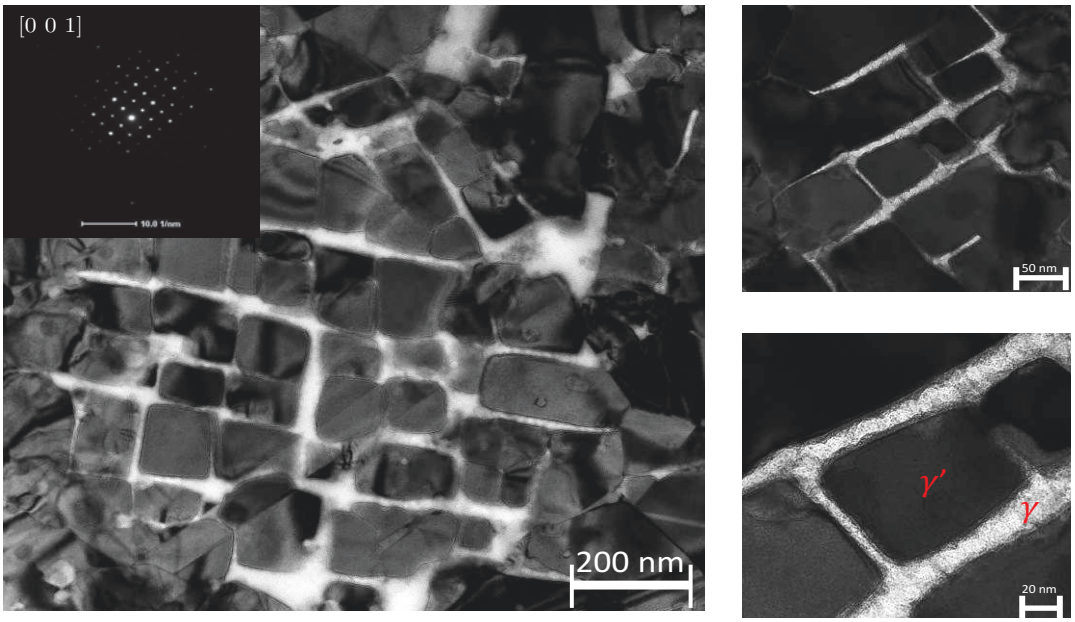

Fig. 5.22 TEM images of the ternary PM cobalt-based alloy after heat treatments

The element distribution of the ternary system is shown in Fig. 5.23. The good distribution of the -Al and -W into the cobalt microstructure is a good reflection of the formation of the ternary precipitate γ' -Co_3(Al,W). The presence of C can contribute to the precipitation of rich carbides, such as Co_3AlC with similar stoichiometry and crystal structure in small cuboidal [148], although in this case, there is no evidence of this type of precipitate.

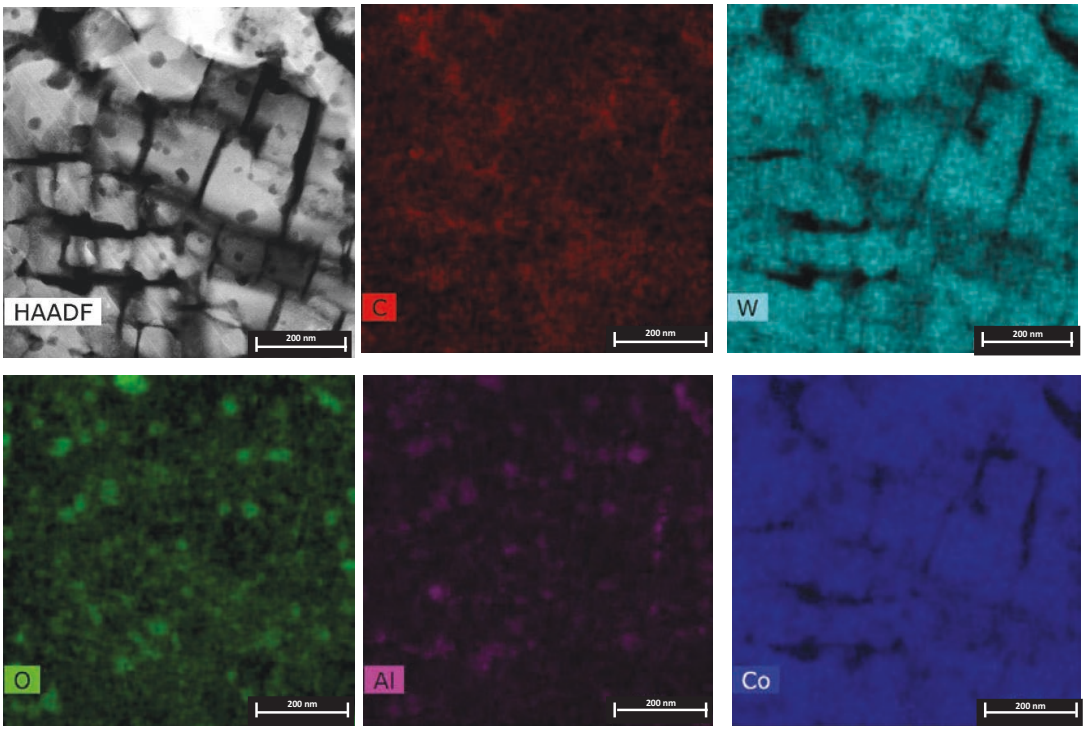

Fig. 5.23 EDX-STEM mapping of the ternary PM cobalt-based alloy

The experimental powder metallurgy alloys investigated were aged for 24 h at 900 °C. To explore the long-term phase stability, ternary and quinary system were aged additionally for 1000 h at 900 °C. An overview of the γ/γ' dual phase microstructure evolution is shown by using BSE-SEM micrographs in Fig. 5.24. After 24 h (left column), it is possible to see how ternary alloy exhibit cuboidal γ' precipitates. The following aged steps at 168 h (center column) and 1000 h (right column), do not show a visual problem in gamma phase etching removal.

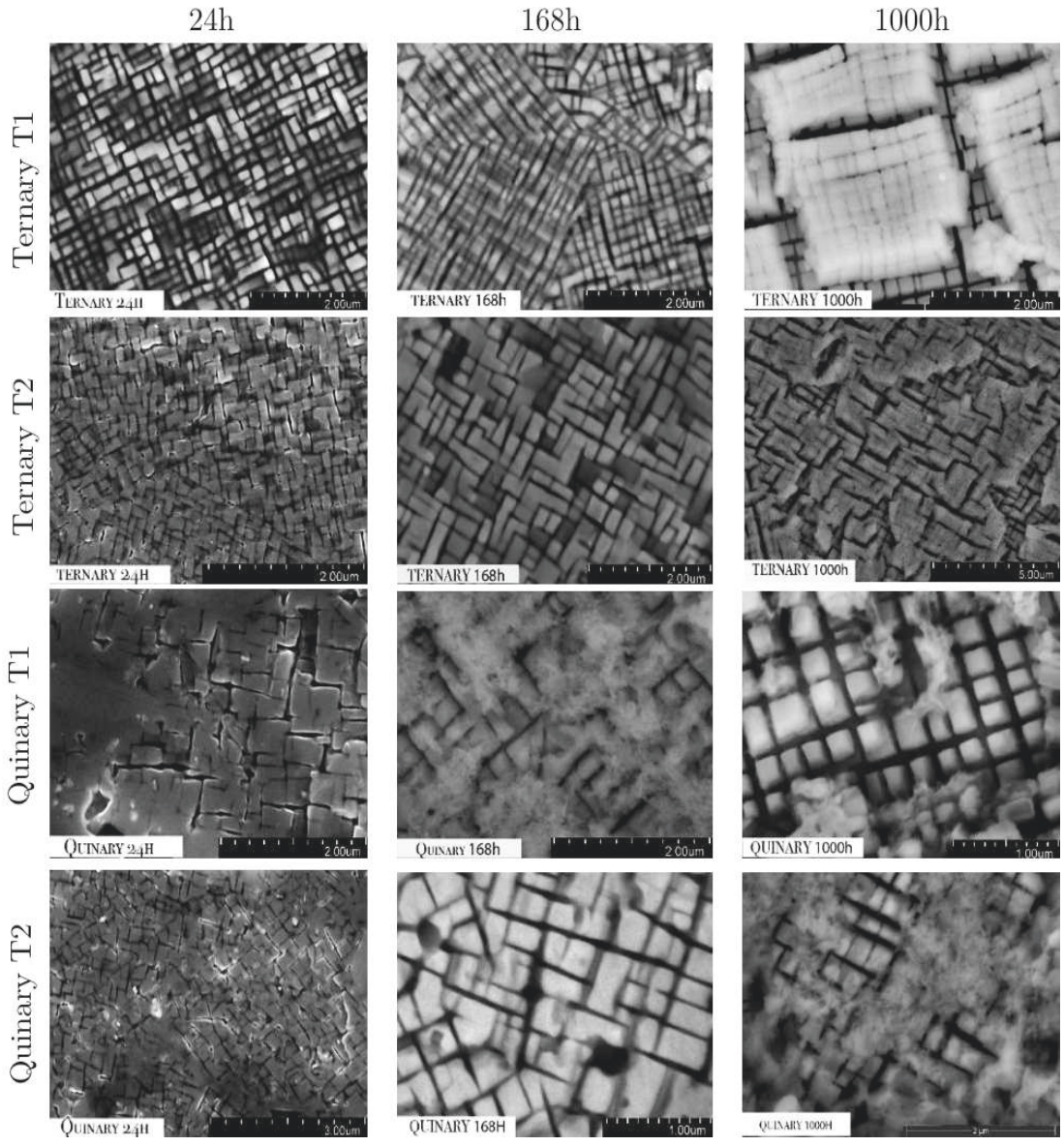

Fig. 5.24 Backscatter scanning electron microscopy micrographs of the annealed ternary and quinary PM alloys after 24h, 168h and 1000h, respectively

Chemical composition of the γ/γ' two-phase microstructure after 1000 h can confirm that no further composition changes have been occurred in both systems, (see: Table. 5.10). Furthermore, long term aging shows for all the samples an increasing size of the γ' precipitates, (see: Table. 5.11). For ternary system, a growing trend exits in γ' precipitates, from 150 – 170 nm to 270 – 280 nm cube edge length. In the case of quinary system, there is a similar growth from 160 – 190 nm to 250 – 270 nm, respectively.

Table. 5.10 Chemical composition of the cuboidal PM microstructure under study measured by EDX in FE-SEM after aging heat treatments

Time (h)	Sample	Co (at.%)	Al (at.%)	W (at.%)	Ti (at.%)	Ta (at.%)
24	T-pm (T1)	73.54	9.66	16.80	-	-
24	Q-pm (T1)	77.89	10.53	8.66	1.64	1.29
24	T-pm (T2)	76.79	9.64	13.57	-	-
24	Q-pm (T2)	81.33	8.04	7.73	1.83	1.07
168	T-pm (T1)	76.95	10.12	12.93	-	-
168	Q-pm (T1)	79.44	9.74	8.61	1.46	0.76
168	T-pm (T1)	78.33	10.04	11.63	-	-
168	Q-pm (T2)	78.94	8.61	9.69	1.64	1.11
1000	T-pm (T1)	72.29	10.21	17.51	-	-
1000	Q-pm (T1)	78.13	5.06	12.60	1.82	2.39
1000	T-pm (T2)	77.63	8.00	14.36	-	-
1000	Q-pm (T2)	76.91	7.25	11.40	2.16	2.28

Volume fraction is also increasing by long-term aging, confirming the good stability of the γ'-phase. There has been not change on the evolution of the γ' volume fraction in ternary and quinary systems, achieving more than 70 % after 1000 h, (see: Fig. 5.25). The small change of the γ' volume fraction suggest that γ'-phase is metastable and the other phases, as γ-Co and Co_3W, are in equilibrium in the system [81].

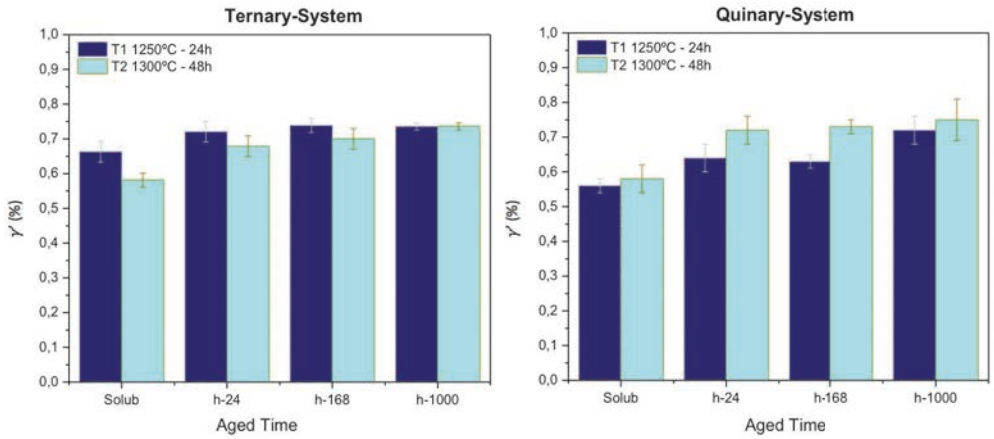

Fig. 5.25. Volume fraction values of γ' phase for ternary (left) and quinary (right) PM alloys after long term aging heat treatments

All the above microstructural properties are reflected on the evolution of the microhardness, as shown in Fig. 5.26. For ternary system (left graph), it can be seen that T1 has better Vickers hardness after aging than the other T2 solution heat treatments. After first 24 h aged, T1 has a Vickers value of 520 HV versus 368 HV obtained by T2. Once 1000 h has been achieved, T1 remains at 458 HV while T2 is reduced to 313 HV. For the quinary system (right graph), the results are inverse to the ternary system, being more profitable to apply T2 solution heat treatments to reach better Vickers hardness after aging. In the first 24 hours, T2 has a Vickers value of 659 HV and T1 has only a 535 HV. At 1000 h aged, T2 still above of T1 with a Vickers value of 610 HV vs 520 HV, respectively.

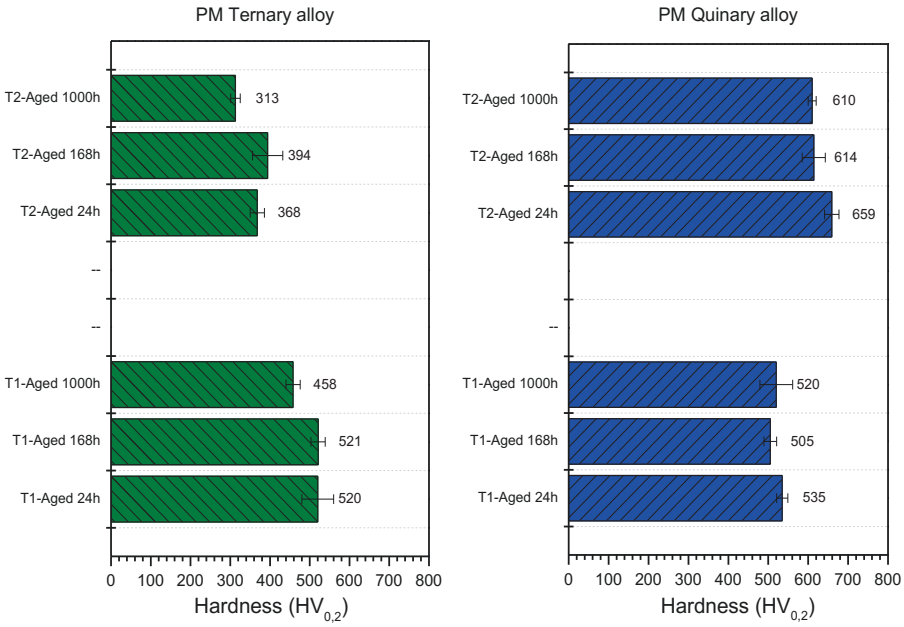

Fig. 5.26 Microhardness of ternary and quinary PM aged specimens after 24, 168 and 1000 h, respectively

Table. 5.11 Average cuboidal size for ternary and quinary PM alloys after aging heat treatments

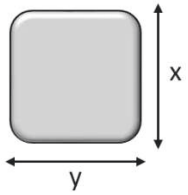		Size (μm)	
Alloy		x	Y
Ternary	$T1_{(24h)}$	150 ± 10	150 ± 20
	T2 $_{(24h)}$	170 ± 30	170 ± 20
	$T1_{(168h)}$	240 ± 10	230 ± 20
	T2 $_{(168h)}$	250 ± 10	250 ± 10
	T1 $_{(1000h)}$	270 ± 20	280 ± 20
	T2 $_{(1000h)}$	260 ± 10	270 ± 10
Quinary	$T1_{(24h)}$	180 ± 20	160 ± 30
	T2 $_{(24h)}$	190 ± 30	190 ± 20
	$T1_{(168h)}$	190 ± 20	200 ± 10
	T2 $_{(168h)}$	220 ± 30	230 ± 20
	T1 $_{(1000h)}$	250 ± 10	250 ± 10
	T2 $_{(1000h)}$	260 ± 20	270 ± 20

5.3. Remarks

In this chapter, the effect of the heat treatments on the desired γ/γ' dual phase microstructure for both cobalt-based superalloys has been studied by following casting and powder metallurgy route. The main outcomes are can be discussed as follow:

- Solution heat treatments:

Despite the processing route, it should be noted that if both compositions are compared, quinary alloy has a resulting microstructure much complex than ternary system, other reported enhanced by without regard to their specific route. Other researchers suggest that this may cause by the secondary precipitates are induced from liquid phase due to the -Ti and -Ta additions. Besides their γ'-former character -Ti and -Ta additions also act a strong carbide former. The formation of MC is also favored. MC carbides, can decomposes into $M_{23}C_6$ and M_6C carbide at high temperature [138].

Both routes can produce a dual phase microstructure with any heat treatment process (T1 and T2). The resulting γ/γ' microstructure varies in cuboidal size, misfit, volume fraction and hardness, depending of the time and temperature applied. Secondary precipitates, such as W-rich carbides, also appear in both routes, but PM can distribute it more efficiently into the dual phase microstructure than casting route. Moreover, Vickers hardness reveal better results when T1 is applied. Much of these properties are related to the increasing of secondary precipitates, where is reflected the need to apply some aging heat treatments in order to dissolve them and thus avoid the possibility of acting as stress fracture mechanisms.

- Aging heat treatments:

The aging heat treatments are fundamental for the stabilization of the γ'-phase once solution heat treatments are achieved. For this reason, a long-term aging study up to 1000 h was done to reach an optimal parameter of time vs main morphology properties of superalloys.

It is clear that both routes and systems improving their morphology properties as the exposure time increases. Volume fraction and cuboidal size increase as the time increases, being much better the first 24 hours. On the other hand, microhardness has a significant decrease the first 24 hours for both systems and routes. Since then, a subsequent increase of time can lead to a tendency to stabilize the morphological properties and microhardness.

A detailed study of each system can help to choose the most suitable heat treatment. Once morphological properties have been known for each alloy and focusing on the powder metallurgy route, it is targeted as materials to study the mechanical properties, ternary system (Co-Al-W) with a T1 solution heat treatment (1250 °C – 24 h) and 24 h aging. In the case of quinary system (Co-Al-W-Ti-Ta) it was proposed a T2 solution heat treatment (1300 °C – 48h) and 24 h aging. An overview of the main morphology properties is listed below in Table. 5.12.

Table. 5.12 Summary of the morphological properties of the selected ternary and quinary alloys processed by powder metallurgy route

	Ternary (Co-Al-W) T1 (1250 °C – 24 h)	Quinary (Co-Al-W-Ti-Ta) T2 (1300 °C – 48 h)
Volume fraction (%)	65	70
Cuboidal Size (nm)	150	190
Microhardness ($HV_{0.2}$)	520	659
Microstructure	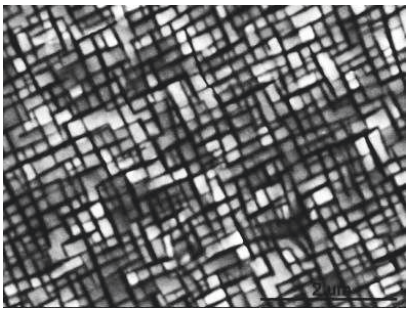	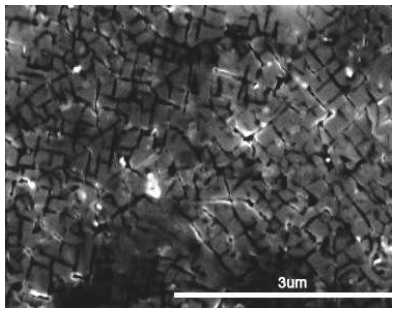

6. Dynamic behavior of powder metallurgy cobalt-based at high strain rate

This chapter is focused on the dynamic behavior of powder metallurgy cobalt-based superalloys with γ/γ' two-phase at high strain rate, once the design of the microstructure and the heat treatments have been achieved. The dynamic loading tests were conducted on a Split Hopkinson Pressure Bar (SHPB) to study the strain-rate effect at different range of temperatures, focusing on the temperature-dependent anomalies of the flow stress at elevated temperatures for both ternary and quinary alloys. In addition, these materials have to consider the strain rate and thermal softening effects. Thus, the Johnson-Cook constitutive model is proposed as a starting point to certificate the material model. Based on the experimental results, a modified model of J-C based of function piece was established for ternary and quinary cobalt-based alloys to be able to capture the anomalous peak of the flow stress, which is dependent on the temperature. It was demonstrated that the yield strength of the superalloys can be predicted over a wide range of temperatures with the modified J-C model.

6.1. Approach of High Strain Rate

It is well known that superalloys have a high resistance to deformation at high fractions of their melting temperature due to the difficulty of shearing the ordered $L1_2$ precipitates at moderate stresses and strain rates, [127, 149]. This class of materials can maintain a high level of ductility and toughness, under high rate conditions, such as, foreign object damage, preventing catastrophic failure.

As it was mentioned in chapter 3, dynamic experiments were performed at strain rates of 1000 s^{-1} over temperature range of 25 - 850 °C, using a Split Hopkinson Pressure Bar (SHPB). For high strain rates at elevated temperatures it is fundamental to heat the sample to the required uniform temperature due to the temperature gradient may exist in the elastic bars, which in turn changes the elastic constants, and thus the mechanical impedance of the bar material, leading to changes in stress wave propagation in the bars [150]. When it compares the flow stress vs temperature, the flow stress decreases to higher temperature ranges. For this class of superalloys, when flow stress is represented as a function of temperature, there is a particular characteristic where a bell-shaped peak is produced in the stress versus temperature curve at high temperature and high strain rate.

Different analytical models performed by computer simulation have been developed to predict the ballistic performance. The vast majority of finite element simulations requires that the data results be presented in terms of true stress and effective true strain. In this case, the Johnson-Cook (J-C) model is the standard for analyzing high strain rate deformations of superalloys [118]. The equation 6.1 gives the yield strength of the material (σ), as a function of effective plastic strain (ε), equivalent plastic strain rate $\dot{\varepsilon}^*$ and homologous temperature, T^* (see: equation 6.2)

$$\sigma = (A + B\,\varepsilon^n)(1 + C\,ln\,\dot{\varepsilon}^*)(1 + T^{*m}) \quad (6.1)$$

$$T^* = \frac{T - T_{room}}{T_m - T_{room}} \quad (6.2)$$

T is the current temperature of the materials in degree Celsius, and T_m is the melting temperature of the materials. The equivalent strain rate Is the adimensionalized strain rate with a value of reference, (see: Equation 6.3), where $\dot{\varepsilon}^*$ is usually 1 s^{-1}, however, other values may be chosen.

$$\dot{\varepsilon}^* = \frac{\dot{\varepsilon}}{\dot{\varepsilon}_0} \quad (6.3)$$

As can be seen in the formula, the first term describes strain hardening, second term describes the increase in strength with increased strain rate, and the last term describe the softening due to heating. One of the most important aspect that is included in J-C model is the thermal softening. Although the J-C model consider this effect, It Is not calibrated for high temperature range, where there is a more extreme environment. Most of the materials used in ballistic are tested at room temperature and extrapolated at high temperature. However, it is well known that plastic deformation generates heat and under high strain rates loading there is not sufficient time to dissipate this heat. As temperature increases, there is an adiabatic heating in the material due to the impact, leading a decrease in the mechanical properties of these materials.

Adiabatic heating can be obtained by the Taylor-Quinney approach [151], where the heat Is due to a fraction of the plastic work given by $dQ = \beta dW$, where β Is this fraction. This expression can be rewritten as:

$$\rho C_p dT = \beta \sigma d\varepsilon_p \quad (6.4)$$

and the temperature increase can be computed as:

$$T = T_0 + \int_0^{\varepsilon_p} \frac{\beta}{\rho C_p} \sigma d\varepsilon \quad (6.5)$$

6.2. The demand for heat treatments

A clear example of the important of heat treatments for high strain rate studies is shown in the stress-strain curves compressed under the strain rate of 1000 s^{-1} and obtained at room temperature (see: Fig. 6.1). These curves, as well as the fracture strain, plotted after Hopkinson bar tests, can demonstrate that heat treatments are fundamental to obtain high degree of plastic flow. As heat treatments are applied (green and black lines), the strain to failure decreased remarkably if compared with as consolidated cobalt-based alloys (red line) where no plastic deformation is appreciated. As consolidated curves demonstrate a pronounced range of strain hardening with the peak stress reaching at 2.25 GPa.

In addition, stress-strain curves with aging heat treatments improve the flow stress with a higher rupture strength value than other with solution heat treatments. This Improvement can be explained because as the γ' volume fraction increases, it also improves their ductility. In any

case, heat treatments enhance tremendously the deformation ductility compared to the as consolidated samples.

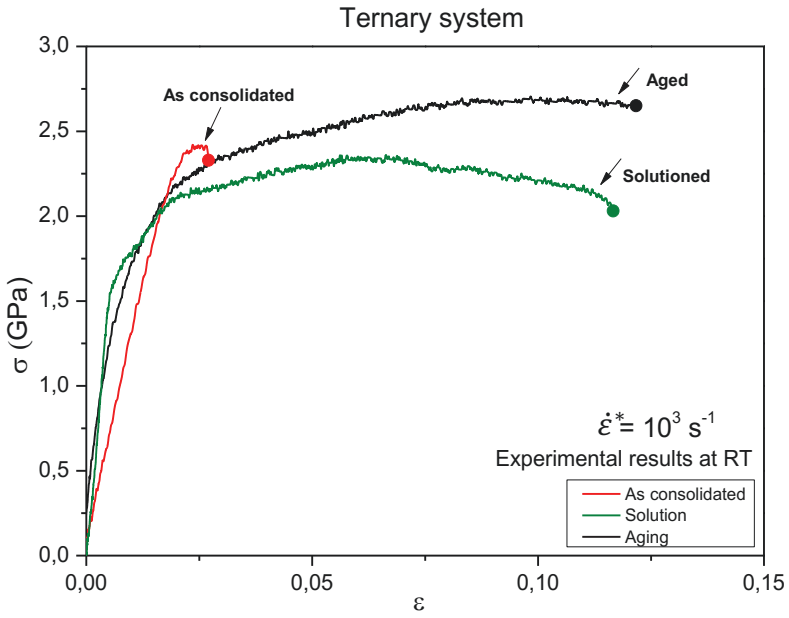

Fig. 6.1 Adiabatic Stress-strain curves in SPHB test of cobalt-based samples with different heat treatments at room temperature

6.3. Analysis of constitutive equation accuracy and Johnson-Cook model

The stress-strain curves of the ternary and quinary cobalt-based alloys at the temperatures ranging from room temperature to 850 °C tested at strain rates of 10^3 s^{-1} are shown in Fig. 6.2. In this case, it has to be considering that the end of the curves does not represent the failure of the material, since all the test were studied in compression. This end is the end of the pulse on the loading bar.

The tested materials show a clear sensitivity to the increase in temperature. The flow stress curves show similar conditions, such as, work-hardening stage caused by dislocation accumulation, followed by a flow softening stage caused by dislocation accumulation, softening caused of recovery and recrystallization, and steady state at high strain zone. In this case, the curves show clearly the elastic to plastic transition. At any particular value of strain rate, the flow stress decreases with the increase of the temperature in the 25 – 750 °C range. However, a thermal softening has to be considered in the temperature range of 700 – 800 °C.

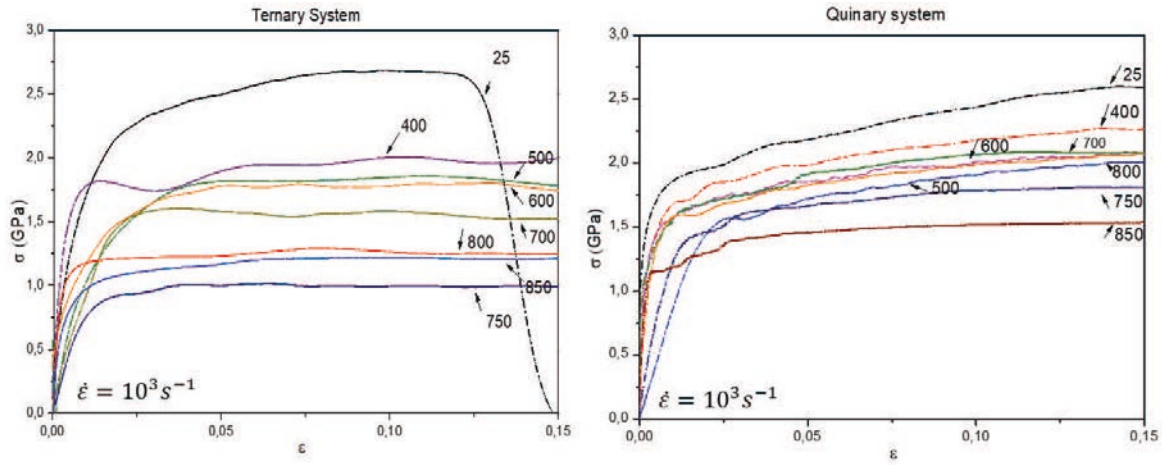

Fig. 6.2 Adiabatic True stress-strain curves of ternary (left) and quinary (right) alloys obtained from SHPB test at different temperatures

As it was mentioned in the experimental procedure (see: Chapter 3), for the development of the Johnson-Cook model, the hardening of the equivalent stress is composed of three independent terms: plastic strain hardening, plastic strain rate hardening and thermal softening. In this case, the Johnson-Cook material model has been obtained considering the behavior of the materials and the strain rate dependent. The material constants of the J-C model for cobalt-based alloy are given in

Table. 6.1 and Table. 6.2 for ternary and quinary systems, respectively. By using these parameters, it is possible to fit the desirable stress-strain curves for ternary alloys.

Fig. 6.3 show a comparison between the experimental results and J-C model of both systems alloys. It is possible to observe how this J-C model can adjust well the stress curves obtained at low temperatures, where thermal softening has no remarkable influence. It is also fundamental to consider the thermal softening due to the plastic strain under dynamic loading, because it is transformed to temperature via adiabatic heating of the materials, where there is not enough time to redistribute the heat generated. This heat increases the dislocations movement and generates thermal hardening. However, it has to be considering that J-C model cannot represents the anomalous thermal behavior from the temperature range of 700 - 750 °C, being necessary to study it in depth.

Table. 6.1 Johnson-Cook material model constants for ternary (Ts) cobalt-based superalloys

Physical properties and isotropic elastic constants for Ts				
E (GPa)	ν	ρ (kg/m^3)	C_p (J/kg°C)	χ
244	0.28	9110	420	0.9

Johnson-Cook constitutive relation for Ts							
Strain hardening			Strain rate hardening			Thermal softening	
A (MPa)	B (MPa)	n	C	$\dot{\varepsilon_0}$(s^{-1})	m	T_r (°C)	T_m (°C)
1500	2000	0.2	0.002	1.0	1.3	20	1300

Table. 6.2 Johnson-Cook material model constants for quinary (Qs) cobalt-based superalloys

Physical properties and isotropic elastic constants for Qs				
E (GPa)	ν	ρ (kg/m^3)	C_p (J/kg°C)	χ
388	0.28	9110	420	0.9

Johnson-Cook constitutive relation for Qs							
Strain hardening			Strain rate hardening			Thermal softening	
A (MPa)	B (MPa)	n	C	$\dot{\varepsilon_0}$(s^{-1})	m	T_r (°C)	T_m (°C)
1200	2500	0.25	0.002	1.0	1.4	25	1650

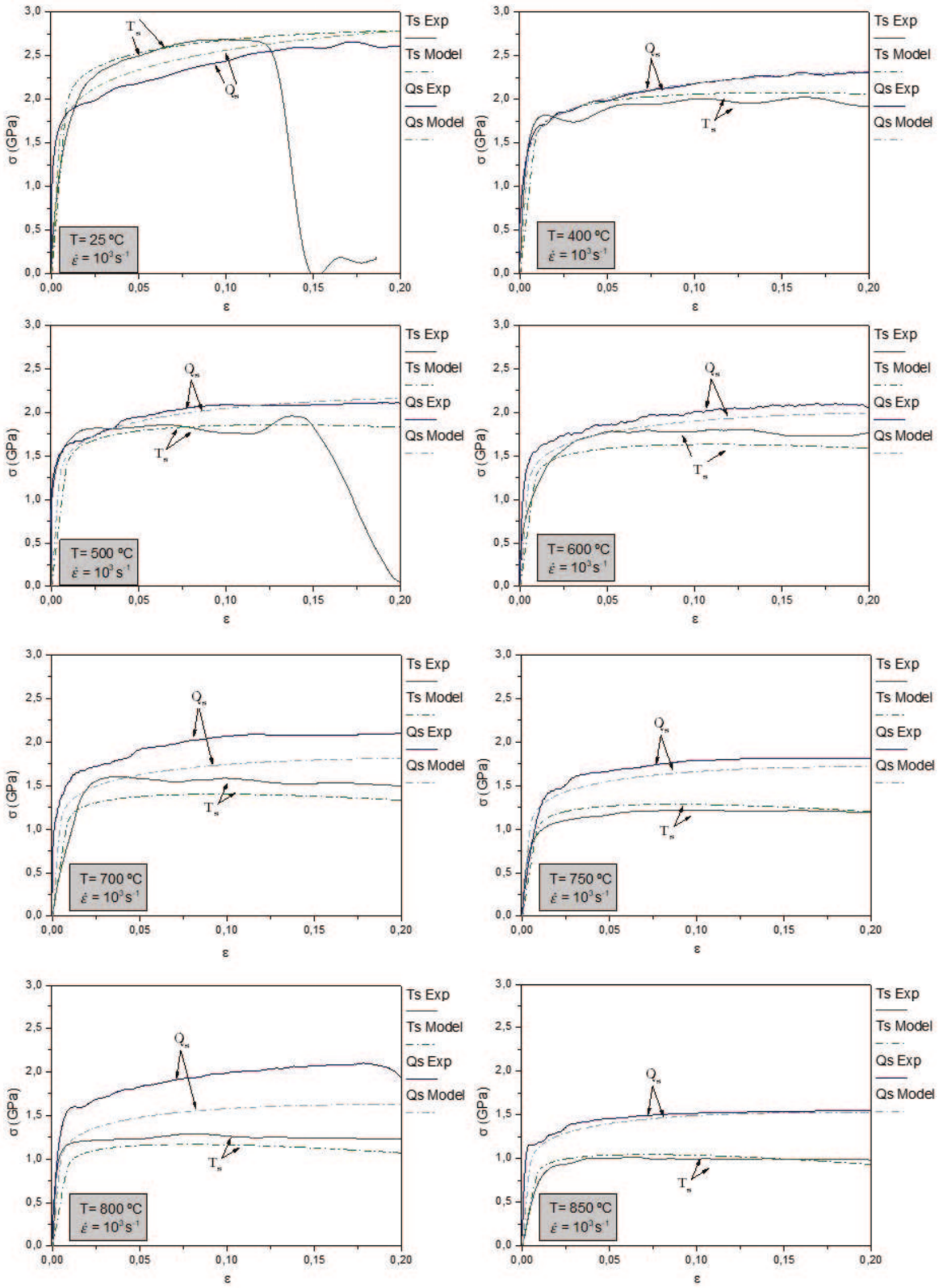

Fig. 6.3 Comparison between experimental (line) and J-C model adjustment (dot line) proposed from resulted ternary and quinary stress-strain curves at different temperatures.

6.4. Anomalous behavior of Cobalt-based superalloys over a wide range of temperatures at high strain rate

The Fig. 6.4 shows the temperature dependence of the yield stress for ternary (green line) and quinary (blue line) cobalt-based system as a function of temperature, obtained from Split Hopkinson Bar Pressure (SHBP) tests at the strain rate of 1000 s^{-1}, as well as the J-C adjustment (dot lines). The yield stress is selected either corresponding to the yield strength average measured from $\sigma_{0.1}$ to $\sigma_{0.15}$. It also should be noted that the temperature rise needs to be considered during the adiabatic process under high strain rate loading [150, 152].

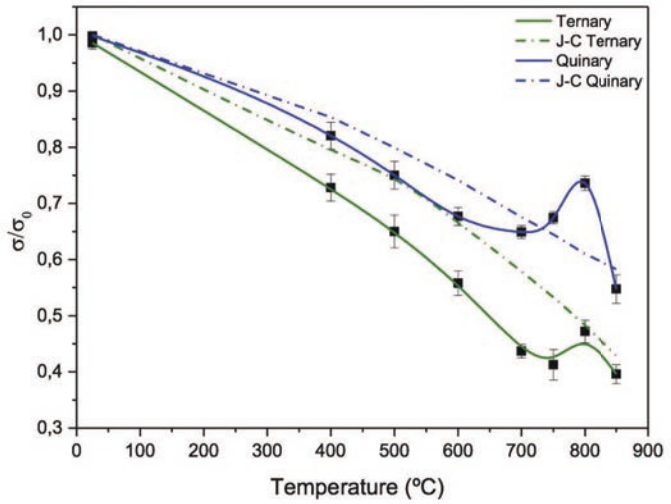

Fig. 6.4 Temperature dependence of the flow stress for high strain rate test and the Johnson Cook adjustment for ternary (green) and quinary (blue) cobalt-based superalloys

For both cobalt-based alloys, it can be seen three different steps of variation. First stage can be identified to the normal decay of flow stress with temperature over the temperature range from the room temperature to 750 °C for ternary and 700 °C for quinary, respectively. In the second variation, there is an anomalous positive temperature discrepancy where the flow stress increases with temperature, being higher in the case of quinary alloys. The last stage again displays a negative temperature variation, which is normal for materials above 50 % of their melting temperature.

On the other hand, it can be shown that the peak temperature is located at 800 °C for both alloys. 2Ta-Ti containing alloys improves their high temperature strength close to 0.35 σ/σ_0 in the peak temperature the with regards to ternary system. Above the peak, the flow stress decreases rapidly for both alloys but in any case, quinary alloys are greater than ternary alloys.

The contrary dependence of the flow stress on temperature and the peak in the flow stress at elevated temperatures has been observed in $L1_2$ and other intermetallics works and also in nickel-based alloys measured in compression with a strain rates of 10^{-4} s^{-1} [8, 66, 110], but not studied yet at strain rate of 1000 s^{-1} in cobalt-based alloys. In these previous works, it has been reported that the anomalous strengthening in γ'-$L1_2$ compounds is causes by pinning of cross-slipped screw segments of superdislocations from the octahedral (1 1 1) plane to the cube (1 0 0) plane; which is driven by elastic anisotropy and lower anti-phase boundary (APB) energy on (0 0 1) planes.

Suzuki and Pollock [127] and Suzuki *et al.* [8], reported that Co-Al-W system with γ/γ' two-phase exhibit the flow stress anomalies above 600 °C due to activation of paired ½(1 1 0) dislocation slip on both octahedral and cube planes in the γ' precipitates; Ta addition improve their strength and deformed in compression at 800 °C, due to its strong flow stress anomaly. It is also reported that this flow stress anomalies are contributed to the activation of multiple slip modes within the γ' precipitates, which include the slip of (1 1 0) dislocations below the peak and thermally activated slip of (1 1 2) dislocations above the peak.

Rhein *et al.* [153], reported that deformation is dominated by shearing with superlattice extrinsic stacking faults (SISF) formation at low temperature, while at the high temperature antiphase boundaries (APB) dominant mechanics is observed. Eggeler *et al.* [154] reported that the mode of γ' shearing is not affected by volume fractions or morphology of the γ' precipitates, indicating that the antiphase boundaries (APB) and stacking faults energies (SFE) must influence the dominant deformation mechanism. For this reason, these energies can be influenced by alloying additions, such as, Ti and Ta.

As can be observed, the proposed J-C model does not reproduce well the anomalous positive temperature dependence in both cases, since a thermal softening at high temperatures are evidenced.

6.5. Determination of modified J-C model for PM cobalt-based superalloys

Sancho *et al.* [155], determined a modified Johnson-Cook model, based on a piece function, to describe the thermal softening and hardening of material with different flow stress temperatures (see: Fig. 6.5). In this case, it is necessary to modify the thermal softening exponent of the equation 6.1 for a new function θ(T). The resumed function θ (T) is defined as, (see: Equation 6.6)

$$\theta(T) = \begin{cases} \theta_1(T) & if \quad T \leq T_1 \\ \theta_2(T) & if \quad T_1 < T \leq T_2 \\ \theta_3(T) & if \quad T_2 < T \leq T_m \end{cases} \quad (6.6)$$

where T_1 y T_2 are temperatures at which some transformation occurs in the cobalt-based material. The $\theta_1(T)$, $\theta_2(T)$, $\theta_3(T)$ are functions defined as (see: Equation 6.7, Equation 6.8 and Equation 6.9)

$$\theta_1(T) = 1 \pm \left(\frac{T-T_r}{T_1-T_r}\right)^{m_1} \frac{\Delta\sigma_1}{\sigma_r} \quad (6.7)$$

$$\theta_2(T) = \theta_1(T_1)\left[1 \pm \left(\frac{T-T_1}{T_2-T_1}\right)^{m_2} \frac{\Delta\sigma_2}{\sigma_1}\right] \quad (6.8)$$

$$\theta_3(T) = \theta_2(T_2)\left[1 \pm \left(\frac{T-T_2}{T_m-T_2}\right)^{m_1}\right] \quad (6.9)$$

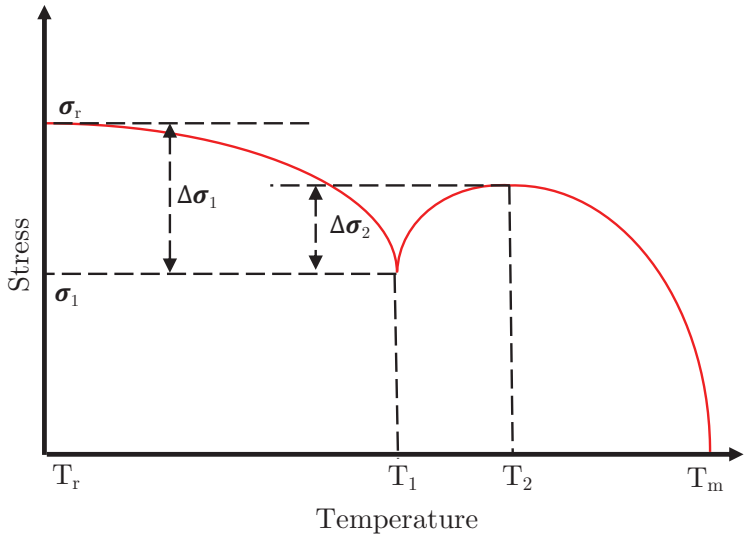

Fig. 6.5 Schematic of the evolution of stress (σ) vs temperature (T) for multiphase material

Once the constants of the modified J-C have been defined in Table. 6.3 for ternary and Table. 6.4 for quinary system, respectively, it has been possible to accurately represent the adjustment of the temperature dependence of the stress flow for high strain rate, as can be seen in Fig. 6.6 for ternary and Fig. 6.7 for quinary system, respectively.

Table. 6.3 Constant of the modified Johnson-Cook for ternary cobalt-based alloys

T_1 (°C)	m_1	$\Delta\sigma_1/\sigma_r$	T_2 (°C)	m_2
750	1.15	0.29	800	0.75
$\Delta\sigma_2/\sigma_1$	m_3	T_m (°C)	T_r (°C)	-
0.04	1.28	1000	25	-

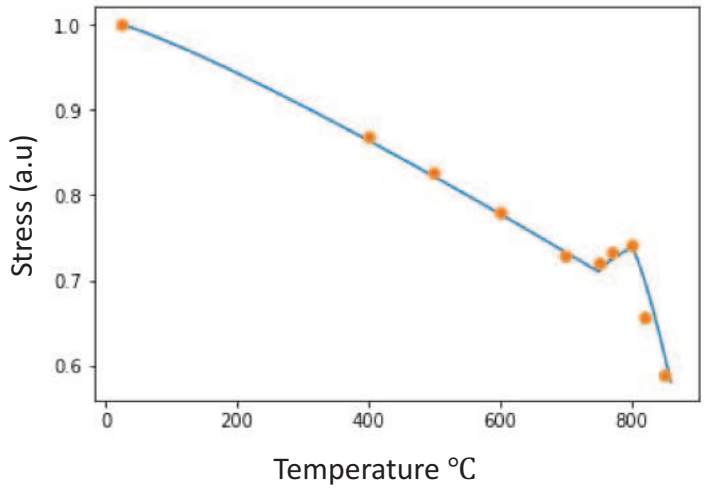

Fig. 6.6 Evolution of experimental stress (σ) vs temperature (T) and fitting model (line) of ternary system

Table. 6.4 Constant of the modified Johnson-Cook for quinary cobalt-based alloys

T_1 (°C)	m_1	$\Delta\sigma_1/\sigma_r$	T_2 (°C)	m_2
700	1.1	0.35	800	1.8
$\Delta\sigma_2/\sigma_1$	m_3	T_m (°C)	T_r (°C)	-
0.15	1.3	1000	25	-

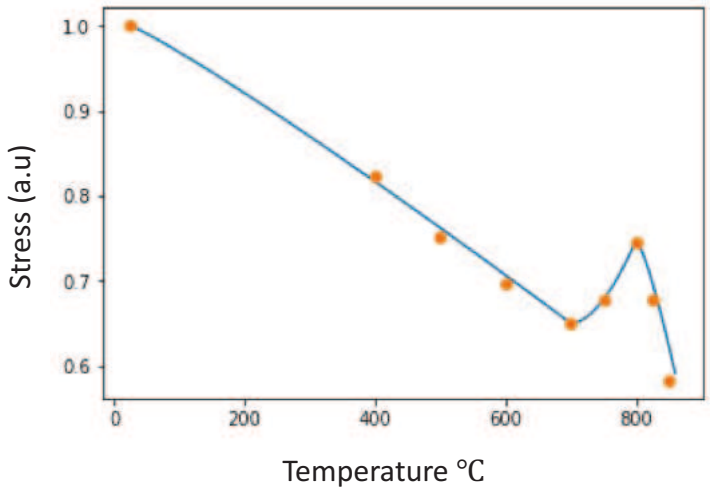

Fig. 6.7 Evolution of experimental stress (σ) vs temperature (T) and fitting model (line) of quinary system

6.6. Remarks

It is well known that microstructural parameters, (i.e., volume fraction, morphology and particle size) can coordinate the mechanical properties of the materials. In this chapter, the positive temperature dependence of flow stress showed for both compositions with the γ/γ'-two phase. A schematic of the typical flow stress as a function of temperature for the resulted composition is shown in Fig. 6.8. As it is explained in previous works, there is three different stages that matches with the ternary and quinary alloys. In the stage II it is possible to appreciate the anomalous bell-shaped peak at 800 °C.

It is clear that γ'-phase is the one of the most important reason for this kind of anomalies. Wang *et al.* [156] reported that during the deformation, the generation and motion of dislocations are restricted in the γ-phase or piled up at the γ/γ' interfaces. Ott and Mughrabi [157] confirmed that the crack can propagate along the γ-channels between the γ' particles in material with cuboidal microstructure. It is also known that the plastic deformation in γ-channels is dominantly under conditions of high temperatures. Suzuki *et al.* [8] reported that Co-Al-W system with γ/γ' two-phase exhibit the flow stress anomalies above 600 °C; and Ta addition improve their flow strength and deformed in compression at 800 °C, due to its strong flow stress anomaly. It is also reported that the peak temperature is almost the same at low compression strain rate for polycrystalline ternary alloys with different volume fraction of γ'-phase [110]. These conditions can be confirmed with the results obtained for both ternary and quinary alloys with a positive peak temperature of 800 °C, where flow stress increases with -Ta and -Ti additions. In addition,

Suzuki *et al.* [8] also reported that there is a significant density of dislocations trapped within the γ' precipitates where hyperfine γ' precipitates are found in the γ microstructure channel during cooling from elevated temperatures. It was also mentioned from Suzuki work [8], that this flow stress anomalies are contributed to the activation of multiple slip modes within the γ' precipitates, which include the slip of ⟨1 1 0⟩ dislocations below the peak and thermally activated slip of ⟨1 1 2⟩ dislocations above the peak. Furthermore, the high level of flow stress detected at 800 - 850 °C in both cobalt-based alloys can be explained by the high solvus temperature, meaning the existence of the γ'-phase at high temperature, and by the solid-solution hardening due to solute W [110].

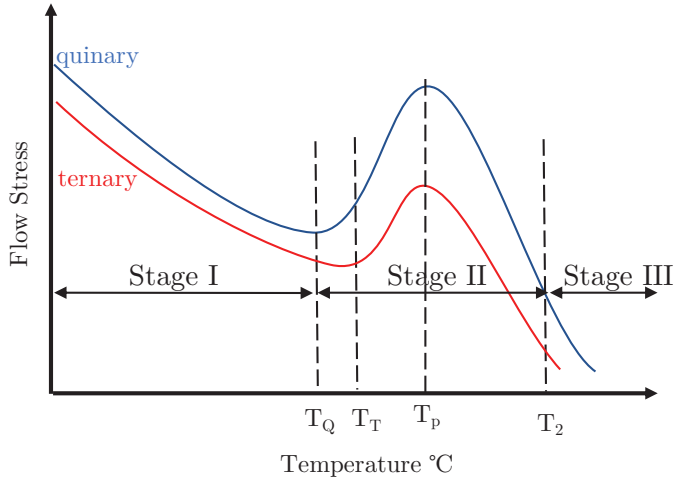

	Stage I	Stage II	T_p	Stage III	γ'-V_f (%)	Max σ/σ_0
Ternary	24 - 700	700 - 850	800	850 - T_m	65 ± 2	0.75 ± 1
Quinary	24 - 700	700 - 850	800	850 - T_m	70 ± 2	0.45 ± 3

Fig. 6.8 Schematic of the flow stress as a function of temperature with different stages at high strain rate. Table with the summary of the critical temperatures as function of volume fraction and maximum flow stress (σ/σ_0). T_Q and T_T are the start temperatures of stage II for quinary and ternary, respectively. T_P is peak temperature and T_2 is the start temperature of a stage III for both compositions.

A constitutive model is developed to calculate the flow stress as a function of the temperature with a piece function on Johnson-Cook model that allow to describe the anomalous positive peak temperature. The model was shown to be able to capture the anomalous peak of the flow stress at high strain rate for both cobalt-based alloys. The stress behavior of the superalloys can be predicted over a wide range of temperatures.

7. Conclusions and future work

In the present research work, a novel cobalt-based superalloy has been processed by powder metallurgy route. The resulted γ/γ' two-phase and their mechanical properties have been analyzed for different mechanisms with the aim of obtaining a good microstructure.

The main conclusions extracted from previous work are summarized as follows:

- It has been possible to confirm the powder metallurgy route as a real possibility for processing novel cobalt-based superalloys with a density greater than 99 %, and mechanical properties similar or even higher than conventional casting route when alloying element as titanium and tantalum are added in the cobalt system. Powders obtained by mechanical alloying depends on the particle size and the relationship between crystallite size and microstrain. However, when W is included in MA-powders, it is not possible to incorporate it totally as solid solution. There is a part of W % that will remain as free element into the particles. Unexpected secondary phases are found in the as-consolidated samples (though they are dissolved after heat treatments)

- Specific heat treatments have been applied on as-consolidated samples to turn them into the required γ' precipitation. Nevertheless, it should be noted that for both cobalt-based alloys, the γ/γ' dual phase appears just after the solution treatment even before applying aging conditions. The resulting γ/γ' microstructure varies in cuboidal size, misfit, volume fraction and hardness depending on the time and temperature applied. It has been shown that it is necessary to design, according to the specific nominal composition, the optimum parameters for the heat treatments. In this study, for ternary cobalt-based alloy, the optimum microstructure was achieved for solution treatment T1 (1250 °C – 24h) with 24h aged condition. However, for quinary alloys with a higher level of refractory elements makes it necessary to increase the solution temperature (T2 - 1300 °C, 48 h) to homogenize better the composition to obtain the dual γ/γ' microstructure. It should be noted that the secondary phases are also present in small quantities after heat treatment in quinary alloys. This may be due to the difficulty associated with dissolving the alloying elements. In aging heat treatments,

both routes improve their properties as the exposure time increases. Volume fraction and cuboidal size increase as the time increases, being much better the first 24 h. Instead, microhardness has a significant decrease the first 24 h. Since then, a subsequent increase of time can lead to a tendency to stabilize the morphological properties and microhardness. In any case, hardness testing showed that both alloys exhibit a good mechanical behavior compared with those examined in previous works. Considering the evolution of microstructures with long-term aging periods of up to 1000 h, promising creep behavior can be expected as the size of the γ' precipitate phase and volume fraction remain almost stable.

- The dynamic behavior at high strain rates performed with Hopkinson bar showed the relationship between flow stress and temperature. Instead, an anomalous positive temperature dependence of flow stress appeared for both cobalt-based alloys in the temperature above 600 °C. It is also seeming clear that γ'-phase is one of the most important reason for this kind of anomalies due to the generation and motion of dislocations are restricted in the γ phase or piled up at the γ/γ' interfaces. It was also confirmed that -Ta addition improve their flow strength and deformed in compression at 800 °C, due to its strong flow stress anomaly. The high level of flow stress detected in both alloys at 800 – 850 °C can be explained by the high solvus temperature, meaning the existence of the γ'-phase at high temperature, and by the solid-solution hardening due to solute W.

- A constitutive model has been established to calculate the flow stress as a function of the temperature with a piece function of Johnson Cook model that allow to describe the anomalous positive peak temperature. The proposed model was shown to be able to capture the anomalous peak of the flow stress at high strain rates for both alloys.

Considering the information gathered during this doctoral thesis and keeping in mid the main objective of developing a novel cobalt-based superalloy by powder metallurgy route, the following suggestions can be given for further research:

- Processing of the powders by gas atomization route**.** The possibility of an additional route for the production of prealloyed powders by Gas Atomization may help to avoid the typical contamination of carbides from high energy milling process.

- Further work could be conducted on the study of the oxidation, fatigue and wear resistance at high temperature. In order to complement the work of this thesis it is proposed to conduct a full characterization of the mechanical properties at high temperature. Previous work in cobalt-based processed by casting route can confirm that cobalt-based exhibit a better behavior of hot corrosion and wear resistance. Because of this, it is suggested to carry out these experiments in cobalt-based processed by powder metallurgy route. Moreover, the measurement of the corrosion resistance at high temperature could be a good option due to the presence of residual porosity located in the surface can affect the specimen.

- Study new alternatives to avoid the use of W such as the ternary Co-Ta-V and Co-Nb-V. Latest research works has focused on substituting some of the W with various γ' forming elements such as Ta and Nb due to their lower density (6.1 and 8.6 g/cm^3 vs 19.3 g/cm^3).

- In order to compare the full validity of the Johnson-Cook model of this superalloy, an extensive numerical analysis could be conducted to implement the proposed modified Johnson Cook model.

List of figures

List of tables

References

[1] J. Sato, T. Omori, K. Oikawa, I. Ohnuma, R. Kainuma, and K. Ishida, "Cobalt-Base High-Temperature Alloys," *Sci. 312*, vol. 90, 2006.

[2] R. Reed, *The superalloys: fundamentals and applications*. Cambridge: Cambridge University Press, 2006.

[3] C. T. Sims, N. S. Stoloff, and W. C. Hagel., *Superalloys II: High-Temperature Materials for Aerospace and Industrial Power*. 1987.

[4] S. Neumeier, L. P. Freund, and M. Goken, "Novel wrought γ-γ′ cobalt base superalloys with high strength and improved oxidation resistance," *Scr. Mater.*, vol. 109, pp. 104–107, 2015.

[5] F. Xue, H. J. Zhou, X. F. Ding, M. L. Wang, and Q. Feng, "Improved high temperature γ' stability of Co-Al-W-base alloys containing Ti and Ta," *Mater. Lett.*, vol. 112, pp. 215–218, 2013.

[6] H. Y. Yan, V. A. Vorontsov, J. Coakley, N. G. Jones, H. J. Stone, and D. Dye, "Quaternary Alloying Effects and the Prospects for a New Generation of Co-Base Superalloys," *Superalloys 2012*, pp. 705–714, 2012.

[7] A. Bauer, S. Neumeier, F. Pyczak, and M. Goken, "Microstructure and creep strength of different γ/γ′- strengthened Co-base superalloy variants," *Scr. Mater.*, vol. 63, no. 12, pp. 1197–1200, 2010.

[8] A. Suzuki, G. C. DeNolf, and T. M. Pollock, "Flow stress anomalies in γ-γ' two-phase Co-Al-W-base alloys," *Scr. Mater.*, vol. 56, no. 5, pp. 385–388, 2007.

[9] A. Suzuki and T. M. Pollock, "High-temperature strength and deformation of γ-γ' two-phase Co-Al-W-base alloys," *Acta Mater.*, vol. 56, no. 6, pp. 1288–1297, 2008.

[10] T. M. Pollock, J. Dibbern, M. Tsunekane, J. Zhu, and A. Suzuki, "New Co-Based γ-γ′ High-temperature Alloys," *JOM*, vol. 58, p. 62, 2010.

[11] F. Xue, H. Zhou, X. Chen, Q. Shi, H. Chang, M. Wang, X. Ding, Q. Feng, "Creep behavior of a novel Co-Al-W-base single crystal alloy containing Ta and Ti at 982 ∘ C," *MATEC Web Conf.*, vol. 14, p. 15002, 2014.

[12] K. Ishida, "Intermetallic compounds in co-based alloys-phase stability and application to superalloys," *Mater. Res. Soc.*, vol. 1128, 2009.

[13] M. J. Donachie and S. J. Donachie, *Superalloys A Technical Guide*. 2002.

[14] T. P. Transformation, S. Crystals, T. O. D. Frequency, N. H. Group, and P. Link, "The Phase Transformation of Cobalt as Observed on Single Crystals*," 1952.

[15] K. Z. F. Frey, W. Prandl, J. Schneider, C. Zeyens, "The HCP-FCC transition in pure Co investigated by neutron scattering," *J. Phys. F Met. Phys.*, vol. 9, no. 4, pp. 603–613, 1979.

[16] A. P. Mouritz, *Introduction to aerospace materials*. Woodhead Publishing materials, 2012.

[17] R. M'Saoubi, D. Axinte, S. Soo, C. Nobel, H. Attia, G. Kappmeyer, S. Engin, M. Sim, "High performance cutting of advanced aerospace alloys and composite materials," *CIRP Ann. - Manuf. Technol.*, vol. 64, no. 2, pp. 557–580, 2015.

[18] Z. Y. Li, X. T. Wei, Y. B. Guo, and M. P. Sealy, "State-Of-Art, Challenges, and Outlook on Manufacturing of Cooling Holes for Turbine Blades," *Mach. Sci. Technol.*, vol. 19, no. 3, pp. 361–399, Jul. 2015.

[19] Y. B. Guo, W. Li, and I. S. Jawahir, "Surface integrity characterization and prediction in machining of hardened and difficult-to machine alloys: a state-of-art research review and analysis," *Mach. Sci. Technol.*, vol. 13, no. 4, pp. 437–470, Nov. 2009.

[20] A. Thakur and S. Gangopadhyay, "State-of-the-art in surface integrity in machining of nickel-based super alloys," *Int. J. Mach. Tools Manuf.*, vol. 100, pp. 25–54, 2016.

[21] T. M. Pollock and S. Tin, "Nickel-Based Superalloys for Advanced Turbine Engines: Chemistry, Microstructure and Properties," *J. Propuls. Power*, vol. 22, no. 2, pp. 361–374, 2006.

[22] M. Zieliñska, M. Yavorska, M. Porêba, and J. Sieniawski, "Thermal properties of cast nickel based superalloys," *Arch. Mater. Sci. Eng.*, vol. 44, no. 1, pp. 35–38, 2010.

[23] C. S. Lee, "Precipitation-Hardening Characteristics of Ternary Cobalt - Aluminum - X Alloys," 1971.

[24] J. M. D. J.M. Blaise, P. Viatour, "Cobalt 49," p. 192, 1970.

[25] D. C. P. Viatour, J.M. Drapier, "Cobalt 3," p. 67, 1973.

[26] D. C. J.M. Drapier, J.L. de Brouwer, "Cobalt 27," p. 59, 1965.

[27] D. C. J.M. Drapier, "Cobalt 39," p. 63, 1968.

[28] N. L. Okamoto, T. Oohashi, H. Adachi, K. Kishida, H. Inui, and P. Veyssière, "Plastic deformation of polycrystals of $Co_3(Al,W)$ with the $L1_2$ structure," *Philos. Mag.*, vol. 91, no. 28, pp. 3667–3684, 2011.

[29] K. Tanaka, M. Ooshima, N. Tsuno, A. Sato, and H. Inui, "Creep deformation of single crystals of new Co–Al–W-based alloys with fcc/$L1_2$ two-phase microstructures," *Philos. Mag.*, vol. 92, no. 32, pp. 4011–4027, Nov. 2012.

[30] C. T. Sims, "A History of Superalloy Metallurgy for Superalloy Metallurgists," *Superalloys 1984 (Fifth Int. Symp.*, pp. 399–419, 1984.

[31] A. Mottura, A. Janotti, and T. M. Pollock, "Alloying effects in the gamma prime phase of Co-base superalloys," *Superalloys 2012 12th Int. Symp. Superalloys.*, p. 685, 2012.

[32] R. M. Forbes Jones and L. a. Jackman, "The structural evolution of superalloy ingots during hot working," *Jom*, vol. 51, no. 1, pp. 27–31, 1999.

[33] M. Durand-charre, *The microstructure of superalloys*. 1997.

[34] C. T. Sims, "A contemporary view of nickel-base superalloys," *JOM*, vol. 18, no. 10, pp. 1119–1130, 1966.

[35] W. H. Jiang, X. D. Yao, H. R. Guan, and Z. Q. Hu, "Secondary M_6C precipitation in a cobalt-base superalloy," *J. Mater. Sci. Lett.*, vol. 18, pp. 303–305, 1999.

[36] C. C. J. Engler-Pinto, C. Noseda, M. Y. Nazmy, and F. Rezai-Aria, "Interaction between creep and thermo-mechanical fatigue of CM 247 LC-DS," *Superalloys 1996*, pp. 319–325, 1996.

[37] J. E. Doherty, B. H. Kea, and A. F. Giamei, "On the origin of the ductility enhancement in Hf-doped Mar-M200," *JOM*, vol. 23, no. 11, pp. 59–62, 1971.

[38] Y. Chen, *F. Xue, S. Mao, H. Long, B. Zhang, Q. Deng, Y. Liu, P. Maguire, H. Zhang, X. Han, Q. Feng.*, "Elemental preference and atomic scale site recognition in a Co-Al-W-base superalloy," *Sci. Rep.*, vol. 7, no. 1, pp. 1–6, 2017.

[39] R. A. Ricks, A. J. Porter, and R. C. Ecob, "The growth of γ′ precipitates in nickel-base superalloys," *Acta Metall.*, vol. 31, no. 1, pp. 43–53, Jan. 1983.

[40] G. Blaine, L. Hugo, and H. Xiao, *Superalloys: Alloying and Performance*. The Materials Information Society, 2010.

[41] M. P. Jackson and R. C. Reed, "Heat treatment of UDIMET 720Li: The effect of microstructure on properties," *Mater. Sci. Eng. A*, vol. 259, no. 1, pp. 85–97, 1999.

[42] H. S. Ko, K. W. Paik, L. J. Park, Y. G. Kim, and J. H. Tundermann, "Influence of rhenium on the microstructures and mechanical properties of a mechanically alloyed oxide dispersion-strengthened nickel-base superalloy," *J. Mater. Sci.*, vol. 33, no. 13, pp. 3361–3370, Jul. 1998.

[43] C. T. Sims, N. S. Stoloff, and W. C. Hagel, "Superalloys II." Wiley, New York, 1987.

[44] P. Zhang, Q. Zhu, G. Chen, H. Qin, and C. Wang, "Effect of heat treatment process on microstructure and fatigue behavior of a nickel-base superalloy," *Materials (Basel).*, vol. 8, no. 9, pp. 6179–6194, 2015.

[45] B. B. Seth, "Superalloys: The Utility Gas Turbine Perspective," *Superalloys 2000 (Ninth Int. Symp.*, pp. 3–16, 2000.

[46] E. C. Caldwell, F. J. Fela, G. E. Fuchs, and N. Rene, "Segregation of Elements in High Refractory Content Single Crystal Nickel Based Superalloys," *Superalloys 2004*, pp. 811–818, 2004.

[47] S. R. Hegde, R. M. Kearsey, and J. Beddoes, "Design of solutionizing heat treatments for an experimental single crystal superalloy," pp. 301–310, 2008.

[48] S. L. Semiatin, R. C. Kramb, R. E. Turner, F. Zhang, and M. M. Antony, "Analysis of the homogenization of a nickel-base superalloy," *Scr. Mater.*, vol. 51, no. 6, pp. 491–495, 2004.

[49] S. Tang, Z. Zheng, and L. K. Ning, "Gamma prime coarsening in a nickel base single crystal superalloy," *Mater. Lett.*, vol. 128, pp. 388–391, 2014.

[50] F. C. Campbell, *Manufacturing Technology for Aerospace Structural Materials*. 2013.

[51] L. Xu, C. G. Tian, C. Y. Cui, Y. F. Gu, and X. F. Sun, "Morphology evolution of unstable γ′ in Ni–Co based superalloy," *Mater. Sci. Technol.*, vol. 30, no. 8, pp. 962–967, 2014.

[52] S. Miura, K. Ohkubo, and T. Mohri, "Mechanical Properties of Co-Based $L1_2$ Intermetallic Compound $Co_3(Al,W)$," *Mater. Trans.*, vol. 48, no. 9, pp. 2403–2408, 2007.

[53] S. Kobayashi, Y. Tsukamoto, T. Takasugi, H. Chinen, T. Omori, K. Ishida, S. Zaefferer, "Determination of phase equilibria in the Co-rich Co-Al-W ternary system with a diffusion-couple technique," *Intermetallics*, vol. 17, no. 12, pp. 1085–1089, 2009.

[54] F. Pyczak, A. Bauer, M. Goken, U. Lorenz, S. Neumeier, M. Oehring, J. Paul, N. Schell, A. Schreyer, A. Stark, F. Symanzik, "The effect of tungsten content on the properties of $L1_2$-hardened Co-Al-W alloys," *J. Alloys Compd.*, vol. 632, pp. 110–115, 2015.

[55] S. K. Makineni, B. Nithin, and K. Chattopadhyay, "Synthesis of a new tungsten-free γ-γ′ Cobalt-based superalloy by tuning alloying additions," *Acta Mater.*, vol. 85, pp. 85–94, 2015.

[56] S. K. Makineni, A. Samanta, T. Rojhirunsakool, T. Alam, B. Nithin, A.K. Singh, R. Banerjee, K. Chattopadhyay, "A new class of high strength high temperature Cobalt based γ-γ′ Co-Mo-Al alloys stabilized with Ta addition," *Acta Mater.*, vol. 97, pp. 29–40, 2015.

[57] E. A. Lass, D. J. Sauza, D. C. Dunand, and D. N. Seidman, "Multicomponent γ'-strengthened Co-based superalloys with increased solvus temperatures and reduced mass densities," *Acta Mater.*, vol. 147, pp. 284–295, 2018.

[58] A. Bauer, S. Neumeier, F. Pyczak, R. F. Singer, and M. Göken, "Creep properties of different γ′-strengthened Co-base superalloys," *Mater. Sci. Eng. A*, vol. 550, pp. 333–341, 2012.

[59] I. Povstugar, P. Choi, S. Neumeier, A. Bauer, C. Zenk, M. Goken, D. Raabe, "Elemental partitioning and mechanical properties of Ti- and Ta-containing Co-Al-W-base superalloys studied by atom probe tomography and nanoindentation," *Acta Mater.*, vol. 78, pp. 78–85, 2014.

[60] F. Xue, M. Wang, and Q. Feng, "Alloying Effects on Heat-Treated Microstructure in Co-Al-W-Base Superalloys at 1300°C and 900°C," *Superalloys 2012*, pp. 813–821, 2012.

[61] R. . Davies and N. S. Stoloff, "On the yield stress of aged NiaAl alloys," *Trans. Met. Soc AIME*, no. 233, p. 714, 1965.

[62] P. H. Thornton and R. G. Davies, "The temperature dependence of the flow stress of gamma prime phases having the Ll2 structure," *Metall. Mater. Trans. B*, vol. 1, no. 2, pp. 549–550, Feb. 1970.

[63] L. Kovarik, R. Unocic, J. Li, P. Sarosi, C. Shen, Y. Wang, M.J. Mills., "Microtwinning and other shearing mechanisms at intermediate temperatures in Ni-based superalloys," *Prog. Mater. Sci.*, vol. 54, no. 6, pp. 839–873, 2009.

[64] C. M. F. Rae and R. C. Reed, "Primary creep in single crystal superalloys: Origins, mechanisms and effects," *Acta Mater.*, vol. 55, no. 3, pp. 1067–1081, 2007.

[65] R. C. Reed, N. Matan, D. C. Cox, M. A. Rist, and C. M. F. Rae, "Creep of CMSX-4 superalloy single crystals: effects of rafting at high temperature," *Acta Mater.*, vol. 47, no. 12, pp. 3367–3381, 1999.

[66] F. Pyczak, A. Bauer, M. Goken, S. Neumeier, U. Lorenz, M. Oehring, "Plastic deformation mechanisms in a crept $L1_2$ hardened Co-base superalloy," *Mater. Sci. Eng. A*, vol. 571, pp. 13–18, 2013.

[67] M. S. Titus, A. Suzuki, and T. M. Pollock, "Creep and directional coarsening in single crystals of new γ–γ′ cobalt-base alloys," *Scr. Mater.*, vol. 66, no. 8, pp. 574–577, 2012.

[68] Benjamin J.S, "Mechanical Alloying," *Sci Amer*, no. 234, pp. 40–49, 1976.

[69] J. Benjamin, E. Arzt, and L. Schultz, "New materials by mechanical alloying techniques," *Oberursel, Ger. DGM Informationgesellschaft*, pp. 3–21, 1989.

[70] J. S. Benjamin and M. J. Bomford, "Dispersion strengthened aluminum made by mechanical alloying," *Metall. Trans. A*, vol. 8, no. 8, pp. 1301–1305, 1977.

[71] J. H. Weber and M. K. B. T. Banerjee, "Nickel-Based Superalloys: Alloying," in *Reference Module in Materials Science and Materials Engineering*, Elsevier, 2016.

[72] M. H. Bocanegra-Bernal, "Hot isostatic pressing (HIP) technology and its applications to metals and ceramics," *J. Mater. Sci.*, vol. 39, no. 21, pp. 6399–6420, 2004.

[73] C. Suryanarayana, "Mechanical alloying and milling," *Prog. Mater. Sci.*, vol. 46, no. 1–2, pp. 1–184, 2001.

[74] W. Cao, "Synthesis of Nanomaterials by High Energy Ball Milling," *Skyspring Nanomaterials, Inc.* .

[75] W. I. Eckert, J.Holzer J.C., C.E. III, and Johnson, "Structural and thermodynamic properties of nanocrystalline fcc metals prepared by mechanical attrition," *J. Mater Res*, vol. 7, p. 1751, 1992.

[76] F. A. Mohamed and Y. Xun, "On the minimum grain size produced by milling Zn-22%Al," *Mater. Sci. Eng. A*, vol. 358, no. 1–2, pp. 178–185, 2003.

[77] M.M. Baloch and H.K.D.H. Bhadeshia;, "Directional recrystallisation in Inconel MA 6000 nickel base oxide dispersion strengthened superalloy," *Mater. Sci. Technol.*, vol. 6, pp. 1236–1246, 1990.

[78] L. Zhang, X. Qu, X. He, D. Rafi-Ud, M. Qin, and H. Zhu, "Hot deformation behavior of Co-base ODS alloys," *J. Alloys Compd.*, vol. 512, no. 1, pp. 39–46, 2012.

[79] A. M. Mebed, M. I. Abd-Elrahman, A. M. Abd-Elnaiem, and M. A. Gaffar, "Thermal analysis study for the phase determination and instable to metastable transformation of the Co–13Cu alloy," *Phase Transitions*, vol. 82, no. 8, pp. 587–598, Aug. 2009.

[80] M. Zhu, X. Z. Che, Z. X. Li, J. K. L. Lai, and M. Qi, "Mechanical alloying of immiscible Pb-Al binary system by high energy ball milling," *J. Mater. Sci.*, vol. 33, no. 24, pp. 5873–5881, 1998.

[81] S. Kobayashi, Y. Tsukamoto, and T. Takasugi, "The effects of alloying elements (Ta, Hf) on the thermodynamic stability of gamma-gamma prime;-Co_3(Al,W) phase," *Intermetallics*, vol. 31, pp. 94–98, 2012.

[82] R. Muñoz-Moreno, E. M. Ruiz-Navas, B. Srinivasarao, and J. M. Torralba, "Microstructural development and mechanical properties of PM Ti-45Al-2Nb-2Mn-0.8vol.% TiB2 processed by field assisted hot pressing," *J. Mater. Sci. Technol.*, vol. 30, no. 11, pp. 1145–1154, 2014.

[83] B. Srinivasarao, J. M. Torralba, M. A. Jabbari Taleghani, and M. T. Perez-Prado, "Very strong pure titanium by field assisted hot pressing of dual phase powders," *Mater. Lett.*, vol. 123, pp. 75–78, 2014.

[84] C. C. Koch and J. D. Whittenberger, "Mechanical milling/alloying of intermetallics," *Intermetallics*, vol. 4, no. 5, pp. 339–355, 1996.

[85] K. Takezawa, S. Ukai, and S. Hayashi, "Microstructure Control of Co-Base ODS Alloys," in *Advanced Materials, CEAM 2011*, 2011, vol. 239, pp. 864–867.

[86] D. Cui, "Preparation of ODS Cobalt Base Superalloy by Mechanical Alloying and Spark Plasma Sintering," pp. 5377–5380, 2011.

[87] H. Yu, S. Ukai, and N. Oono, "Tensile properties of Co-based oxide dispersion strengthened superalloys," *J. Alloys Compd.*, vol. 714, pp. 715–724, 2017.

[88] T. Sasaki, K. Takezawa, S. Ukai, N. Oono, and S. Hayashi, "Effect of heat treatment on the hardness and microstructure in Co-3Al-1.5Y_2O_3-1.2Hf ODS alloy," *Mater. Sci. Eng. A*, vol. 601, pp. 139–144, 2014.

[89] H. Yu, S. Ukai, S. Hayashi, and N. H. Oono, "Effect of Cr and Y_2O_3 on the oxidation behavior of Co-based oxide dispersion strengthened superalloys at 900 °C," *Corros. Sci.*, vol. 127, no. October 2016, pp. 147–156, 2017.

[90] L. Zhang, S. Ukai, T. Hoshino, S. Hayashi, and X. Qu, "Y_2O_3 evolution and dispersion refinement in Co-base ODS alloys," *Acta Mater.*, vol. 57, no. 12, pp. 3671–3682, 2009.

[91] L. Zhang *et al.*, "Microstructural Formation in Novel Co-Base ODS Alloys Produced by Mechanical Alloying," *Adv. Mater. Res.*, vol. 415–417, pp. 1136–1139, 2011.

[92] L. Zhang, X. Qu, M. Qin, Rafi-Ud-Din, X. He, and Y. Liu, "Microstructure and mechanical properties of γ' strengthened Co-Ni-Al-W-base ODS alloys," *Mater. Chem. Phys.*, vol. 136, no. 2–3, pp. 371–378, 2012.

[93] D. Moon and J. . Campbell, "Effects of Moderately High Strain Rates on the Tensile Properties of Metals," p. 9, 1961.

[94] P. S. Follansbee, "High strain rate deformation in fcc metals and alloys," *Los Alamos Rep.*, p. LA-UR-85-3026, 1985.

[95] G. T. (Rusty) Gray, "High-Strain-Rate Deformation: Mechanical Behavior and Deformation Substructures Induced," *Annu. Rev. Mater. Res.*, vol. 42, no. 1, pp. 285–303, 2012.

[96] B. Hopkinson, "The effects of momentary stresses in metals," *Proc. R. Soc. London*, pp. 498–506, 1904.

[97] J. Hopkinson, "On the rupture of iron wire by a blow," *Manchester Lit. Philos. Soc.*, vol. 11, pp. 40–45, 1872.

[98] J. Hopkinson, "Further experiments on the rupture of iron wire," *Manchester Lit. Philos. Soc.*, vol. 11, pp. 119–121, 1872.

[99] B. Hopkinson, "A method of measuring the pressure produced in the detonation of high explosives or by the impact of bullets," *Phil. Trans R. Soc. London*, vol. 213, p. 438, 1913.

[100] H. Kolsky, "An investigation of the mechanical properties of materials at very high rate of loading," *Proc. Phys. Soc London*, no. 62, pp. 676–700, 1949.

[101] R. S. Cadenas, "A review of the Split Hopkinson Bar System," Escuela Técnica Superior de Ingenieros de Caminos, Canales y Puertos, 2016.

[102] H.L. Lukas, S. G. Fries, and B. Sundman, *Computational Thermodynamics – The Calphad Method*. Cambridge, 2007.

[103] M. Cartón-Cordero, B. Srinivasarao, M. Campos, A. García-Junceda, and J. M. Torralba, "On the role of processing parameters in sintered new Co-based (W,Al) alloys," *J. Alloys Compd.*, vol. 674, pp. 406–412, 2016.

[104] A. García-Junceda, M. Rincón, and J. M. Torralba, "Development of Duplex Stainless Steels by Field-Assisted Hot Pressing: Influence of the Particle Size and Morphology of the Powders on the Final Mechanical Properties," *Metall. Mater. Trans. A Phys. Metall. Mater. Sci.*, vol. 49, no. 1, pp. 264–271, 2018.

[105] N. V. Kazantseva, S.L. Demakov, A.S. Yurovskikh, N.N. Stepanova, N.I. Vinogradova, D.I. Davydov, S.V. Lepikhin, "Phase diagram of the Co–Al–W system. structure and phase transformations near the Co_3(Al, W) intermetallic composition range," *Phys. Met. Metallogr.*, vol. 117, no. 7, pp. 701–709, 2016.

[106] K. Tanaka, T. Ohashi, K. Kishida, and H. Inui, "Single-crystal elastic constants of $Co_3(Al,W)$ with the $L1_2$ structure," *Appl. Phys. Lett.*, vol. 91, no. 18, pp. 1–4, 2007.

[107] C. H. Zenk, A. Bauer, P. Goik, S. Neumeier, H. J. Stone, and M. Göken, "Microstructure, Lattice Misfit, and High-Temperature Strength of γ′-Strengthened Co-Al-W-Ge Model Superalloys," *Metall. Mater. Trans. A Phys. Metall. Mater. Sci.*, vol. 47, no. 5, pp. 2141–2149, 2016.

[108] L. Shi, J. J. Yu, C. Y. Cui, and X. F. Sun, "Effect of Ta additions on microstructure and mechanical properties of a single-crystal Co-Al-W-base alloy," *Mater. Lett.*, vol. 149, pp. 58–61, 2015.

[109] J. Zhu, M. S. Titus, and T. M. Pollock, "Experimental Investigation and Thermodynamic Modeling of the Co-Rich Region in the Co-Al-Ni-W Quaternary System," *J. Phase Equilibria Diffus.*, vol. 35, no. 5, pp. 595–611, 2014.

[110] K. Shinagawa, T. Omori, K. Oikawa, R. Kainuma, and K. Ishida, "Ductility enhancement by boron addition in Co-Al-W high-temperature alloys," *Scr. Mater.*, vol. 61, no. 6, pp. 612–615, 2009.

[111] P. Scherrer, "Bestimmung der Grösse und der inneren Struktur von Kolloidteilchen mittels Röntgenstrahlen," *Nachr. Ges. Wiss. Göttingen*, vol. 26, pp. 98–100, 1918.

[112] S. Swapp, "Scanning Electron Microscopy (SEM)," *University of Wyoming.* .

[113] C. F. C. Anthony, *Introduction to contact mechanics*. New York: Springer-Verlag, 2000.

[114] W. C. Oliver and G. M. Pharr, "Measurement of hardness and elastic modulus by instrumented indentation: Advances in understanding and refinements to methodology," *J. Mater. Res.*, vol. 19, no. 01, pp. 3–20, 2004.

[115] W. C. Oliver and G. M. Pharr, "experiments," *J. Mater Res*, vol. 7, no. 6, pp. 1564–1583, 1992.

[116] W. Yan, C. L. Pun, and G. P. Simon, "Conditions of applying Oliver-Pharr method to the nanoindentation of particles in composites," *Compos. Sci. Technol.*, vol. 72, no. 10, pp. 1147–1152, 2012.

[117] F. Gálvez, D. Cendón, A. Enfedaque, V. Sánchez-Gálvez, "High strain rate and high temperature behaviour of metallic materials for jet engine turbine containment," *J. Phys. IV Fr.*, vol. 134, no. 26 July 2006, pp. 269–274, 2006.

[118] G. Johnson and W. Cook, "A constitutive model and data for metals subjected to large strains, high strain rates and high temperatures," *Proc. 7th Int. Symp. Ballist.*, pp. 541–547, 1983.

[119] G. R. Johnson and W. H. Cook, "Fracture characteristics of three metals subjected to various strains, strain rates, temperatures and pressures," *Eng. Fract. Mech.*, vol. 21, no. 1, pp. 31–48, Jan. 1985.

[120] Y. F. Cui, X. Zhang, G. L. Xu, W. J. Zhu, H. S. Liu, and Z. P. Jin, "Thermodynamic assessment of Co-Al-W system and solidification of Co-enriched ternary alloys," *J. Mater. Sci.*, vol. 46, no. 8, pp. 2611–2621, 2011.

[121] S. Y. Yang, M. Jiang, and L. Wang, "Thermodynamic Description of the γ' Phase in the Co-Al-W Based Superalloys," *Mater. Sci. Forum*, vol. 747–748, pp. 654–658, 2013.

[122] P. Wang *et al.*, "Thermodynamic re-assessment of the Al-Co-W system," *Calphad Comput. Coupling Phase Diagrams Thermochem.*, vol. 59, no. September, pp. 112–130, 2017.

[123] T. Omori, Y. Sutou, K. Oikawa, R. Kainuma, and K. Ishida, "Shape memory and magnetic properties of Co-Al ferromagnetic shape memory alloys," *Mater. Sci. Eng. A*, vol. 438–440, no. SPEC. ISS., pp. 1045–1049, 2006.

[124] R. W. Fountain and W. D. Forgeng, "Phase Relations and Precipitation in Cobalt-Titanium Alloys," *Trans. AIME*, vol. 215, pp. 998–1008, 1959.

[125] M. Korchynsky and R. W. Fountain, "Precipitation phenomena in cobalt-tantalum alloys," *Trans. AIME*, vol. 215, pp. 1033–1043, 1959.

[126] R. W. Fountain;, G. M. Faulring, and W. D. . Forgeng, "Structural relationships between precipitate and matrix in cobalt-rich cobalt–titanium alloys," *Trans. Met. Soc AIME*, no. 221, pp. 747–751, 1961.

[127] A. Suzuki and T. M. Pollock, "High-temperature strength and deformation of γ/γ′ two-phase Co–Al–W-base alloys," *Acta Mater.*, vol. 56, no. 6, pp. 1288–1297, 2008.

[128] M. Ooshima, K. Tanaka, N. L. Okamoto, K. Kishida, and H. Inui, "Effects of quaternary alloying elements on the γ′ solvus temperature of Co-Al-W based alloys with fcc/L12 two-phase microstructures," *J. Alloys Compd.*, vol. 508, no. 1, pp. 71–78, 2010.

[129] R. Lizárraga, F. Pan, L. Bergqvist, E. Holmström, Z. Gercsi, and L. Vitos, "First Principles Theory of the hcp-fcc Phase Transition in Cobalt," *Sci. Rep.*, vol. 7, no. 1, p. 3778, 2017.

[130] T. Bachaga, R. Daly, L. Escoda, J. J. Suñol, and M. Khitouni, "Amorphization of Al50(Fe2B)30Nb20 Mixture by Mechanical Alloying," *Metall. Mater. Trans. A*, vol. 44, no. 10, pp. 4718–4724, 2013.

[131] M. Adamiak, J. B. Fogagnolo, E. M. Ruiz-Navas, L. A. Dobrzañski, and J. M. Torralba, "Mechanically milled AA6061/(Ti3Al)P MMC reinforced with intermetallics - The structure and properties," *J. Mater. Process. Technol.*, vol. 155–156, no. 1–3, pp. 2002–2006, 2004.

[132] A. J. McAlister, "The Al-Co (Aluminum-Cobalt) system," *Bull. Alloy Phase Diagrams*, vol. 10, no. 6, pp. 646–650, 1989.

[133] D. I. Davidov, N. N. Stepanova, N. V. Kazantseva, M. B. Rigmant, and D. A. Shishkin, "Study of the magnetic properties, structure, and phase transformation in the alloys of the Co-Al-W system," vol. 020035, p. 020035, 2015.

[134] H. Y. Yan, J. Coakley, V. A. Vorontsov, N. G. Jones, H. J. Stone, and D. Dye, "Alloying and the micromechanics of Co-Al-W-X quaternary alloys," *Mater. Sci. Eng. A*, vol. 613, pp. 201–208, 2014.

[135] A. Tomaszewska, G. Moskal, D. Migas, M. Mikus, and T. Macia, "Thermal parameters determination of Co – Al – W as-cast alloy homogenization by DTA analysis," vol. 4, 2018.

[136] A. Epishin, N. Petrushin, G. Nolze, G. Gerstein, and H. J. Maier, "Investigation of the γ′-Strengthened Quaternary Co-Based Alloys Co-Al-W-Ta," *Metall. Mater. Trans. A*, 2018.

[137] A. Bauer, S. Neumeier, F. Pyczak, and M. Goken, "Microstructure and creep strength of different γ-γ'- strengthened Co-base superalloy variants," *Scr. Mater.*, vol. 63, no. 12, pp. 1197–1200, 2010.

[138] W. Gui, H. Zhang, M. Yang, T. Jin, X. Sun, and Q. Zheng, "The investigation of carbides evolution in a cobalt-base superalloy at elevated temperature," *J. Alloys Compd.*, vol. 695, pp. 1271–1278, 2017.

[139] F. R. Morral, "The Metallurgy of Cobalt Alloys," *Ournal Met.*, no. July, pp. 52–59, 1968.

[140] J. Murray, *ASM alloy phase diagrams center, chapter binary alloy phase diagrams.*, ASM Intern. ASM, 2007.

[141] M. S. . Karunaratne, P. Carter, and R. . Reed, "Interdiffusion in the face-centred cubic phase of the Ni–Re, Ni–Ta and Ni–W systems between 900 and 1300°C," *Mater. Sci. Eng. A*, vol. 281, no. 1–2, pp. 229–233, Apr. 2000.

[142] C. H. Zenk, S. Neumeier, H. J. Stone, and M. Göken, "Mechanical properties and lattice misfit of γ-γ' strengthened Co-base superalloys in the Co-W-Al-Ti quaternary system," *Intermetallics*, vol. 55, pp. 28–39, 2014.

[143] M. S. Titus, A. Suzuki, and T. M. Pollock, "Creep and directional coarsening in single crystals of new γ-γ' Cobalt-base alloys," *Scr. Mater.*, vol. 66, no. 8, pp. 574–577, 2012.

[144] A. Bauer, S. Neumeier, F. Pyczak, and M. G??ken, "Creep Strength and Microstructure of Polycrystalline γ' - Strengthened Cobalt-Base Superalloys," *Superalloys 2012*, pp. 695–703, 2012.

[145] M. Jiang, G. Saren, S. Y. Yang, H. X. Li, and S. M. Hao, "Phase equilibria in Co-rich region of Co-Ti-Ta system," *Trans. Nonferrous Met. Soc. China (English Ed.*, vol. 21, no. 11, pp. 2391–2395, 2011.

[146] E. A. Lass, D. J. Sauza, D. C. Dunand, and D. N. Seidman, "Multicomponent γ'-strengthened Co-based superalloys with increased solvus temperatures and reduced mass densities," *Acta Mater.*, vol. 147, pp. 284–295, 2018.

[147] M. Cartón-Cordero *et al.*, "Microstructure and compression strength of Co-based superalloys hardened by γ′ and carbide precipitation," *Mater. Sci. Eng. A*, vol. 734, no. August, pp. 437–444, 2018.

[148] L. Freund, Patricia, A. Bauer, L. Benker, S. Neumeier, and G. Mathias, "Formation of Cuboidal Co 3 AlC Precipitates in Carbon - Containing Co - Al - W-Based Superalloys," pp. 1–6, 2015.

[149] T. M. Pollock and R. D. Field, *Dislocations in Solids vol 11.* Elsevier, 2002.

[150] J. Wang, W. G. Guo, X. Gao, and J. Su, "The third-type of strain aging and the constitutive modeling of a Q235B steel over a wide range of temperatures and strain rates," *Int. J. Plast.*, vol. 65, pp. 85–107, 2015.

[151] G. I. Taylor and H. Quinney, "The Latent Energy Remaining in a Metal after Cold Working," *Proc. R. Soc. A Math. Phys. Eng. Sci.*, vol. 143, no. 849, pp. 307–326, 1934.

[152] R. Kapoor and S. Nemat-Nasser, "Determination of temperature rise during high strain rate deformation," *Mech. Mater.*, vol. 27, no. 1, pp. 1–12, 1998.

[153] R. K. Rhein *et al.*, "Creep Behavior of Quinary γ′-Strengthened Co-Based Superalloys," *Metall. Mater. Trans. A*, 2018.

[154] Y. M. Eggeler, M. S. Titus, A. Suzuki, and T. M. Pollock, "Creep deformation-induced antiphase boundaries in L12-containing single-crystal cobalt-base superalloys," *Acta Mater.*, vol. 77, pp. 352–359, 2014.

[155] R. S. Cadenas, D. Cendón, and F. Gálvez, "Modelo del comportamiento mecánico de materiales con cambios microestructurales," 2016, pp. 1–6.

[156] J. Wang, W. G. Guo, Y. Su, P. Zhou, and K. Yuan, "Anomalous behaviors of a single-crystal Nickel-base superalloy over a wide range of temperatures and strain rates," *Mech. Mater.*, vol. 94, pp. 79–90, 2016.

[157] M. Ott, U. Tetzlaff, and H. Mughrabi, "Influence of directional coarsening on the isothermal high-temperature fatigue behaviour of the monocrystalline nickel-base superalloys CMSX-6 and CMSX-4," vol. 272, pp. 24–30, 1999.

List of publications

Scientific articles in peer-reviewed journals

Authors	**R. Casas**, F. Gálvez, M. Campos
Title	Microstructural development of powder metallurgy cobalt-based superalloys processed by field assisted sintering techniques (FAST)
Review	Materials Science & Engineering A Volume 724, (2018), pp 461-468 DOI 10.1016/j.msea.2018.04.004

Abstract

This study reports the microstructural evolution, physical and mechanical properties of cobalt-based superalloys processed from mechanical alloyed powders and consolidated by field-assisted sintering techniques (FAST). After an initial thermodynamic simulation of the ternary diagram by Thermocalc® to determine the composition, a sequential milling process was carried out at room temperature up to 40 h milling of two different alloying systems: Co-12Al-10W (at. %) and Co-12Al-10W-2Ti-2Ta (at. %). Characterization of the powders was performed by using X-Ray diffraction, scanning electron microscope with energy-dispersive X-ray spectroscopy (EDS) and particle-size analyzer. Consolidated samples were also characterized in terms of density, microhardness and hardness. In order to promote the dual γ/γ' microstructure, both alloys were aged after solution annealing heat treatment, improving a new route of consolidation with a new level of performance.

Authors	**R. Casas**, F. Gálvez, M. Campos
Title	Effect of heat treatments on γ/γ' microstructures and strengthening in cobalt-based superalloys produced by powder metallurgy
Review	Under review – Submitted to journal

Abstract

The main research of this work is focused on the influence of heat treatments on the development of the γ/γ' two-phase microstructure, once cobalt-based superalloy has been manufactured by powder metallurgy route (PM). Cobalt-based specimens with a nominal composition of Co12Al10W (at.%) and Co+2Ti/2Ta (at.%), obtained by mechanical alloying (MA) and consolidated by the field assisted sintering technique (FAST) were chosen to promote the required γ/γ' dual phase by heat treatments. A specific study at different temperatures and times of solution and annealing was

performed. Characterization of microstructure was determined by using scanning electron microscope (SEM) with energy-dispersive X-ray spectroscopy (EDS), and X-Ray diffraction (XRD). The results are linked to the final γ'-phase features such as volume fraction and misfit, which depend on composition, temperatures and times selected during both steps of heat treatment. Micro and nano hardness measurements of both alloys demonstrate that -Ti and -Ta containing additions increase the strength of the superalloy.

Authors	**R. Casas**, M. Campos, F. Gálvez
Title	High strain rate deformation of a cobalt-based alloys processed by powder metallurgy route over a wide range of temperatures
Review	In preparation

Abstract

The aim of this work is focused on the dynamic behavior of a novel powder metallurgy cobalt-based superalloy with γ/γ' two-phase at high strain rate over a temperature range of 25 – 850 °C and over a strain rate range of 1000/s. The dynamic loading tests were conducted on a Split Hopkinson Pressure Bar (SHPB) to study the strain-rate effect at different range of temperatures, focusing on the temperature-dependent anomalies of the flow stress at elevated temperatures for ternary and quinary alloys. In addition, these materials have to consider the strain rate and thermal softening effects. Thus, the Johnson-Cook (J-C) constitutive model is proposed as a starting point to certificate the material model. Based on the experimental results, a modified model of J-C based of function piece was established for ternary and quinary cobalt-based alloys to be able to capture the anomalous peak of the flow stress, which is dependent on the temperature. It was demonstrated that the yield strength of the superalloys can be predicted over a wide range of temperatures with the modified J-C model

Conference contributions

Congress	XIV Congreso Nacional de Materiales Gijón (España), June 2016
Authors	**R. Casas**, M. Campos, F. Gálvez
Title	Aleaciones base Co sinterizadas para su aplicación en condiciones severas: Diseño de microestructuras γ/γ'
Participation	Oral

Abstract

El reciente hallazgo de una fase estable intermetálica $Co_3(Al,W)$, con un tipo de estructura $L1_2$, ofrece en aleaciones de base Co una microestructura dual γ/γ', que pueden competir con las súper aleaciones base Ni para su correspondiente aplicación en condiciones severas a altas temperaturas. Hasta ahora, esta familia de aleaciones se ha desarrollado empleando técnicas metalúrgicas convencionales, donde, se requiere una atención especial para evitar algunos defectos como, macro o micro segregaciones, contracción en la solidificación del metal, o inclusiones de segunda fase. La tecnología de polvos puede ayudar a encontrar nuevas rutas en un futuro, con avances en conceptos de enfriamiento e innovación del diseño microestructural de las aleaciones. En esta investigación, el enfoque PM debe contener la obtención de polvos prealeados a partir de una atomización y su correspondiente consolidación a través de técnicas HIP o SPS. El sistema ternario Co-Al-W se ha investigado usando programas de simulación CALPHAD, para predecir la región optima rica en Co. Una vez localizada, se diseñó una aleación para elaborar polvos prealeados y se consolidó a partir de una alta densificación para promover la precipitación de γ'

Congress	World PM 2016 Hamburg (Germany), October 2016 ISBN: 978-1-899072-48-4
Authors	**R. Casas**, M. Campos, F. Gálvez
Title	High Temperature Co alloys processed by PM route: Designing γ/γ' microstructures.
Participation	Oral

Abstract

The recent discovery of the stable $Co_3(Al,W)$ intermetallic with an ordered $L1_2$ structure, provides a potential dual phase γ/γ' microstructures in Co-base alloys that can compete with Ni-base superalloys for high T applications. This family of alloys have been developed always using conventional metallurgy, where, proper care needs to be taken in order to avoid defects such as macro and micro segregation, solidification shrinkage or second phase inclusions.PM technology can aid to develop new routes with advances cooling concepts allowing

innovations microstructural designs in the future. In this case, PM approach should include the development of the powder by atomization and fully-dense consolidation by HIP or SPS. Ternary system Co-Al-W was investigated with CALPHAD method to predict Co-rich region. Once the alloy design was set, the experimental information was used to develop fully prealloyed powders. Consolidation was conducted through high densification PM route to promote the γ' precipitation.

Congress	AMPT 2016 Kuala Lumpur (Malaysia), November 2016
Authors	M. Cartón, **R. Casas**, M. Campos, José M. Torralba
Title	Microstructural possibilities of Co-Al-W alloys processed by SPS: Effects of Al and W contents.
Participation	Oral

Abstract

Expand the knowledge on phase equilibria in the ternary system Co-A-W is crucial basis for the proper design of future γ-γ' Co superalloys. In the present work, starting from powdered metals, ternary Co-Al-W with Al contents between 8 and 12 at. % and W contents between 8 and 10 at. % were investigated with respect to microstructural phase evolution. This work explores as well, the ability of near net shape technologies (by powder metallurgy –PM–) to overcome common defects of ingot metallurgy, and to take the advantages of a recognized cost-effective technology. Therefore, this family of alloys have been obtained by gas atomizing and high energy milling. Afterwards, processed powders were consolidated by field assisted hot pressing (FAHP), followed by solution treatment up to 1250 °C for 24 h to better determine the effect of composition on γ+γ'→ γ transformation temperature by thermal analysis (STA). Microstructural characteristics of consolidated alloys were determined by means of X-ray diffraction, SEM, TEM and STEM. Besides the effect of Ti and Ta as γ' forming elements was also investigated, to understand the consequences on γ' solvus temperature.

Congress	VI Congreso Nacional de Pulvimetalurgia Ciudad Real (España), June 2017 ISBN: 978-84-697-3650-0
Authors	**R. Casas**, M. Campos, F. Gálvez
Title	Diseño de microestructuras γ-γ' mediante tratamientos térmicos para la obtención de aleaciones de cobalto por vía pulvimetalúrgica
Participation	Oral

Abstract

Dada la importancia de las denominadas *superaleaciones*, se están realizando numerosos estudios para el desarrollo de una microestructura de fase tipo dual γ *(*cúbica centrada en las caras) / γ' ($L1_2$). La fase γ' presenta una morfología muy característica con finos precipitados, obtenida por diferentes tratamientos térmicos. Los efectos de dichos tratamientos térmicos aún no han sido analizados para las aleaciones base Co obtenidas por vía pulvimetalúrgica. Este trabajo se centra en los efectos ocurridos en la microestructura final tras los tratamientos térmicos de solubilización y maduración realizados a diferentes temperaturas y tiempos. Para su consecución, se ha partido de dos composiciones específicas (Co-12Al-10W at. %) y (Co-12Al-10W-2Ti-2Ta at%), fabricadas por molienda mecánica de alta energía y consolidadas mediante prensado en caliente por campo asistido. El resultado final está ligado a la fracción volumétrica de *γ',* que depende directamente de la temperatura y tiempo fijado durante ambos tratamientos térmicos. Además, se ha calculado la microdureza sobre la microestructura resultante de ambas composiciones. Por otro lado, se ha estudiado la temperatura de *solvus* de γ' en los tratamientos térmicos seleccionados, debido a la importancia en la estabilidad de la microestructura $L1_2$ a altas temperaturas.

Congress	EuroPM 2017 Milan (Italy), October 2017 ISBN: 978-1-899072-49-1
Authors	**R. Casas**, M. Campos, F. Gálvez, David C. Dunand, David N. Seidman
Title	Design of γ-γ' microstructures through heat treatments for strengthening Co base PM alloys

Participation

Abstract

Given the importance of the superalloys, studies are currently being conducted on promoting new dual phase γ (face-centered cubic)/ γ'($L1_2$) microstructure. The γ' phase has a characteristic morphology and fine precipitates, obtained by a specific heat treatment. For PM Co base alloys the effect of these heat treatments is not already explored. Starting from two particular compositions (Co-12Al-10W at. %) and (Co-12Al-10W-2Ti-2Ta at.%) processed by Mechanical Alloying (MA) and consolidated by Field Assistant Hot Pressing (FAHP), this work is focused on the effect of solubilization and ageing parameters on final microstructure. The results are linked to the final vol% of γ' depending on the temperature and time set during both steps of the heat treatment. Microhardness of both compositions are also calculated. Besides, as γ' solvus temperature is essential for high temperature microstructure stability, it has been studying the solvus temperature related to Co alloy composition and heat treatment selected.

Congress	Eurosuperalloys 2018 Oxford (United Kingdom), September 2018
Authors	**R. Casas**, M. Campos, F. Gálvez
Title	Poster Research on design of γ/γ' microstructures in cobalt-based superalloys processed by powder metallurgy route
Participation	Poster